# Nonlinear Mixing and Synchronization in Dusty Plasma

Thesis submitted for the award of the Degree

of

## 𝕯𝖔𝖈𝖙𝖔𝖗 𝖔𝖋 𝕻𝖍𝖎𝖑𝖔𝖘𝖔𝖕𝖍𝖞

in the

**Department of Physics**

by

## Ajaz Ahmad Mir

(2018RPH0028)

Under the supervision of

## Dr. Sanat Kumar Tiwari



भारतीय प्रौद्योगिकी
संस्थान जम्मू
**INDIAN INSTITUTE OF
TECHNOLOGY JAMMU**

विद्याधनं सर्वधन प्रधानम्

**Indian Institute of Technology Jammu**

**May 2023**

# Declaration

I hereby declare that the matter embodied in this thesis entitled **"Nonlinear Mixing and Synchronization in Dusty Plasma"** is the result of investigations carried out by me in the **Department of Physics, Indian Institute of Technology Jammu (IIT Jammu), India**, under the supervision of **Dr. Sanat Kumar Tiwari** and it has not been submitted elsewhere for the award of any degree or diploma, membership *etc.* In keeping with the general practice in reporting scientific observations, due acknowledgements have been made whenever the work described is based on the findings of other investigators. Any omission that might have occurred due to oversight or error in judgment is regretted. A complete bibliography of the books and journals referred in this thesis is given at the end of the thesis.

May 2023

Indian Institute of Technology Jammu

Ajaz Ahmad Mir

(2018RPH0028)

*I am delightfully dedicating my PhD thesis work to my respected parents **(Ms. Habla Begum & Mr. Mohd Maqbool Mir )** and my beloved elder brother **(Mr. Tariq Ahmad Mir)**.*

# Abstract

Dusty plasma is a collection of heavily charged particles immersed in an electron-ion plasma. The dust particles are heavy compared to ions by a few orders of magnitude. Hence, their inertia and forces around them lead to slow modes. Also, the high charge on dust particles brings in the existence of different phases of the dust system. In a fluid regime, plasma supports the dust acoustic wave (DAW) due to the balance between dust inertia and the background plasma pressure. However, a two-dimensional monolayer lattice, formed due to strong Coulomb coupling between the dust grains, supports the longitudinal dust lattice waves (DLWs). This thesis provided a theoretical model for the nonlinear mixing of DLWs and synchronization of DAWs. While the mixing is studied using a forced Korteweg-de Vries (fKdV) model, the synchronization is explored using a forced Korteweg-de Vries-Burgers (fKdV-B) model. The results from the thesis work are in excellent agreement with dusty plasma experimental observations based on the mixing of DLWs and synchronization of DAWs.

The nonlinear dynamical evolution of dusty plasmas as charged fluid is usually represented by fluid-Poisson equations. In the weak nonlinear dynamical regime, these coupled fluid-Poisson equations reduce to KdV and KdV-B equations with and without the viscous damping mechanism. These one-dimensional models are convenient to solve and provide good visualization of nonlinear longitudinal collective acoustic modes with reasonable accuracy.

Nonlinear mixing is a collective phenomenon in which the nonlinear interaction of two or more modes in the presence of a nonlinear medium generates a cascade of coherent modes. The characteristic features of the mixed-mode spectrum primarily depend on the nature of nonlinearity and dispersion in the medium. Using the fKdV model, we theoretically model the nonlinear mixing in dusty plasma. The nonlinear mixing features captured from the fKdV-based model remarkably resemble the dusty plasma experiment on mixing compressional acoustic waves in a dusty plasma. The origin of modes in the spectrum is due to the three-wave mixing confirmed using the bispectral analysis—the bispectral profiles of the fKdV model capture features of the bispectral profiles of the dusty plasma experiment.

Synchronization is also a collective nonlinear phenomenon in which a weak nonlinear interaction between the natural mode and an external driver adjusts the natural mode's rhythms. We have established that the fKdV-B equation provides a realistic theoretical framework for explaining synchronization in dusty or other dispersive systems. The synchronization domains are delineated as Arnold tongue in the two-dimensional parametric space of the forcing frequency and forcing amplitude. Results from the fKdV-B equation-based model showed excellent quantitative agreement with the dusty plasma experiment based on the synchronization of DAWs.

This thesis provides a simple, efficient, and accurate theoretical description of the mixing and synchronization of nonlinear waves in agreement with previous experiments. The presented model is extendable to similar nonlinear waves in plasmas at other lengths and time scales and in fluid-like mediums governed by convective nonlinearity and dispersion. The models may also have applicability in understanding the dynamical evolution of space junk or space debris and the nonlinear plasma excitation in the lower earth orbit.

# Acknowledgements

# Contents

# List of Figures

# List of Tables

# List of Symbols

| Symbol | Description |
|--------|-------------|
| $n(x,t)$ | Dust density field |
| $v(x,t)$ | Dust velocity field |
| $\phi(x,t)$ | Dust potential field |
| $\alpha$ | Nonlinearity coefficient |
| $\beta$ | Dispersion coefficient |
| $\eta$ | Viscous damping coefficient |
| $cn$ | Jacobi elliptic function |
| $\kappa$ | Jacobi elliptic modulus |
| $K(\kappa)$ | Complete elliptical integral of first kind |
| $F_s(x,t)$ | Spatio-temporal forcing |
| $F_s(t)$ | Time-dependent forcing |
| $B(F_1, F_2)$ | Bispectrum |
| $\gamma(F_1, F_2)$ | Bicoherence |
| $\langle E_p \rangle$ | Average Coulomb potential energy |
| $\langle E_k \rangle$ | Average thermal kinetic energy |
| $\phi^Y(r)$ | Yukawa potential |
| $\kappa_D$ | Debye screening parameter |
| $\lambda_D$ | Debye length |
| $Q_d$ | Dust charge |
| $M_d$ | Dust mass |
| $T_d$ | Dust temperature |
| $a$ | Average inter-particle separation or Wigner-Seitz radius |
| $\Gamma$ | Coulomb coupling parameter |
| $\nu$ | Friction coefficient |
| $\epsilon_0$ | Electric permittivity of free space |
| $k_B$ | Boltzmann constant |
| $e$ | Electron charge |

# List of Abbreviations

| Abbreviation | Description |
| --- | --- |
| NLM | Nonlinear Mixing |
| KdV | Korteweg-de Vries |
| fKdV | forced KdV |
| KdV-B | Korteweg-de Vries-Burgers |
| fKdV-B | forced Korteweg-de Vries-Burgers |
| VdP | Van der Pol |
| fVdP | forced VdP |
| DDW | Dust Density Wave |
| DAW | Dust Acoustic Wave |
| DLW | Dust Lattice Wave |
| ISS | International Space Station |
| PK-4 | Plasma Kristall-4 |
| PSD | Power Spectral Density |
| RF | Radio-frequency |
| DC | Direct-current |
| IMD | Inter-Modulation Distortion |
| LEO | Low Earth Orbit |
| GHD | Generalized hydrodynamic |
| MHD | Magneto-hydrodynamic |
| MD | Molecular Dynamics |
| LAMMPS | Large-scale Atomic/Molecular Massively Parallel Simulator |
| SCP | Strongly Coupled Plasma |
| OCP | One Component Plasma |
| YOCP | Yukawa OCP |

# Chapter 1

# Introduction

This thesis provides theoretical models for nonlinear mixing and synchronization in dusty plasma. This chapter introduces these phenomena and delineates their widespread applicability to physical systems. It also introduces dusty plasmas and acoustic waves supported in their fluid and solid phases, an application test-bed for studies of the above nonlinear phenomena. Thesis briefs about the previously used oscillator-based qualitative model. It motivates the need for a new theoretical model with an appropriate form of nonlinearity supported in dusty plasmas. We discuss the full-fluid model for dusty plasma and the reduced Korteweg-de Vries model in the weak nonlinear dynamical regime. Including driving and damping effects associated with dusty plasma medium, we propose forced KdV and forced KdV-Burgers models for nonlinear mixing and synchronization. The chapter concludes with a summary of all upcoming chapters of the thesis.

---

## 1.1 Nonlinear mixing and synchronization

We commonly observe the transition of water flow turning from streamlined to turbulent as we increase the flow rate in the sink tap; we also observe the transition from laminar to turbulent flow in a plume of smoke [1]. Likewise, we observe the rhythmic chirping of birds in the morning and the rhythmic flashing of fireflies in the evening [2]. Each of these is an outcome of some physical process; while the former two are caused due to the turbulent mixing, the latter is due to the ability of birds and fireflies to work in unison. More specifically, turbulent mixing is an outcome of "nonlinear mixing," and the ability to work in unison is due to "synchronization". With scientific advancements, we can explain these two physical phenomena through nonlinear mathematical models. The presence and form of nonlinearity are significant in both phenomena' existence and characteristics.
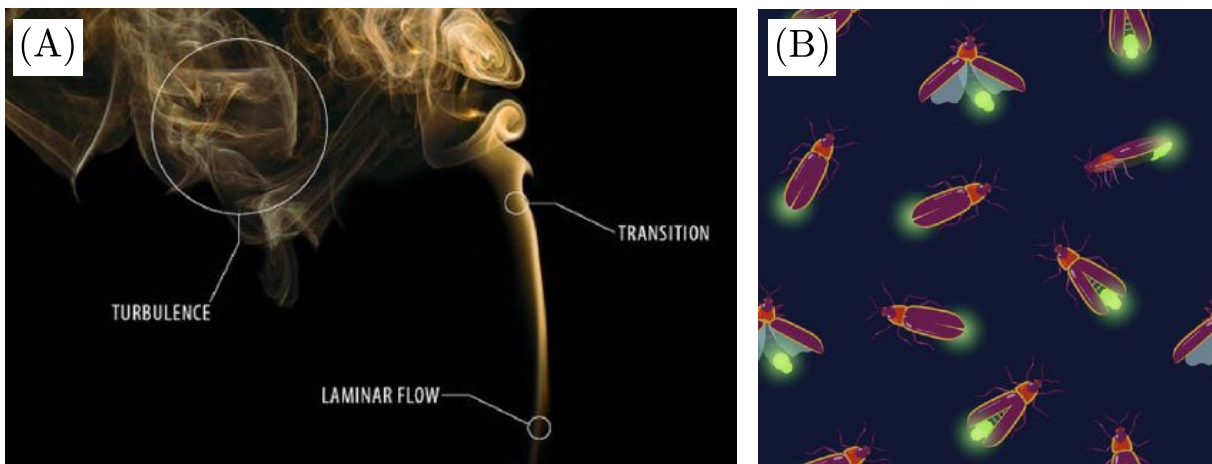


Figure 1.1: (A) The transition from laminar to turbulent flow of plume of smoke *Credit: https://www.bronkhorst.com*. The basic principle behind the turbulent nature is the nonlinear mixing of modes. In a typical gas, the Navier-Stokes equations govern the complex nonlinear dynamics of turbulent mixing, in which nonlinear interaction between the modes leads to generating a cascade of modes [3]. (B) Synchronization of fireflies via rhythmic flashing *Credit: https://www.123rf.com*. Theoretically, the Kuramoto model provides insights into the dynamics of the synchronization of fireflies, in which each firefly is mimicked as a nonlinear oscillator with an intrinsic rhythm [4].

The above two examples are among a huge number of physical processes that, for understanding, require some nonlinear modelling. Some widely used models include Navier-Stokes equations, Coupled oscillators, Schrodinger equations and kinetic models with an ensemble of particles interacting through pairwise interaction. All these models utilize different nonlinear mechanisms (explicitly or implicitly) to explain collective dynamical phenomena in different physical paradigms. Also, a single physical process, such as propagation and dispersion of longitudinal waves, requires different models relevant to given physical systems. In a nonlinear dynamical regime, various mediums, such as optical fibres, water surfaces, plasmas *etc.,* support solitons whose behaviour strongly depends on the nature of the medium's nonlinearity.

Nonlinear mixing (NLM) occurs whenever two or more modes interact through a nonlinear medium and generate a cascade of modes via a three-wave or higher-order mixing mechanism. Synchronization, on the other hand, is an adjustment of rhythms in two are more systems due to their weak nonlinear interaction. The features of both phenomena depend on the characteristic nonlinearity of the medium.

Figure 1.2: Collective phenomenon observed in nature and their representative mathematical models. (A) The flocking of birds is reasonably understood through the Vicsek model [5] *Credit: UCDAVIS/College of Biological Sciences.* (B) The Hurricane Jeanne in which the vortex formation is governed by Navier-Stokes equations [6] *Credit: NASA's Aqua satellite.* (C) The dynamics of Bose-Einstein condensate [7] is governed by nonlinear Schrödinger equation (Gross-Pitaevskii equation) [8] *Credit: NASA/JPL-Caltech.*

Based on our theoretical understanding of physical phenomena, a few systems with different characteristic nonlinearity are optical systems, fluid flows, quantum collective dynamics and waves in solids. This thesis proposes a theoretical model for both phenomena in fluid and fluid-like nonlinear mediums. A convective spatio-temporal nonlinearity supports the nonlinear interaction in these systems. We have adopted the dusty plasma as a test bed because the available experimental observation makes it easy to validate the proposed theoretical models.

The phenomenon of nonlinear mixing and synchronization of waves are ubiquitous. Nonlinear mixing of waves have been observed in plasmas [9–15], acoustics [16, 17], plasmons [18–20], meta-materials [21, 22], nonlinear optical systems [23–27] and nonlinear dispersive fluid media [28]. Synchronization has been found in biological systems like rhythmic processes in physiology [29], cardiac pacemaker cells [30, 31], chemical systems [32, 33], and in physical systems like quantum mechanically entangled systems [34, 35], laboratory plasmas [36–42], and nonlinear optical systems [43, 44]. The nonlinearity involved in the aforementioned systems differs for different physical systems. Our goal in this thesis work is to understand the mixing and synchronization of nonlinear waves in systems where the source of nonlinearity is spatio-temporal convective nonlinearity of the mathematical form $(\vec{v} \cdot \nabla)\vec{v}$, where $\vec{v}$ is the velocity field.

In this thesis, we have established one-dimensional theoretical models for NLM and synchronization based on the Korteweg-de Vries (KdV) equation, a weakly nonlinear dynamical model representation of fluids and plasmas. This model retains the dispersion and fluid-like convective nonlinearity and has exact analytical solutions in a particular physical regime. We have proposed and established that a forced KdV (fKdV) model can explain nonlinear mixing [45] and the fKdV model with viscous damping also known as fKdV-Burgers (fKdV-B) model can explain synchronization [46]. The nonlinear mixing of waves is explored on the fKdV model by solving it analytically for time-dependent force and numerically for travelling wave forcing. On the other hand, the synchronization of waves is explored in the fKdV-B model through its numerical solution.

The proposed models in this thesis are theoretically derived and validated in a dusty plasma. The framework choice is due to two primary reasons 1) the models can be exactly derived from dust fluid dynamical equations, and 2) the outcomes from our models could be compared with available experimental

observations. The mixing profiles from the fKdV model [45] are in excellent agreement with those obtained from the interaction of two lattice waves in a dusty plasma experiment [15] barring minor differences due to simplified model choice. The fKdV-B model [46] for synchronization of nonlinear dust density waves agrees with the synchronization experiment in dusty plasma [36]. There is still a scope to improve both models further to capture all the possible experimental findings of the dusty plasma experiments based on the mixing [15] and synchronization [36] of nonlinear waves.

## 1.2 Dusty plasma

A dusty (complex) plasma is composed of four components and is formed when nanometer to micrometre particles are immersed in a typical electron-ion plasma [47–51]. The dust grains acquire a high negative charge due to the high mobility of electrons compared to ions over the surface of dust grains. Dusty plasmas are not only artificially prepared in the laboratory. However, they are ubiquitous, like planetary rings, comet tails, interstellar clouds, and earth's ionosphere [51–56]. The dusty plasmas in such systems have orders of magnitude differences in mass, charge, grain size and density [51, 52].

Table 1.1: Various physical parameters of a wide range of dusty plasmas [51, 52]. $n_e$, and $T_e$ is electron density and temperature, respectively. $n_d$, and $r_d$ is dust density and dust grain radius, respectively. $n_n$ is the neutral density.

| | $n_e$ (cm$^{-3}$) | $T_e$ (K) | $n_d$ (cm$^{-3}$) | $r_d$ ($\mu$ m) | $n_n$ (cm$^{-3}$) |
|---|---|---|---|---|---|
| **Discharge dusty plasma** | $10^8 - 10^{12}$ | $10^3 - 10^4$ | $10^3 - 10^5$ | $0.1 - 10$ | $-$ |
| **Noctilucent clouds** | $10^3$ | $150$ | $10$ | $0.1$ | $10^{14}$ |
| **Saturn's rings** | $10$ | $10^5 - 10^6$ | $10$ | $1$ | $-$ |
| **Rocket exhaust** | $10^{13}$ | $10^3$ | $10^8$ | $0.1$ | $10^{18}$ |
| **Halley's comet** | $10^2 - 10^4$ | $0.1 - 1$ | $10^3 - 10^8$ | $0.01 - 10$ | $10^{10}$ |
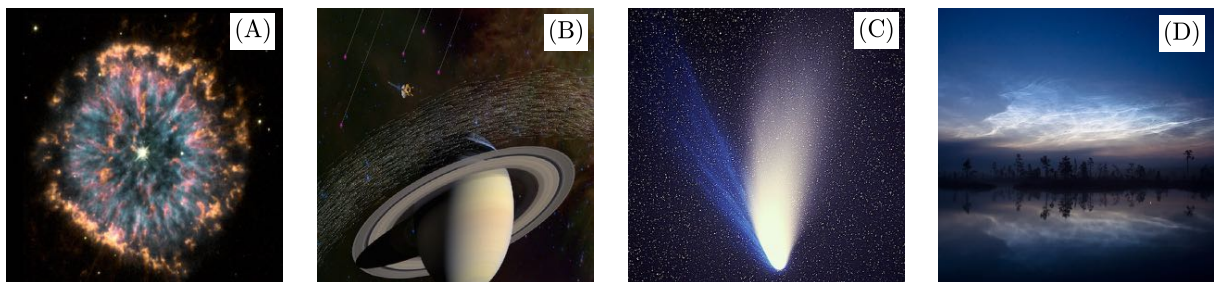


Figure 1.3: A wide range of dusty plasmas exists in nature. (A) The glowing eye Crab nebula *Credit: NASA*, (B) Saturn's rings *Credit: NASA*, (C) the comet Hale–Bopp with white dust tail *Credit: Wikipedia*, and (D) the Noctilucent clouds *Credit: Wikipedia*.

According to the kinetic model, the dust particles are treated as an ensemble of charged particles which interact via screened Coulomb (Yukawa) potential given by

$$\phi^Y(r) = \frac{Q_d^2}{4\pi\epsilon_0 r} \exp(-r/\lambda_D). \tag{1.1}$$

(I) Wave dynamics   (II) Vortex dynamics   (III) Precursor soliton dynamics   (IV) Phase separation

(V) Void formation
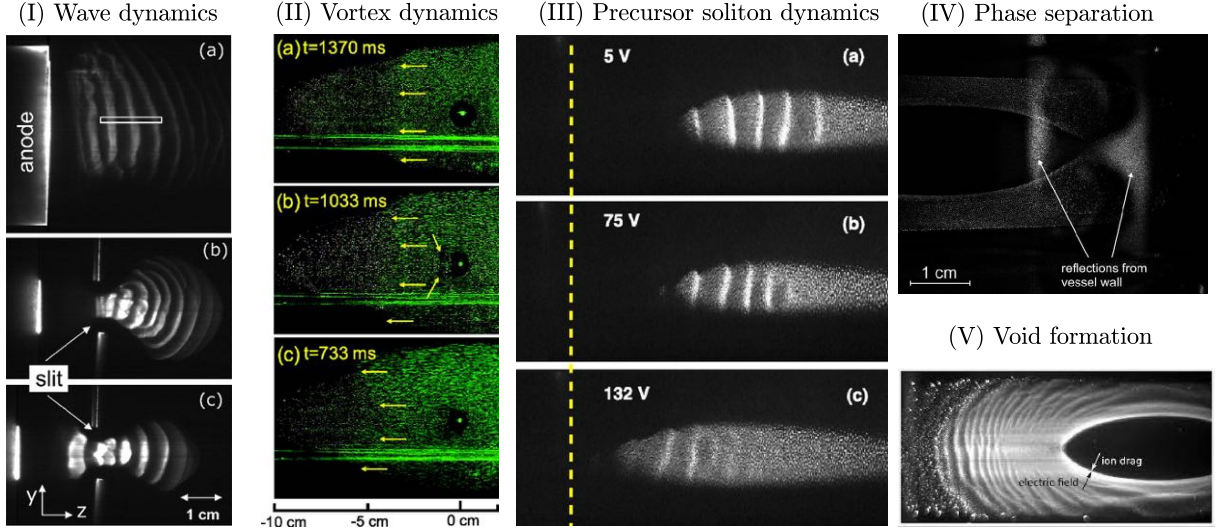


Figure 1.4: Wide variety of physical phenomena observed in laboratory dusty plasmas experiments. (I) The quasi-planar dust acoustic waves, and cylindrical dust acoustic waves and shocks [57], (II) Vortex formation in a strongly coupled dusty plasma [58], (III) Excitation of precursor solitons in dusty plasma [59], (IV) phase separation processes in binary dusty plasmas in parabolic flights[60], and (V) the void formation in dusty plasma under microgravity [61].

Where $Q_d$ is the dust grain charge, $\lambda_D$ is the Debye screening length and $\epsilon_0$ is the electrical permittivity of free space. The background electrons and ions provide the shielding between the dust particles, which is quantified by the Debye screening/shielding parameter given by

$$\kappa_D = a/\lambda_D. \tag{1.2}$$

Where $a$ is the average inter-particle separation or the Wigner-Seitz radius. The dusty plasma shows the dynamics both of a normal fluid and a crystalline state, which is governed by the Coulomb coupling parameter $\Gamma$ defined a the ratio of average Coulomb potential energy $\langle E_C \rangle$ to average thermal kinetic energy $\langle E_T \rangle$

$$\Gamma = \frac{\langle E_C \rangle}{\langle E_T \rangle} = \frac{Q_d^2}{4\pi\epsilon_0 a} \frac{1}{k_B T_d}. \tag{1.3}$$

Where $T_d$ is the kinetic temperature of a dusty plasma and $k_B$ is the Boltzmann constant. The heavy dust particles introduce new low-frequency modes due to dust dynamics and the existing modes due to ion dynamics. Based on the dust grain charge, the average inter-particle separation between the dust grains and the temperature of the dusty plasma, dusty plasmas are mainly categorised into two regimes, namely weak coupling (fluid) regime for which Coulomb coupling strength $\Gamma \leq 1$ and strong coupling (lattice) regime for which Coulomb coupling strength $\Gamma \gg 1$.

Dusty plasmas typically show phases of gas ($\Gamma \ll 1$), liquid ($1 \leq \Gamma \leq 150$) and solid (Coulomb crystal formation) ($\Gamma \gg 1$) [47, 62–64] due to which it supports a variety of physical phenomenon like the formation of waves [65–69], instabilities [70–73], vortices [58, 74–79], solid-liquid phase transition [47, 80–85], phase-separation [86], shock melting [87]. It supports formation of shocks [88–93], mach cones [94–97] and solitons/solitary waves [98, 99], and Peregrine solitons [100]. The dusty plasma medium supports the dust density wave (DDW) or dust acoustic wave (DAW) mostly in the weak coupling regime and the

dust lattice wave (DLW) in the strong coupling regime.

## 1.2.1 Dust Density Wave

The DDW is a longitudinal mode self-excited due to ion streaming, and its propagation direction is at an oblique angle to the ion flow. The DAW is a special case of the DDW in which the propagation direction of the wave is parallel to the ion flow direction. The DDWs/DAWs are often explored in the dusty plasmas' weak coupling regime ($\Gamma \leq 1$), where it behaves like a charged fluid.
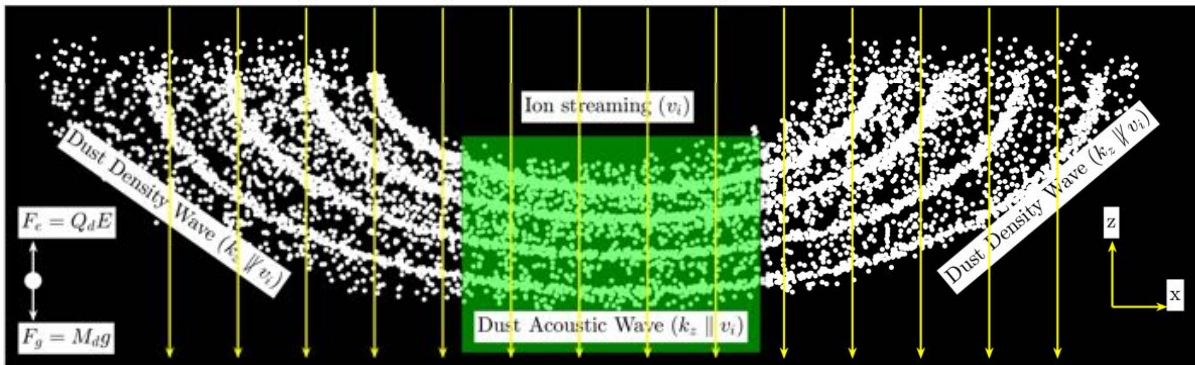


Figure 1.5: A cartoon representing the propagation of dust density waves at an arbitrary angle in a dusty plasma [101]. When the propagation direction is parallel to the ion streaming, it is known as a dust acoustic wave. The DDW is excited spontaneously due to ion-streaming instability [102]. Typically, the wavelength, frequency and phase velocity of DDWs are in the range of 1-15 mm, 10-100 Hz, and 1-20 mm/s, respectively.

In dusty plasma, the DAWs [103] are spontaneously generated due to the ion streaming instability [102], which is assisted by the ambient electric field of the background plasma. The DAWs have been studied in ground based experiments [104–119] and microgravity conditions using parabolic flights [101, 120, 121] and the International Space Station (ISS) [122–128].

## 1.2.2 Dust Lattice Wave

The dust grains in strongly coupled regime ($\Gamma \gg 1$) form two-dimensional (2D) and three-dimensional lattices, which is due to the fact that the dust grains attain a high negative charge of the order of tens of thousand due to which they acquire the nature of a crystalline system due to Coulomb repulsion between the dust grains. The background plasma's electrons and ions contribute to the dust particles' screening, quantified by a Debye screening parameter $\kappa_D$.

The dust grains form a layered structure in 3D, which forms different crystal lattices in 3D. The strongly coupled dusty plasma has been found to form a hexagonal close packing (HCP), body-centred cubic (BCC) and face-centred cubic (FCC) lattices in the 3D [48, 129–131]. The dust grains, often under gravity, have an effective potential that makes them settle down to a 2D monolayer. In 2D monolayer configuration the dusty plasmas form square, pentagon and hexagon lattices [47, 131–133].

The dust lattice supports both the longitudinal and the shear (transverse) waves in a strongly coupled regime due to its behaviour similar to solids [66, 69]. Our interest is the longitudinal mode of the dust

lattice, known as the dust lattice wave. We will confine ourselves to the 2D monolayer, which often supports the excited DLws due to the external forcing.
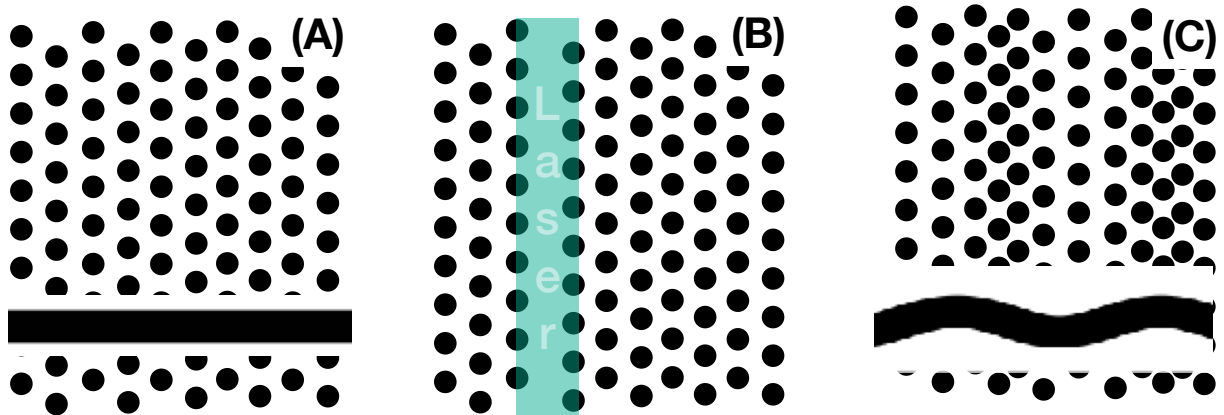


Figure 1.6: A cartoon of DLW propagation in a 2D monolayer dust lattice. (A) The unperturbed dust lattice, (B) localized perturbation via a laser sheet [134, 135], and (C) the DLW excitation due to laser radiation pressure and propagation.

The DLW is a longitudinal compressional mode in a dust lattice excited by an external forcing [67, 68, 134–137]. The DLWs waves are often studied in the 2D dust lattice due to the less complexity involved than the 3D lattices. There are a few key differences between DDWs and DLWs. The first is DDWs are excited spontaneously due to the ambient electric field from the background plasma, while the DLWs are excited by external forcing. The DDW is often observed in dusty plasma's fluid regime ($\Gamma \ll 1$), while the DLW is only excited in the solid regime ($\Gamma \gg 1$) of dusty plasma. The ion-streaming instability is the energy source for the self-excitation of DDWs, while for the DLWs, the energy is provided by the external source. In DDWs, all three species of electrons, ions and dust play an important role in the wave dynamics, while in the DLWs, only the dust plays an important role in the wave dynamics other two species only shield the dust grains.

## 1.3 The fluid model for dusty plasma

The dusty plasma in a weak coupling regime ($\Gamma \leq 1$) shows the traits of a charged-fluid [51]. The Navier-Stokes and Poisson equations collectively govern the dynamics of charged dust fluid in an electrostatic regime. The full fluid-Poisson set of the equation reduces to the Korteweg-de Vries equation in a weakly nonlinear dynamical regime and, in the presence of viscous damping, to the Korteweg-de Vries-Burgers equation. The KdV and KdV-B model keeps the essence of fluid or fluid-like systems by retaining the spatio-temporal convective nonlinearity. We are concerned about the dust fluid dynamics, and the background plasma is Boltzmannian due to a lack of inertia compared to dust grains.

### 1.3.1 The fluid-Poisson model

The 1D fluid-Poisson model for dusty plasma comprises continuity, momentum and Poisson equations [51, 138, 139]. The continuity equation is given by

$$\frac{\partial n}{\partial t} + \frac{\partial (nv)}{\partial x} = 0 \tag{1.4}$$

is based on the conservation of mass in fluid dynamics. Here $n, v$ represents the dust density and velocity fields, respectively. The momentum equation is given by

$$\frac{\partial v}{\partial t} + v\frac{\partial v}{\partial x} = \frac{Z_d e}{M_d}\frac{\partial \phi}{\partial x} \tag{1.5}$$

is based on the conservation of momentum in fluid dynamics. Here $\phi$ is the electrostatic potential field of the dust fluid. $Q_d = Z_d e$ and $M_d$ are the charge and mass of the dust grain, respectively. $e$ is the electron charge and $Z_d$ is a natural number indicating the number of electrons residing on a dust grain. The Poisson equation is given by

$$\frac{\partial^2 \phi}{\partial x^2} = -4\pi e(n_i - n_e - Z_d n) \tag{1.6}$$

$n_e$ and $n_i$ are the electrons, and ion density fields, respectively. The electrons and ions being inertia-less as their mass is several orders less than that of the dust particles follow the Boltzmann distribution.

$$n_{e,i} = n_{e0,i0} \exp\left(\pm\frac{e\phi}{k_B T_{e0,i0}}\right) \tag{1.7}$$

where, $n_{e0,(i0)}$ represent the equilibrium electron (ion) density, and $T_{e0,(i0)}$ represent the equilibrium electron (ion) temperature.

In an actual dusty plasma experiment, the ion streaming, neutral drag and viscous damping are a few important factors that affect the collective dust dynamics. The KdV model is developed by neglecting all these effects and is subsequently used to understand nonlinear mixing. However, we can also get a KdV model incorporating ion streaming. The KdV model is an excellent model where the dissipation effects don't play an important role. The dissipation effects, when considered by the fluid-Poisson model, leads to the KdV-B model, which is an excellent model for understanding the collective dust dynamics where dissipation plays an important role.

The current research focuses on the mixing and synchronization of longitudinal electrostatic waves in dusty plasma. Both phenomena can be explored by considering only one dimension with infinite extension in other dimensions. A one-dimensional model is expected to capture all the essence of compression and rarefaction of a longitudinal wave without losing the generality. Moreover, the KdV can also be derived from a one-dimensional fluid model.

### 1.3.2 The Korteweg-de Vries model

The KdV equation is derived from the full set of fluid Poisson equations using a reductive perturbation technique [51, 138, 140–144] for dusty plasma applications. The KdV model has been found to govern the dynamics of the dust acoustic solitons [51, 145, 146], ion-acoustic waves [140], dust acoustic waves [138, 147] and shallow water surface waves [148], magneto-sonic solitons [149], a reflection of a dust acoustic solitary wave [150] and the dust lattice wave [151, 152], pinning solitons [153] and precursor solitons [59, 154, 155]. The set of Eq. (1.4), (1.5), (1.6), and (1.7) when solving using the reductive perturbation technique, we get

$$\frac{\partial n(x,t)}{\partial t} + \alpha n(x,t)\frac{\partial n(x,t)}{\partial x} + \beta\frac{\partial^3 n(x,t)}{\partial x^3} = 0 \tag{1.8}$$

The coefficients $\alpha$ and $\beta$ represent the strengths of the nonlinear and dispersive contributions. The coefficients $\alpha$ and $\beta$ can be derived in terms of experimental plasma parameters [153, 154, 156, 157]. The KdV equation has exact analytic solutions like the soliton and cnoidal wave solutions.

### 1.3.3 The Korteweg-de Vries-Burgers model

The KdV-B model is a nonlinear partial differential equation incorporating dispersion and dissipation and describes wave propagation under the weakly nonlinear dynamical regime of fluids [158]. The KdV-B model explains the surface waves in conducting liquids [159], internal solitary waves generated by gravitational collapse [160], ion-acoustic solitary waves [161, 162] and dust acoustic shock waves in dusty plasmas [91, 92, 163, 164], dust acoustic waves in strongly coupled visco-elastic medium [147, 165], and head-on collision of dust acoustic solitary waves [92]. The KdV-B model also describes the nonlinear wave propagation in elastic tubes filled with a viscous fluid [166]. There are various damping mechanisms present in the experiment that softens the amplitude of the wave and competes with the nonlinearity of the medium. The viscous damping dissipates all modes in the system indiscriminately. The KdV-B model considers the viscous damping effect of the dusty plasma medium, which is important in many dusty plasma experiments [91, 92, 162, 167]. The viscous damping is incorporated in the fluid model through the momentum equation *i.e.,* Eq. (1.5)

$$n\left[\frac{\partial v}{\partial t} + v\frac{\partial v}{\partial x}\right] = \frac{Z_d e}{M_d}\frac{\partial \phi}{\partial x} + \frac{\eta^*}{M_d}\frac{\partial^2 n}{\partial x^2} \tag{1.9}$$

where $\eta^*$ is the viscosity of the dusty plasma fluid. The set of Eq. (1.4), (1.9), (1.6), and (1.7) when solving using the reductive perturbation technique, reduces the model to a single partial differential equation called the Korteweg-de Vries-Burgers equation given by [159, 162, 165, 168]

$$\frac{\partial n(x,t)}{\partial t} + \alpha n(x,t)\frac{\partial n(x,t)}{\partial x} + \beta\frac{\partial^3 n(x,t)}{\partial x^3} - \eta\frac{\partial^2 n(x,t)}{\partial x^2} = 0 \tag{1.10}$$

Where $\eta$ is the normalized viscosity that gives the strength of the viscous damping term.

## 1.4 The ubiquity of nonlinear mixing

Nonlinear mixing is a phenomenon generating a cascade of waves (modes) by the interaction of two nonlinear waves (modes) in any nonlinear medium [15, 23, 169, 170]. It's broad domain includes optical media [171, 172], plasmas [13, 15], fluids [28] and material science [18, 173]. A few distinct examples include the mixing of vortices in a Kerr-like nonlinear medium [24], generation of short wavelength light due to laser interaction [23], and nonlinear mixing in meta-materials [174, 175].

Different mathematical models have been developed to explain the mixing patterns in different physical domains. The wave and Rayleigh-Plesset equations that couple the acoustic pressure field with the bubble vibrations have been used for NLM in bubbly fluids [176]. The Navier-Stokes and mass-fraction equations describe the nonlinear fluid-mixing [28]. Nonlinear Schrödinger equation is used to explain optical vortex mixing [24]. There is a gap in the literature to understand the dynamics of the nonlinear mixing of waves in fluid or fluid-like systems based on a single equation which incorporates the spatio-temporal convective nonlinearity. We model nonlinear mixing based on the Korteweg-de Vries equation, which keeps the essence of the fluid nonlinearity and dispersion of the medium and is a simplified model with available analytical solutions. The KdV model has provided reasonable conclusive experimental validation to explain the weakly nonlinear dynamics of dust lattice waves in the dusty plasma. The model is a sufficiently accurate one-dimensional model, we believe that the driven KdV model can explain the features of mixing of DLWs observed in the dusty plasma experiment [15]. The fKdV model is in general applicable to any nonlinear dispersive medium where the different modes interact in presence of the convective fluid nonlinearity.
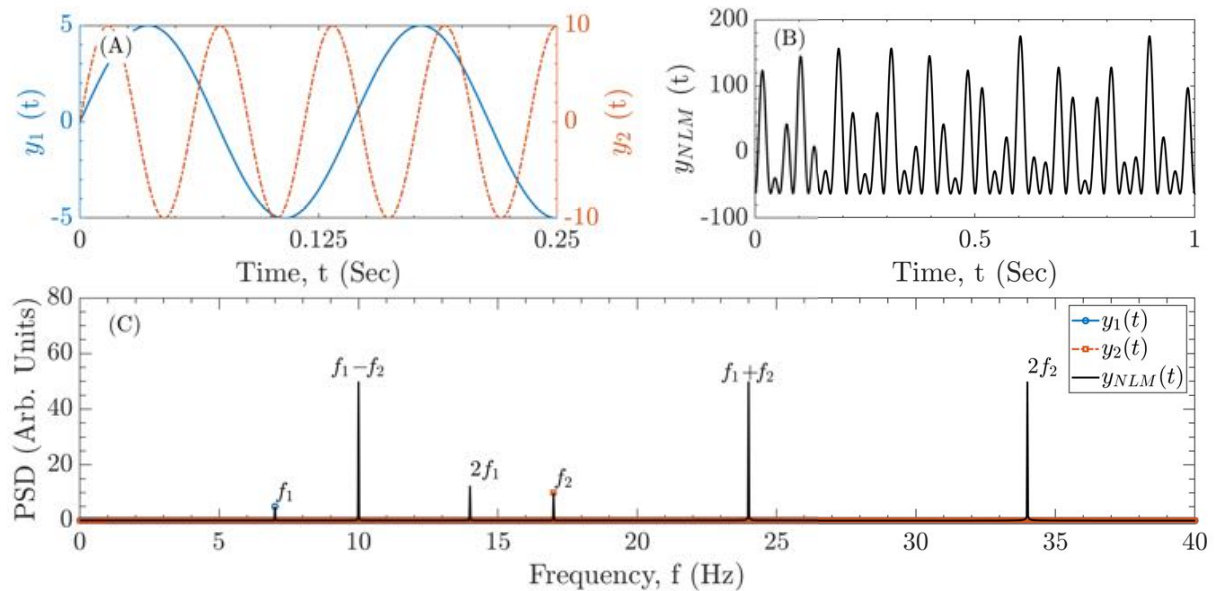


Figure 1.7: Demonstration of nonlinear mixing of two waves in a nonlinear medium. (A) Two linear waves of the form $y_1(t) = A_1 \sin(2\pi f_1 t)$ with $A_1 = 5$, $f_1 = 7$ Hz and $y_2(t) = A_2 \sin(2\pi f_2 t)$ $A_2 = 10$, $f_2 = 17$ Hz interact via a nonlinear medium having a nonlinearity of the combination of linear and quadratic terms which leads to a resultant nonlinear profile of form (B) $y_{NLM}(t) = y_1 + y_2 + (y_1 + y_2)^2$. (C) The PSD of time-series of $y_1$, $y_2$, and $y_{NLM}$ shows the generation of addition, subtraction and harmonic frequencies due to mixing.

### 1.4.1   The forced Korteweg-de Vries model of nonlinear mixing in dusty plasma

The Eq. (1.8), when driven externally with a forcing $F_s$, is called a forced Korteweg-de Vries-Burgers equation. The generalized fKdV-B equation is given by

$$\frac{\partial n(x,t)}{\partial t} + \ \alpha n(x,t)\frac{\partial n(x,t)}{\partial x} + \ \beta\frac{\partial^3 n(x,t)}{\partial x^3} = \ F_s(x,t) \tag{1.11}$$

The fKdV model that Sen *et al.* [140] proposed for driven nonlinear acoustic waves and subsequently developed to study nonlinear precursor solitons in dusty plasma experiments [154, 155], pinned solitons created by a supersonically moving object in a fluid [153] and electromagnetic pinned solitons for space debris detection in Low Earth Orbit (LEO) region [177]. The fKdV equation has also been used to model the electrostatic excitation of ion-acoustic precursor solitons by a charged debris object [140]. The fKdV model also describes the excitation of long nonlinear water waves by a moving pressure distribution [178] and is a simple mathematical model capable of describing the physics of a shallow layer of fluid driven by external forcing [179].

## 1.5   The kinetic model of nonlinear mixing in dusty plasma

A kinetic approach to model dusty plasma assumes it is a collection of charged dust particles. Such a model is primitive and realistic as the pairwise interaction potential is known as Coulomb. As electrons and ions dynamics have fast time scales compared to the dust particles, both species mostly act as shielding backgrounds to dust particles. This leads to dust particles interacting with each other with effective shielded-Coulomb potential. The system becomes a one-component plasma with Yukawa integration between the particles. Hence, the dusty plasma is treated as an ensemble of charged particles interacting via Yukawa (screened-Coulomb) potential known as Yukawa one-component plasma (YOCP). The effect of the plasma environment is incorporated in the shielding of the dust species. Due to the high negative charge, the dusty plasma often becomes a strongly coupled plasma (SCP). The thermodynamic equilibrium of Yukawa-type SCPs is governed by the Coulomb coupling parameter $\Gamma$ and the screening/shielding parameter $\kappa_D$ [180, 181]. Due to heavy dust mass, the motion of each particle in the ensemble is governed by the classical Newton's equation of motion given by

$$M_d\ddot{\mathbf{r}} = -\nabla\phi^Y(r) \tag{1.12}$$

The particle trajectories $\mathbf{r}(t)$ are generated for all particles by integrating Eq. (1.12). The Yukawa interaction neglects the boundary effects and takes into consideration only the bulk properties of the dusty plasma medium.

We performed 2D Langevin MD simulations (as explained in chapter 4) to study the mixing of DLWs in such strongly coupled dusty plasma. We have excited two dust lattice waves by mimicking the laser

force used to excite the same in the experiment [15]. The two DLWs interact in the YOCP, giving rise to a rich spectrum of mixing profiles that agrees with our fKdV model [45].

## 1.6 The ubiquity of synchronization

The tendency to attain rhythmic synchronization (self-organization in time) has been observed in various natural and artificial systems. Two identical clocks hung on a wooden beam and eventually followed each other. Christiaan Huygens observed this for the first time in 1663 [182, 183]. Similarly, a swarm of fireflies develop cooperation in their otherwise random expected flashing [184]. All these rhythmic harmonies originate through a weak nonlinear interaction among participants, and this collective mechanism is called "*synchronization*" [4, 185].

Synchronization is often studied in two different scenarios, namely *partial* and *global* synchronization. For understanding purposes, below, we explain them with the help of nonlinear oscillators. However, many continuum nonlinear media supporting propagating waves also show these synchronisation phenomena.

1. When a large ensemble of oscillators with random frequencies attain a synchronized phase through a non-equilibrium phase transition in which they develop clusters that oscillate at constant frequencies is called *partial* synchronization. The threshold nonlinear coupling for the phase transition depends on the frequency disorder. In other words, whenever a system of nonlinear oscillators self-organizes into different frequency clusters without any external driving source is known as *partial* synchronization. That is why it is also called as *frequency clustering* [120, 186, 187]

2. When an external driver synchronizes a natural nonlinear oscillator or an ensemble of nonlinear oscillators, this type of synchronization is called the *global* synchronization [36, 37, 41]. The oscillators (a natural system and an external driver) only attain the phase-locking condition if the coupling strength is above a threshold value. This threshold nonlinear coupling increases with the frequency detuning of oscillators. The detuning means how far from the system's natural frequency is driven by an external driver. The "Arnold tongue diagram" refers to the set of coupling (in our case, the amplitude of the driver) and frequency detuning values for which phase or frequency locking occurs.

### 1.6.1 The forced Van der Pol model of synchronization

The forced Van der Pol (fVdP) equation is a widely used theoretical model used to explain the global synchronization of nonlinear point oscillators and is given by

$$\frac{d^2x}{dt^2} - (c_1 - c_2x^2)\frac{dx}{dt} + \omega_0^2 x = A_{dr}\cos(2\pi f_{dr}t). \tag{1.13}$$

Here $x$ is the displacement of a harmonic oscillator with a natural frequency $\omega_0$. The model includes nonlinear damping $c_2x^2dx/dt$, a source of energy for self-excitation $c_1dx/dt$, and a periodic driving
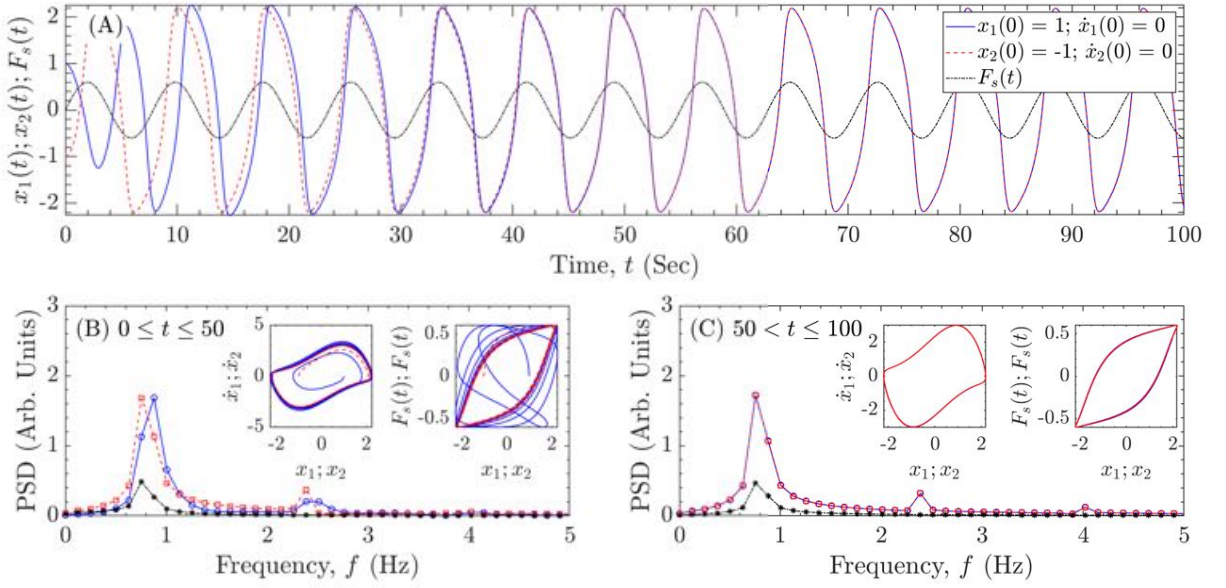
Figure 1.8: Synchronization in forced Van der Pol oscillator (*i.e.*, Eq. (5.1)) with $c_1 = c_2 = 1$, $\omega_0 = 1$, $\omega_{dr} = 2\pi f_{dr} = 0.8$ and $A_{dr} = 0.6$ for two initial conditions $x_1 = 1; \dot{x}_1 = 0$ and $x_2 = -1; \dot{x}_2 = 0$. (A) The fVdP profile (blue solid line) for $x_1 = 1; \dot{x}_1 = 0$, (red dash-dash line) for $x_2 = -1; \dot{x}_2 = 0$ and (black dash-dotted) for the forcing $F_s(t) = A_{dr} \cos(\omega_{dr}t)$. (B) The unsynchronized state of the fVdP oscillator and (C) the synchronized state of the fVdP oscillator by attaining a limit cycle.

source of amplitude $A_{dr}$ at a frequency $f_{dr}$. The fVdP oscillator exhibits "harmonic" ($f_{dr}/f_0 \approx 1$), "super-harmonic" ($f_{dr}/f_0 > 1$), and "sub-harmonic" ($f_{dr}/f_0 < 1$) synchronization states. Harmonic synchronization means the system is driven in the vicinity of the fundamental mode and synchronizes at that frequency. The super-harmonic synchronization means the system is driven in the vicinity of the first harmonic (1:2) or second harmonic (1:3) and synchronizes at half or one-third of the driver. The sub-harmonic synchronization means the system is driven in the vicinity of one-half (2:1) or one-third (3:1) of the fundamental frequency and is synchronised at double or thrice the driver frequency. The ensemble of coupled VdP oscillators is a useful model to explain the cluster or partial synchronization [188, 189].

Both the partial and global synchronization of nonlinear oscillators is often modelled by the fVdP model. Typically in plasmas, these scenarios of frequency clustering [120, 186, 187] and the global synchronization [36, 41, 42, 190] have been studied experimentally. The investigation of the mutual synchronization between two plasma devices [39, 40, 191] has also been explored in plasmas which have been explained through a coupled-VdP oscillators [39]. Specifically, the global synchronization of dust acoustic waves to an external driver has been widely studied in an anodic [41], radio-frequency (RF) and direct-current (DC) plasmas [36–38]. Pilch *et al.* [41] reported the entrainment of DAWs through a driving modulation to the anode. Ruhunusiri *et al.* [36] reported observation of harmonic, super-harmonic, and sub-harmonic synchrony of self-excited cnoidal DAWs. Williams *et al.* [38] compared DAW synchronization in RF and DC-generated plasmas. Deka *et al.* [37] observed the synchronization of self-excited DDW and bifurcation of DDW by modulating ion streaming with an external sinusoidal driver.

The fVdP oscillator model has been used as a qualitative reference for characterizing synchronization phenomena in plasmas and other media that support the propagation of waves [36, 37, 39, 192]. It also explained frequency clustering of propagating DDWs [120] under microgravity conditions [101] through a chain of coupled Van der Pol oscillators [193]. However, it is worth mentioning that as a point oscillator model, its dynamics are restricted to nonlinear oscillations, and it cannot correctly represent nonlinear waves. The VdP oscillator equation is mathematically an ordinary differential equation different from a wave or partial differential equation. The nonlinearity in the VdP model is time-dependent only, which is not a good representative of nonlinearity in fluid or fluid-like systems with spatio-temporal convective nonlinearity.

Moreover, one must invoke a coupled van der Pol equation system for a propagating wave. This complex procedure would require making arbitrary assumptions about the oscillators' coupling and determining each dust particle's initial frequencies and phases. The inadequacy of the VdP model to describe nonlinear waves is meant for a single VdP equation and not a system of coupled VdPs. The fKdV-B model, on the other hand, accomplishes that through a single equation. Hence, we believe it is appropriate to use the fKdV-B model for investigating the global synchronization of a nonlinear dispersive propagating wave, in a medium with spatio-temporal convective nonlinearity, to an external driver.

### 1.6.2 The forced Korteweg-de Vries-Burgers model of synchronization in dusty plasma

The Eq. (1.10), when driven externally with a forcing $F_s$, is called a forced Korteweg-de Vries-Burgers equation. The generalized fKdV-B equation is given by

$$\frac{\partial n(x,t)}{\partial t} + \alpha n(x,t)\frac{\partial n(x,t)}{\partial x} + \beta\frac{\partial^3 n(x,t)}{\partial x^3} - \eta\frac{\partial^2 n(x,t)}{\partial x^2} = F_s(x,t) \tag{1.14}$$

The fKdV-B model was used to study temporal or spatial chaos using a randomly time-varying [194] or randomly space-varying [195] driving term. The fKdV-B model has shown that with a spatial driver, the system undergoes a period-doubling and shows weak chaos and developed chaos [196]; in the first type, only a small chaotic deviation from the periodic solution occurs, and in the second type, a random sequence of uncorrelated shocks is formed. Also, the model explains nonlinear wave propagation in an elastic tube filled with a Newtonian fluid with variable viscosity [197].

## 1.7 Numerical approach

We have solved the KdV equation numerically using the pseudo-spectral method [198] and used the periodic boundary conditions. We perform the Fourier transform $(f(x,t) \to \tilde{f}(k,t))$ of the partial differential equation in space, which converts the KdV to an ordinary differential equation in time. The RK-4 method has been used for the time integration with an accuracy of $O(h^4)$ with Richardson extrapolation.

1. *Time-series collection method:* The time-series collection of fluid field (density here) is the only
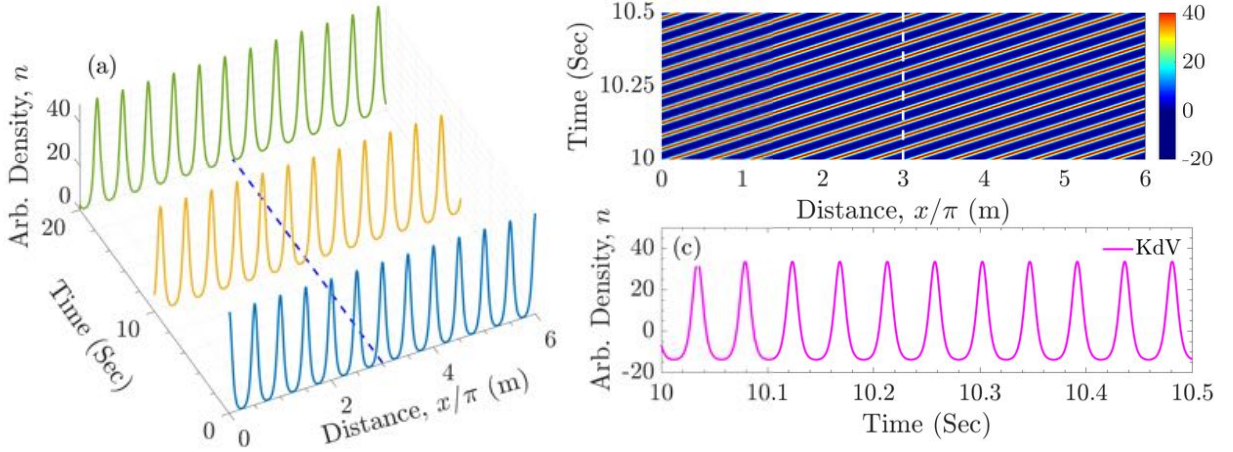
Figure 1.9: Time-series collection for KdV evolution (Eq. 1.8) with initial perturbation of the cnoidal-square form. Panel (a) shows the evolution of the density profile at times 0, 10 and 20 $\omega_{pd}^{-1}$ respectively. Panel (b) shows the spatio-temporal evolution of the density perturbation. Panel (c) is the collected time-series at a specific spatial location ($x = 3\pi$) as marked by the blue and white dashed lines in panels (a) and (b), respectively. The coefficients $\alpha = 2.3$, $\beta = 0.5$ and simulation system size $L_x = 6\pi$.

measurement during the evolution for diagnostics purposes. Figure 1.9(a) show the evolution of cnoidal-square initial perturbation of the form $n(x,0) = A_0 \, cn^2[2K(\kappa_0)\{x/\lambda_0\}; \, \kappa_0]$ through KdV (*i.e.,* Eq. (1.8)) with $A_0 = 40.32$, $\kappa_0 = 0.9$ and $k_0 = 4$ with system size $L_x = 6\pi$. Figure 1.9(b) shows the complete spatio-temporal evolution, and Fig. 1.9(c) provides the collected time-series at an arbitrary point in space (marked by the blue or white dashed vertical line in subplots (a) or (b), respectively).

Although we have demonstrated the collection of time-series for the KdV equation (*i.e.,* Eq. (1.8)), the same procedure is applied for the fKdV-B model to collect its time-series for further analysis. It should be noted that the time-series of KdV, KdV-B, fKdV and fKdV-B density profiles and forcing profile have been time-averaged to zero *i.e.,* $n(x,t) = n(x,t) - \langle n(x,t) \rangle$ and $F_s(x,t) = F_s(x,t) - \langle F_s(x,t) \rangle$, respectively. This helps to remove the dc component in the time-series when we take the Fourier transform. Once the time-series is collected at any specific location, its power spectrum determines dominant modes. We carry out the bispectral analysis for the same time-series to further understand the physical origin of observed modes in the spectrum. The detailed analysis is provided in chapter 3.

2. *Bench-marking and establishing the numerical accuracy of the code:* We have also compared the numerical solution of KdV and fKdV with its analytic solution [169] to establish our simulation approach's numerical stability and accuracy as shown in Fig. 1.10. Moreover, the code was bench-marked by reproducing earlier results for the KdV and fKdV equations [45, 140]. To numerically evolve the KdV equation, we have developed our own C++ code for this purpose. The post-processing analysis of the numerical data has been done using MATLAB software to identify the various features of the evolved system.
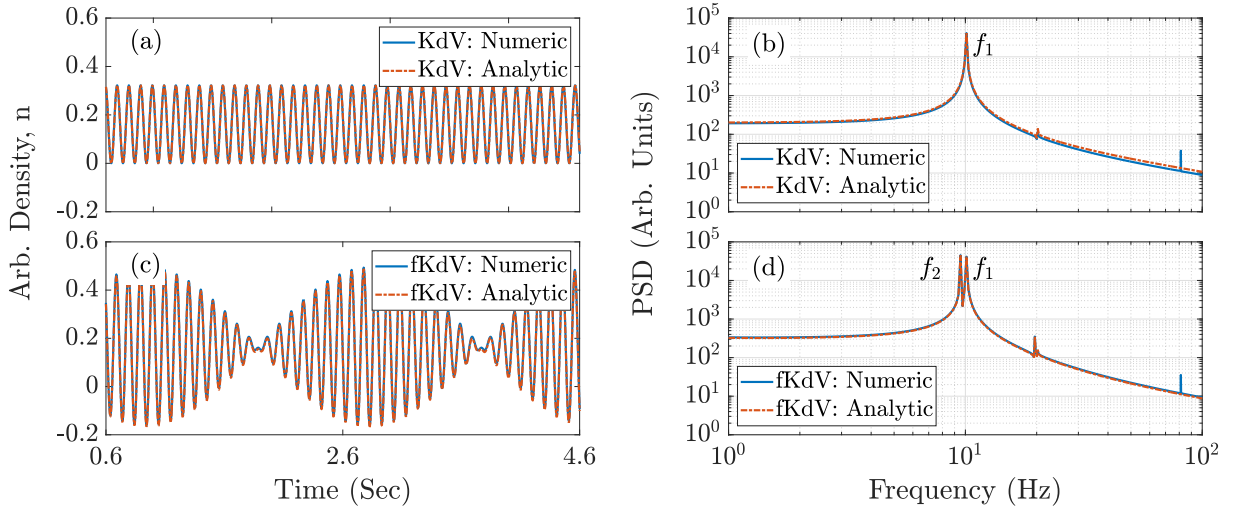
Figure 1.10: Comparison of the time-series obtained numerically (solid line) and the analytically (dash-dotted line) of the KdV (*i.e.,* Eq. (1.8)) and fKdV (*i.e.,* Eq. (1.11)) given in Ref [169]. (a) KdV equation with initial numerical perturbation $n(x, 0) = 0.1611 + 0.1611 \sin(4x + \pi/2)$ and analytic solution with parameters $\mu = 0.3221$ and $\kappa = 0.01$. (b) fKdV equation with initial numerical perturbation is $n(x, 0) = 0.1611 \sin(4x + \pi/2)$ and forcing $F_s = 10 \sin(60t)$ for both the numerical and analytic solution. The coefficients $\alpha = \beta = 1$ and simulation system size $L_x = 2\pi$.

## 1.8 Motivation of the thesis

The phenomena of nonlinear mixing and synchronization have been observed in table-top dusty plasma experiments by multiple leading researchers in the last decade. However, the majority of these works provided ad-hoc or qualitative theoretical support. Though these qualitative theoretical models reflected limited agreement with experiments, they lacked the appropriate nature of nonlinearity of the medium, an important aspect of both mentioned physical phenomena. The current thesis work is motivated to frame such a theoretical model which can incorporate plasma dispersion and keep the essence of fluid and fluid-like convective nonlinearity. Other than proposing a theoretical model that includes spatio-temporal nonlinearity, another vision is to bring forward a simplified mathematical model of dusty plasma. One benefit to looking for a simplified model is the possibility of exploring analytic solutions that are otherwise not possible for a full set of fluid-Maxwell set of equations representing the dynamics of dust fluid in general. As it is a well-established fact that the KdV equation represents the acoustic wave dynamics very well in the weak nonlinearity domain, we chose to build models keeping KdV equation as the foundation. Further, depending on the physical requirements, we incorporated the medium's driving mechanism and damping. Keeping all facts in view, we present fKdV and fKdV-B models to quantitatively explain nonlinear mixing and synchronization in a dusty plasma medium.

## 1.9 Summary of the thesis

This thesis work develops a theoretical framework based on the fKdV [169] and fKdV-B [46] equations for the nonlinear mixing and synchronization of waves, respectively. The nonlinear mixing patterns from the fKdV model show agreement with nonlinear mixing of compressional longitudinal dust lattice waves in dusty plasma experiment [15] and the synchronization of dust acoustic waves from the fKdV-B model show excellent qualitative features as were observed in dusty plasma experiment [36]. Even though

the findings from these models were validated with the previously done experiments in a dusty plasma medium, however, both models have the capability they can be easily implemented in other fluid and fluid-like mediums governed by the spatio-temporal convective nonlinearity.

## 1.10   Organization of the thesis

This dissertation comprises six chapters, including the current chapter, which serves as an introduction. The organization and content of these chapters are outlined as follows:

**Chapter 2:** The chapter discusses the results based on the nonlinear mixing of DLWs based on the fKdV model. In this chapter, we have derived the analytic solution of the fKdV model with time-dependent sinusoidal forcing. The model can capture features of mixing profiles of the dusty plasma experiment based on the analytic solution of the fKdV model. The power spectral analysis gives quick evidence of generating the various modes due to the nonlinear interaction between the sinusoidal driver and the natural KdV mode.

**Chapter 3:** The chapter can be outlined based on three things. Firstly, the NLM based on the different sinusoidal and non-sinusoidal time-dependent and travelling wave forcing is thoroughly studied. Second, the bispectral analysis technique used on the time-series provides evidence of the three-wave mixing mechanism. Finally, we have studied the effect of driver frequency on the mixing profiles.

**Chapter 4:** This chapter mainly focuses on the kinetic simulations of dusty plasma treated as an ensemble of charged particles interacting via pair-wise Yukawa potential. The mixing of DLWs is studied using the Langevin molecular dynamics simulations. The results based on the MD simulations show a good agreement with the fKdV model. Power spectral and bispectral analyses capture the presence of the excited modes and their physical origin, respectively.

**Chapter 5:** This chapter describes the synchronization of DAWs based on the fKdV-B model. We have utilized the numerical solution of the fKdV-B model to explain the synchronization of DAWs. The results from this chapter are in excellent qualitative agreement with the dusty plasma experiment. The characterization techniques used to distinguish between the synchronized and the unsynchronized stated are the power spectral analysis, phase-space plots and Lissajous figures. The effect of amplitude and frequency of the external forcing is captured in the famous Arnold tongue diagram, which identifies the different synchronization domains.

**Chapter 6:** This chapter provides a comprehensive conclusion of the theoretical findings obtained throughout the dissertation. The study illustrates that the fKdV model successfully explains the nonlinear mixing of DLWs in dusty plasma experiments. In contrast, the fKdV-B model could successfully capture the synchronization of DAWs in dusty plasma experiments. Moreover, the possible future scope of our theoretical models and their applicability to other fluid media is also outlined in this chapter.

# Chapter 2

# A forced Korteweg-de Vries model for nonlinear mixing of waves in a dusty plasma

This chapter provides a detailed analysis of the nonlinear mixing of dust lattice waves. The analysis includes the forced-KdV model formulation, its applicability in explaining dust lattice wave mixing, and comparison with experimental findings in the literature. Presented results include mixing characteristics for a dust lattice wave's interaction with time-dependent sinusoidal external driving. An analytic solution exists for such a system, and its power spectrum shows the existence of various modes. While the results agree with experiments, a small deviation still exists, and the same shortcoming of the present model has been improvised in the following chapter.

---

## 2.1 Introduction

Nonlinear mixing (NLM) is a phenomenon found in many physical systems that can sustain waves of large amplitudes [156, 199–201]. In a dusty plasma, compressional waves can easily attain large amplitudes, even if the electric potential variation is only a few millivolts, and this is due to the large electric charge of thousands of elementary charges [112, 156] residing on a dust particle.

Two kinds of compressional waves in dusty plasmas are the dust-acoustic wave (DAW) and the longitudinal dust lattice wave (DLW) [104, 136, 202]. The dust-acoustic wave propagates in a three-dimensional cloud of charged dust particles which are immersed in a mixture of electrons and ions; all three of these charged species participate in compression and rarefaction. If there is an ambient steady electric field, it will drive an ion current that can easily self-excite the DAW through an instability [102], which commonly occurs in laboratory gas-discharge plasmas [108, 203]. On the other hand, the longitudinal DLW propagates in a different situation; while the electrons and ions fill a three-dimensional volume, the dust particles do not; they are instead confined to a planar layer which is thin and often is just a monolayer. Because of the paucity of dust particles, the electrons and ions are not significantly affected by the dust particles, and for the most part, they just contribute to the Debye screening of the inter-particle repulsion among the dust particles [202]. Unlike the DAW, the longitudinal dust lattice wave is not necessarily excited by an ambient DC electric field, so that in the laboratory, it is common to excite it by an external forcing [67, 134].

In this work, we consider the longitudinal dust lattice wave, with two sinusoidal external excitations at large amplitude, to cause nonlinear mixing. By perturbing a two-dimensional crystalline layer of dust particles using two laser beams of different frequencies, three-wave mixing was experimentally demonstrated by Nosenko *et al.* [15]. In this work, we theoretically demonstrate the nonlinear mixing phenomenon in a dusty plasma system using an analytic solution of a sinusoidally forced Korteweg-de Vries model equation. The model solution can also be usefully employed to predict the existence of nonlinear mixing in a variant of the two-dimensional experimental dusty plasma experiment reported in Ref. [15].

In their experiment, the authors of Ref. [15] used a horizontal monolayer of dust, which consisted of precision polymer microspheres that were levitated above a lower electrode of a radio-frequency glow-discharge plasma. Using video microscopy, they verified that the equilibrium state of this cloud of particles was a triangular lattice with a six-fold symmetry. The charge on a microsphere was $-9400\,e$ (where $e$ is the charge of an electron), the crystalline lattice constant was 675 microns, and the mass of the 8 micron microspheres was sufficiently high that the compressional sound speed in the lattice was only 22 mm/s.

The experimenters of Ref. [15] launched two longitudinal lattice waves, with sinusoidal waveforms at different frequencies $f_1$ and $f_2$. Each of these two waves were propagating waves, and they were each excited externally by the radiation-pressure force, using laser manipulation with a steady-state laser that was amplitude modulated at the desired low frequency. The dust cloud was a horizontal monolayer. The

excitation regions for the two waves were physically separate, which is a point that is important for the present work. The spatial localization of the excitation regions was achieved by making the laser beams incident on the dust layer at an angle of 10 degrees. The experimenters then observed waves at various difference and sum frequencies, including $f_1 + f_2, f_2 - f_1, 2f_2 - f_1$, and so on. They confirmed using bi-spectral analysis that these were the products of nonlinear mixing. In this way, they provided an experimental observation of three-wave mixing in a dusty plasma.

The physical system in that experiment can be modelled theoretically by several descriptions, including a point-like particle description and a continuum description of the dust layer. The latter approach was used by Avinash *et al.* [152], who modelled the long-wavelength compressional waves in the monolayer triangular lattice as obeying an evolution equation described by a variant of the Korteweg-de Vries (KdV) equation.

In this work, we predict theoretically that nonlinear mixing can occur also in a different excitation configuration, where only one of the two excitation frequencies $f_1$ has a propagating wave that is excited locally, while the other frequency $f_2$ is a non-localized oscillation. In both cases, the external forcing can be provided by any physical force, including the radiation pressure force that was used in Ref. [15]. Unlike Ref. [15], only the frequency $f_1$ has a propagating wave that is excited in a spatially localized region, and as a crucial difference, frequency $f_2$ has a spatially uniform force, varying sinusoidally in time but not in space. This construction should be feasible simply by performing an experiment with a two-dimensional monolayer of dust as in the experiment of Ref. [15] but with one of the two laser beams incident on the particle cloud at zero degrees instead of ten degrees. A schematic sketch of the excitation configuration is shown in Fig. 3.1.
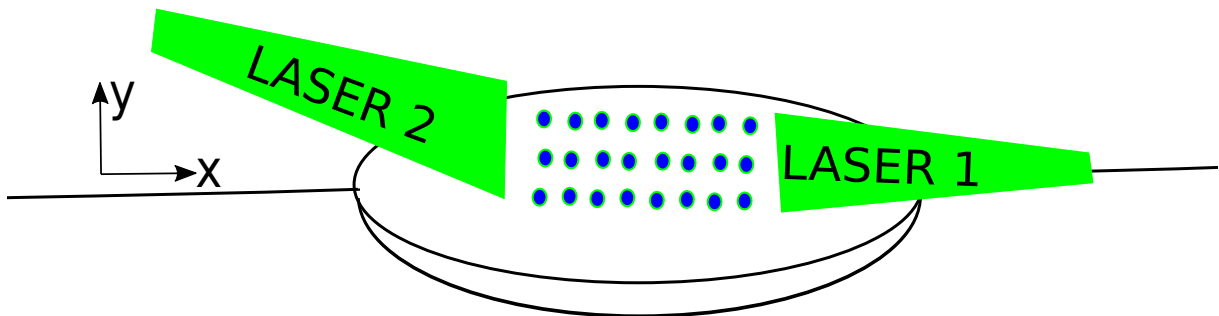


Figure 2.1: A cartoon representation of a proposed experimental configuration with one of the laser beams incident on the dust at zero degrees to provide a non-localized driving oscillation. Thousands of charged dust particles, shown schematically here as a few dots, are levitated in a single horizontal layer in an electric sheath above a powered lower electrode, shown schematically as a disk at the bottom of this diagram.

Although we are mainly concerned here with the nonlinear mixing of the longitudinal lattice wave, we can mention another kind of nonlinear effect which has been observed experimentally, and that is synchronization. In synchronization, there is an inherent oscillation at one frequency and an external forcing at a second frequency. The second frequency must be close to that of the inherent oscillation, or one of its harmonics. Although synchronization has long been understood for point oscillators, it

can also occur in the more complicated case of propagating waves, and indeed it is known to occur in three-dimensional dust clouds that sustain the dust acoustic wave. The DAW is self-excited at an inherent frequency due to ion flow, and an external sinusoidal forcing can be applied, for example, by a voltage applied to the entire cloud by an electrode so that the entire cloud experiences a global modulation [36, 37]. The result of synchronization is that the inherent oscillation is shifted in its frequency, for example, to match the frequency of the external forcing. This is different from the case of mixing, where the two original waves maintain their frequencies and a third wave appears at yet another frequency. Another distinction in comparing synchronization and mixing is that the original two oscillations can have frequencies that differ greatly in the case of mixing, whereas, for synchronization, it is necessary for there to be a small difference in the two frequencies or their harmonics.

## 2.2 The forced Korteweg-de Vries model

Our theoretical approach relies on two basic premises - (i) nonlinear compressional waves in a dusty plasma system can be modelled by a KdV equation, and (ii) the forced KdV equation can model their dynamics in the presence of an external driving force. For a three-dimensional dust cloud, the KdV equation as a model description of nonlinear DAWs is well established. It was first derived by Rao *et al.* [138] using a fluid representation of the dusty plasma and has subsequently been widely used in many theoretical and experimental studies [98, 156, 204, 205]. An fKdV model, within the fluid prescription, was first derived by Sen *et al.* [140] for describing driven nonlinear ion acoustic waves. The generic form of this model equation was subsequently shown to apply for driven DAWs as well and was successfully used to interpret the excitation of precursor dust acoustic solitons in a laboratory dusty plasma device [59, 154].

For the dust lattice wave, the KdV model has also been shown by Farokhi *et al.* [151] to theoretically describe the nonlinear evolution of waves in a two-dimensional dust lattice system. Thus one can expect the fKdV model to also successfully describes the dynamics of driven DLWs in the case of a two-dimensional lattice system subject to external forcing. Hence as a paradigmatic model for driven compressional nonlinear oscillations in a dusty plasma system, we adopt the generic fKdV equation given as,

$$\frac{\partial n(x,t)}{\partial t} + \alpha \, n(x,t)\frac{\partial n(x,t)}{\partial x} + \beta\frac{\partial^3 n(x,t)}{\partial x^3} = F_s(x,t) \tag{2.1}$$

where $n$ is a perturbed physical quantity (representing the perturbed dust density for example) and $F_s(x,t)$ is the driving source term. The coefficients $\alpha$ and $\beta$ represent the strengths of the nonlinear and dispersive contributions, respectively. Dissipative effects, such as may occur due to frictional damping from neutral gas particles, are not included in this model so that it cannot describe phenomena such as synchronization that need dissipation. For $F_s(x,t) = 0$, Eq. (2.1) represents the standard KdV equation that has been extensively studied in the past to describe nonlinear wave propagation in neutral fluids [206, 207], plasmas [208, 209], dusty plasmas [98, 138, 145, 152, 210] and other nonlinear dispersive media [211, 212].

The KdV equation has a variety of solutions including solitons and cnoidal wave solutions. The latter are relevant for our present work and are given by [213, 214]

$$n(x,t) = \mu \; cn^2 \left[ \frac{\sqrt{\mu\alpha}}{2\sqrt{\beta\kappa(\kappa+2)}} \left( x - \frac{\kappa + \kappa^2 - 1}{\kappa(\kappa+2)} \alpha\mu t \right); \; \kappa \right] \tag{2.2}$$

where $cn$ is a Jacobi elliptic function. The parameter $\mu$ represents the amplitude, which can be chosen to be any value (for example, in an experiment by adjusting the amplitude of an external forcing). The elliptic parameter $\kappa$ indicates the response of the medium to that amplitude. The value of the parameter $\kappa$ determines the shape of the cnoidal function so that it serves as a quantitative measure of nonlinearity. For $\kappa = 0$, which is the linear case, the cnoidal solution becomes a cosine function, while for the highly nonlinear case of values close to unity, the waveform has sharp peaks and flattened bottoms. The cnoidal solution, Eq. (2.2), was recently shown to provide an excellent fit to experimental observations of spontaneously generated nonlinear DAWs in a three-dimensional dusty plasma cloud sustained in an RF discharge plasma [156].
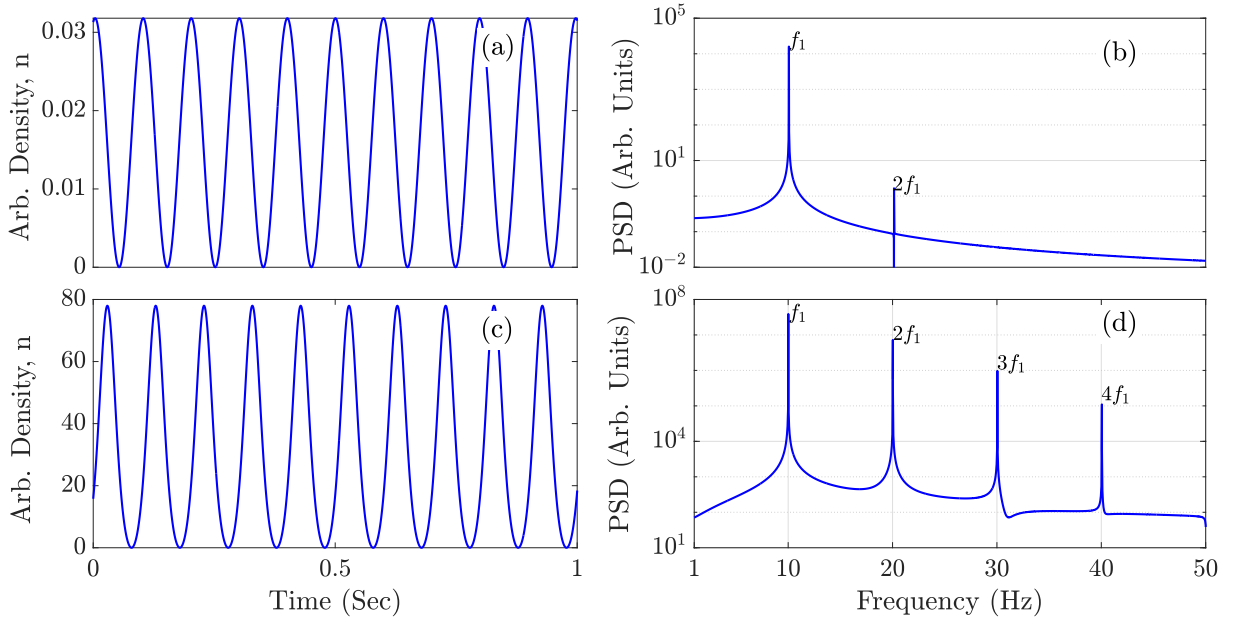


Figure 2.2: Time series and the corresponding power spectra for an arbitrary spontaneous density perturbation, $n$, as given by Eq. (2.2). (a) Sinusoidal-like wave with $\kappa = 0.001$, $\mu = 0.0318$ such that $f_1 = 10$ Hz. (b) Power spectrum of (a). (c) Nonlinear wave form with $\kappa = 0.8$, $\mu = 78$ and $f_1 = 10$ Hz. (d) Power spectrum of (c).

The spatial wave length $\lambda$ and frequency $f_1$ of the periodic wave, Eq. (2.2), are given by

$$\lambda = 4K(\kappa)\sqrt{\frac{\beta(2\kappa + \kappa^2)}{\alpha\mu}} \qquad \text{and} \qquad f_1 = \frac{\beta}{4K(\kappa)}(\kappa^2 + \kappa - 1)\left(\frac{\alpha\mu}{\beta(2\kappa + \kappa^2)}\right)^{3/2} \tag{2.3}$$

Here, $K(\kappa)$ is the complete elliptical integral of the first kind. Expressions for the wavelength $\lambda$ and frequency $f_1$ are obtained by comparing Eq. (2.2) with the following form of the solution by Dingemans [215] and Liu *et al.* [156]

$$n(x,t) = \mu \; cn^2 \left[ 2K(\kappa)\left(\frac{x}{\lambda} - f_1 t\right); \; \kappa \right]. \tag{2.4}$$

To illustrate the nature of the solution, Eq. (2.2), and its spectral properties we will choose $\alpha = \beta = 1$ and plot the solution for several values of $\kappa$ and $\mu$. In Fig. 2.2(a) we plot the time series obtained from Eq. (2.2) at a fixed value of $x$ for $\mu = 0.0318$ and $\kappa = 0.001$ (such that $f_1 = 10$ Hz). The corresponding frequency spectrum is shown in Fig. 2.2(b). For this low value of $\kappa$, the waveform is approximately sinusoidal and shows a single dominant frequency $f_1 = 10$ Hz in the spectrum. A small peak at $2f_1$ due to the nonzero nonlinearity ($\kappa \neq 0$) is also observed. For a higher value of $\kappa = 0.8$ and $\mu = 78$ (such that $f_1$ is still 10 Hz) the waveform is more nonlinear in character, as shown in Fig. 2.2(c), and the spectrum Fig. 2.2(d) shows the appearance of higher harmonics at $2f_1$, $3f_1$ etc..

### 2.2.1 The exact nonlinear solution of the fKdV equation

We next examine the solution of the fKdV model equation, Eq. (2.1), with a specific form of the driving term. For a sinusoidally time-varying driver, $F_s(x,t) = A_s \sin(2\pi f_2 t)$, Eq. (2.1) has an exact analytic solution (derived using Hirota's method as in Salas *et al.* [216]) given by

$$n(x,t) = -\frac{A_s \cos(2\pi f_2 t)}{2\pi f_2} + \mu\, cn^2\left[\frac{\sqrt{\mu\alpha}}{2\sqrt{\beta\kappa(\kappa+2)}}\left(x - \frac{\kappa + \kappa^2 - 1}{\kappa(\kappa+2)}\alpha\mu t + \frac{A_s\alpha}{(2\pi f_2)^2}\sin(2\pi f_2 t)\right); \kappa\right] \quad (2.5)$$

## 2.3 Nonlinear mixing in the fKdV model
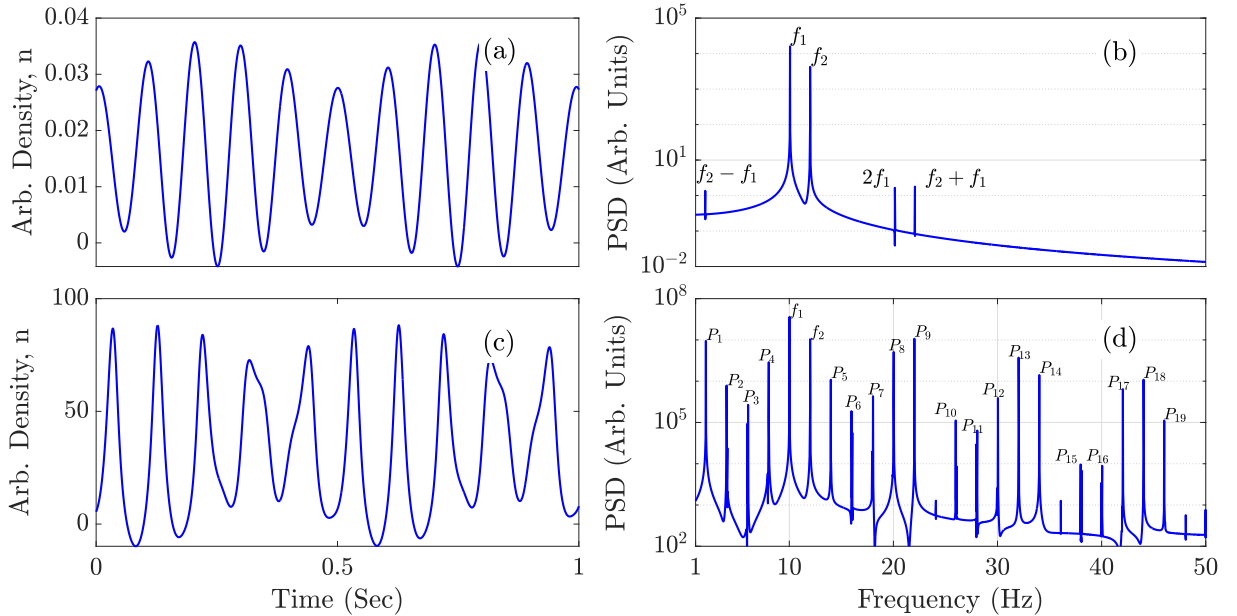


Figure 2.3: Time series and the corresponding power spectra for a density perturbation, $n$, driven at $f_2 = 12$ Hz from Eq. (2.5). (a) Time series with weak nonlinearity ($\kappa = 0.001$, $\mu = 0.0318$, $f_1 = 10$ Hz, $A_s = 0.318$) and (b) the corresponding power spectra showing $f_1, f_2$ and their sum and difference frequencies. (c) Time series with large nonlinearity ($\kappa = 0.8$, $\mu = 78$, $f_1 = 10$ Hz, $A_s = 780$) and (d) its corresponding power spectra showing $f_1, f_2$, their sum and difference frequencies and their harmonics.

To explore the phenomenon of wave mixing in various nonlinear regimes, we will use this exact solution for different values of the parameters, $\kappa$ and $\mu$. Now that we are driving not only at frequency $f_1$, but also at frequency $f_2$, we see a modulation in the time series of Fig. 2.3(a) and 2.3(c), obtained from Eq. (2.5). The corresponding spectra are shown in Fig. 2.3(b) and 2.3(d), respectively. The conditions are for a

Table 2.1: Dominant frequencies observed in the fKdV model Eq. (2.5) as shown in Fig. 2.3(d).

| Nomenclature | Frequency (Hz) | Nomenclature | Frequency (Hz) |
|---|---|---|---|
| $f_1$ | 10 | $P_{10}$ | $3f_2 - f_1$ |
| $f_2$ | 12 | $P_{11}$ | $4f_2 - 2f_1$ |
| $P_1$ | $f_2 - f_1$ | $P_{12}$ | $3f_1$ |
| $P_2$ | $2(f_2 - f_1)$ | $P_{13}$ | $2f_1 + f_2$ |
| $P_3$ | $3(f_2 - f_1)$ | $P_{14}$ | $2f_2 + f_1$ |
| $P_4$ | $4(f_2 - f_1)$ | $P_{15}$ | $4f_2 - f_1$ |
| $P_5$ | $2f_2 - f_1$ | $P_{16}$ | $4f_1$ |
| $P_6$ | $3f_2 - 2f_1$ | $P_{17}$ | $3f_1 + f_2$ |
| $P_7$ | $4f_2 - 3f_1$ | $P_{18}$ | $2(f_1 + f_2)$ |
| $P_8$ | $2f_1$ | $P_{19}$ | $f_1 + 3f_2$ |
| $P_9$ | $f_2 + f_1$ | | |

weakly nonlinear amplitude in Fig. 2.3(a) and 2.3(c), with $\mu = 0.0318$, $\kappa = 0.001$ and $A_s = 0.318$. The amplitude is greater and more nonlinear in Fig. 2.3(b) and 2.3(d), with $\mu = 78$, $\kappa = 0.8$ and $A_s = 780$. In all cases for Fig. 2.3, $f_1 = 10$ Hz, $f_2 = 12$ Hz, and $\alpha = \beta = 1$. The spectrum shows peaks at $f_1$, $f_2$, sum-frequency $f_2 + f_1$ and difference-frequency $f_2 - f_1$.

Nonlinear mixing is revealed by the presence of combination frequencies in the spectra of Fig. 2.3. Especially in Fig. 2.3(d) with the higher amplitude and greater nonlinearity, we see many combination frequencies such as $2f_2 - f_1$ which is labelled as peak $P_5$, and $2f_1 + f_2$ which is labelled as peak $P_{13}$. There is a rich variety of these combination frequencies, and they are listed in Table I. The presence of peaks at harmonics such as $2f_1$, $3f_1$ and $4f_1$ are not attributed to mixing but rather just the presence of nonlinearity ($\kappa > 0$) in the excitation.

### 2.3.1 Comparison of NLM in the fKdV model with dusty plasma experiment

We will now provide experimental evidence of the nonlinear mixing of waves in a dusty plasma experiment that shows good agreement with our fKdV model. The mixing spectrum of the fKdV model shown in the Fig. 2.4(a) is quite similar to nonlinear mixing exhibited in the experimental spectrum [15] shown in the Fig. 2.4(b). This experimental spectrum includes peaks at combination frequencies such as $2f_2 - f_1$ and $2f_1 + f_2$. (The experiment also has peaks at harmonics such as $2f_1$ and $3f_1$, but those can occur in the absence of mixing due to the non-sinusoidal distortion of a periodic waveform, as is common under nonlinear effects.)

It is significant that the spectrum from our solution of the fKdV equation shows peaks at the same combination frequencies as for the experiment of Ref. [15]. This observation gives us some confidence that we are observing nonlinear mixing. The model, even though it is simple, adequately captures salient
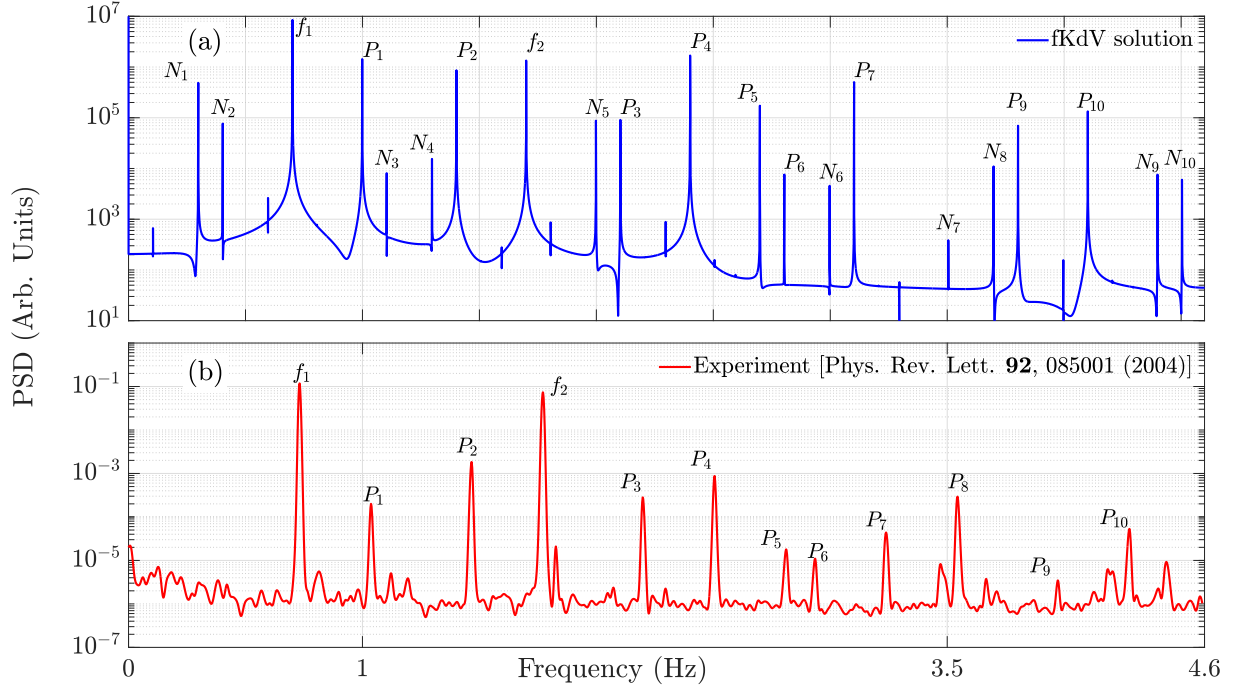
Figure 2.4: Comparison of time series power spectra for [a] obtained from the fKdV model, Eq. (2.5), and [b] we have replotted the same experimental data points that were originally reported in Ref. [15]. Parameters used for the theoretical model are $\mu = 18.5, \kappa = 0.7$ (corresponds to $f_1 = 0.7$ Hz), $A_s = 18.5$ and $f_2 = 1.7$ Hz.

mechanisms for nonlinear mixing, yielding the same signatures of combination frequencies as in a specimen experimental system.

Although for Fig. 2.4(a), we used the same excitation frequencies $f_1 = 0.7$ Hz and $f_2 = 1.7$ Hz as for the experiment of Ref. [15], we should mention several ways that the model's assumptions differ from that of the experiment. First, there is frictional damping from gas in the experiment. This friction can inhibit nonlinear effects unless a threshold is exceeded, which would not be the case in the model where there was no friction. Second, the experimental system was finite in size and could exhibit an overall sloshing mode oscillation in the presence of the external confining potential, which is provided by a curved sheath above the horizontal electrode. Thus, the experimental spectrum could potentially include the signature of a sloshing mode oscillation or the mixing of that oscillation with the excitation at $f_1$ or $f_2$. This behaviour would not be described by our model. Third, the model was constructed so that it assumes that the excitation at one of the two frequencies is not a propagating wave but is uniformly applied throughout the medium, as sketched in Fig. 3.1. This third difference might be less substantial than one might expect, however, because the wavelength at the low frequency $f_1 = 0.7$ Hz in the experiment could have been substantial as compared to the finite size of the cloud of charged dust particles.

We also note that the spectral peaks obtained from the theoretical fKdV model in Fig. 2.4(a) are not limited to all those present in the experimental spectrum shown in Fig. 2.4(b). In Table II, we list those peaks $P_1$-$P_{10}$ of the theoretical model that are also present in the experimental spectrum while peaks $N_1$-$N_{10}$ are only present in the theoretical model. The latter frequency peaks represent different combinations of the sum and difference of $f_1$, $f_2$ and their higher harmonics. Their absence in the

Table 2.2: Frequencies observed in the dusty plasma experiment [15] and fKdV model Eq. (2.5) as shown in Fig. 2.4(a) and (b), respectively.

| Frequency (Hz) | Fig. 2.4(a) | Fig. 2.4(b) | Frequency (Hz) | Fig. 2.4(a) | Fig. 2.4(b) |
|---|---|---|---|---|---|
| $f_1$ | 0.7 | 0.7 | $P_{10} = 2f_2 + f_1$ | ✓ | ✓ |
| $f_2$ | 1.7 | 1.7 | $N_1 = f_2 - 2f_1$ | ✓ | |
| $P_1 = f_2 - f_1$ | ✓ | ✓ | $N_2 = 3f_1 - f_2$ | ✓ | |
| $P_2 = 2f_1$ | ✓ | ✓ | $N_3 = 4f_1 - f_2$ | ✓ | |
| $P_3 = 3f_1$ | ✓ | ✓ | $N_4 = 2f_2 - 3f_1$ | ✓ | |
| $P_4 = f_1 + f_2$ | ✓ | ✓ | $N_5 = 2(f_2 - f_1)$ | ✓ | |
| $P_5 = 2f_2 - f_1$ | ✓ | ✓ | $N_6 = 3(f_2 - f_1)$ | ✓ | |
| $P_6 = 4f_1$ | ✓ | ✓ | $N_7 = 5f_1$ | ✓ | |
| $P_7 = 2f_1 + f_2$ | ✓ | ✓ | $N_8 = 3f_2 - 2f_1$ | ✓ | |
| $P_8 = 2f_2$ | | ✓ | $N_9 = 3f_2 - f_1$ | ✓ | |
| $P_9 = 3f_1 + f_2$ | ✓ | ✓ | $N_{10} = 4f_1 + f_2$ | ✓ | |

experimental spectrum could be due to the effect of gas friction, which can prevent weak nonlinear effects from being observed.

## 2.4   Summary

Finally, to conclude, we have presented a simple mathematical model consisting of a forced KdV equation with a time-varying sinusoidal forcing term that shows the existence of nonlinear wave mixing in a dusty plasma medium. Physically the model represents wave mixing arising from the temporal modulation of a nonlinear dust compressional wave. This is a situation that can be easily realized in an experiment using the radiation pressure of lasers or time-varying electric potentials to modulate self-excited or externally driven large amplitude compressional waves.

One advantage of the present model is the existence of an exact analytic solution which can be conveniently used to map various parametric regimes without recourse to a numerical solution of the nonlinear equation. This solution not only shows the existence of wave mixing phenomenon in this simple model system but may also be useful in predicting nonlinear wave mixing for a proposed experimental configuration in a two-dimensional dusty plasma medium.

The theoretical model in this chapter is primitive yet nicely shows experimental results. The model only looks into a sinusoidal form of driving which has a benefit of an exact analytic solution. We know that driving forces in actual experimental or natural scenarios are nonlinear and of the travelling waveform. We also need to establish the exact origin of newly generated modes we strongly believe are an outcome of nonlinear mixing. These two facts have been discussed in the following chapter.

# Chapter 3

# Bispectral analysis of nonlinear mixing in a periodically driven Korteweg–de Vries system

This chapter examines the nonlinear mixing of dust lattice (and dust acoustic) waves using the fKdV model with various forms of external driving (forcing). We have used a semi-analytic model of the fKdV equation for time-dependent forcing forms and a full numerical model for the travelling wave forcing form. This comprehensive study is to understand the effect of the nonlinear form of external forcing over the mixing profile. Our results for the model involving the travelling wave forcing form quantitatively fit with experimental observations, overcoming the shortcomings of only the time-dependent forcing model in the previous chapter. Further, we analyzed the resultant time series with a bispectral analysis to confirm the origin of new modes as an outcome of the three-wave mixing process.

## 3.1 Introduction

The Korteweg-de Vries (KdV) model equation has served as a standard paradigm for the description of many low-frequency nonlinear phenomena in various nonlinear dispersive media such as neutral fluids, plasmas, optical fibres, vibrating lattices *etc.* [206, 211, 212, 217–221]. As a fully integrable partial differential equation, the KdV equation admits a variety of exact solutions, including solitons, cnoidal waves, dispersive shocks *etc.* that have been used to describe experimental observations of nonlinear wave phenomena in the aforementioned systems. In plasmas, the KdV equation has successfully modelled the existence and evolution of ion and dust acoustic shocks as well as solitary waves [98, 146, 209]. More recently, a forced KdV (fKdV) model was used to explain the emission of precursor magneto-sonic solitons, created by a charge bunch moving in a magnetized plasma [222].

The KdV model has also been investigated in the presence of an external time and space varying perturbation in order to investigate the response of a driven nonlinear medium. Such a forced KdV equation that had a travelling wave source was used to determine the conditions for the resonant excitation of nonlinear oscillatory waves in a dispersive medium by Vainberg *et al.* [223]. Using a chirped frequency driving perturbation, Friedland *et al.* [224] studied the anomalous autoresonance threshold for the excitation of large amplitude travelling waves in a KdV model system. Aranson *et al.* [225] took a similar approach of chirping the frequency of the driver to excite solitons in the system. In particular, for plasmas, the fKdV model predicts existence of precursor and pinned solitons [153, 154]. These nonlinear emissions can prove useful in space awareness applications, such as in the indirect detection of charged space debris orbiting in the earth's ionosphere [140]. More recently, Mir *et al.* [169] used the fKdV model to study nonlinear wave mixing in a dusty plasma system and related their findings to past experimental observations of Nosenko *et al.* [15]. The form of the driver, in their case, was chosen to be a simple time-varying sinusoidal function for which an exact analytic solution of the model could be obtained. Using such an exact solution, time series data of the system response was obtained for parameters close to the experimental conditions and the power spectrum of this model data was compared with the experimental power spectrum. Nonlinear mixing (NLM) was revealed by the presence of the combination of frequencies of various harmonics of the inherent mode of the system and the driving wave.

While such identification of combination frequencies provides quick first-hand evidence of nonlinear wave mixing, it does not conclusively establish the origin of the combination due to a three-wave mixing process. This is because the power spectrum does not explicitly provide the phase coupling information about the interactions. A more precise tool for establishing the physical origin of the wave mixing is a bispectral analysis [226–228] that looks at the triple-correlation of the time series of any dynamical quantity. A finite correlation is obtained for a frequency triad $F(f_1)$, $F(f_2)$ and $F(f_1 + f_2)$ when they are formed by a coherent phase coupling mechanism (where $F$ is the discrete Fourier component at a given frequency). There will be no correlation among frequencies if they are spontaneously excited modes, i.e., no coherent phase coupling is involved. Bispectral analysis has been extensively used in the past to investigate coherent nonlinear interactions in plasmas [229–231] as well as in many biomedical [232, 233]

and engineering applications [234, 235].

In this work, we extend the earlier spectral analysis of Mir *et al.* [169] and carry out a bispectral analysis to firmly establish the nature of the nonlinear mixing phenomenon. We also expand the scope of their model calculations by going beyond the simple time-varying sinusoidal driver to examine the influence of different functional forms of the driver on the mixing process. These different functional forms of the driver can arise in a variety of situations. For example, in a typical experimental situation, if the driving wave is one of the normal modes of the system, then it is likely to be of a nonlinear form, *e.g.* ion acoustic waves or dust acoustic waves (DAWs) have been observed to grow nonlinearly into cnoidal or cnoidal square waveforms in many experiments [36, 39, 107, 112]. The presence and evolution of nonlinear modes or disturbances are, in fact, generic to nonlinear media such as cnoidal waves in metamaterials [236], cnoidal-square waveforms of dust acoustic waves [156], and sawtooth-like shock waves [203]. When the driving wave is applied externally, it can also take a variety of waveforms, such as using a cnoidal waveform electrical or optical signals to generate frequency combs in Kerr microresonators [237], use of a sawtooth wave for higher harmonic generation in a plasma [238] and the use of cnoidal waves to generate nonlinear frequency combs in microring resonators [239]. The present work is aimed at studying the impact of such waveforms on the nonlinear mixing phenomena in plasmas.

It is seen that changing the profile and functional dependence of the driver can significantly alter the response pattern of the system. In particular, a travelling wave source is seen to excite additional frequencies that are not seen in response to purely time-varying sources.This enhanced spectrum is shown to bear a closer resemblance to the dusty plasma experimental data of Nosenko *et al.* [15] than the model system studied by Mir *et al.* [169]. In addition to changing the functional form of the driver, we also examine the effect of changing the driver frequency relative to the natural frequency of the non-driven system. We find a significant difference in the resultant spectral patterns depending upon whether the driver frequency is larger or smaller than the natural frequency. This asymmetry in the response pattern is explained based on a higher-order mixing process. Our findings thereby offer a means of tailoring the response patterns of driven systems that may find practical applications.

The work is organized as follows. The model fKdV equations with different forms of purely time-dependent forcing terms $F_s(t)$ or with a spatio-temporal forcing term $F_s(x,t)$ are described in section 3.2. The effect of different forcing forms on nonlinear mixing is first discussed in section 3.3 in terms of the differences in the power spectral densities (PSD) of the time series data of the numerical solutions of the fKdV model. This is followed up in section 3.4 by a bispectral analysis of the same data and its physical interpretation. Section 3.5 is devoted to a discussion on the effect of tunable drivers on the NLM process and a discussion on the physical origin of the asymmetry in the driven response. A brief discussion and some concluding remarks are given in section 3.6.

## 3.2    The forced Korteweg-de Vries model

A generalized form of the fKdV equation for the perturbed density, $n(x,t)$, can be written down as [169]:

$$\frac{\partial n(x,t)}{\partial t} + \alpha\, n(x,t)\frac{\partial n(x,t)}{\partial x} + \beta\frac{\partial^3 n(x,t)}{\partial x^3} = F_s(x,t). \tag{3.1}$$

The Eq. (3.1) can be derived from the full set of cold fluid equations for the dust component in the weakly nonlinear and weakly dispersive regime [140]. The ions and electrons, as lighter species compared to the dust, are assumed to obey Boltzmann relations. $\alpha$ and $\beta$ are the characteristic parameters quantifying nonlinearity and dispersion of the medium, respectively. $F_s(x,t)$ is the external spatio-temporal forcing. For $F_s(x,t) = 0$ one recovers the standard KdV equation that admits exact nonlinear solutions in the form of solitons [98, 206, 209, 240] and periodic cnoidal waves [156, 241]. In the context of dusty plasmas, Liu *et al.* [156] have shown that a cnoidal wave solution provides an excellent fit to their experimental observations of self-excited dust acoustic waves sustained in an RF plasma [242].

### 3.2.1    Korteweg-de Vries model with a time-dependent forcing, $F_s(t)$

An analytic solution of Eq. (3.1) with a purely time-dependent sinusoidal forcing that is based on Hirota's approach [216] has been presented earlier in Ref. [169] and is given by:

$$n(x,t) = \phi(t) + \mu\, cn^2\left[\frac{\sqrt{\mu\alpha}}{2\sqrt{\beta\kappa(\kappa+2)}}\left(x - \frac{\kappa+\kappa^2-1}{\kappa(\kappa+2)}\alpha\mu t - \alpha\psi(t)\right);\ \kappa\right] \tag{3.2}$$

In Eq. (3.2), $cn$ is the Jacobi elliptic function, $\mu$ is the amplitude of the cnoidal wave, and $\kappa$ is the elliptic modulus that quantifies the nonlinear nature of the cnoidal wave. In the context of dusty plasma, the elliptic modulus $\kappa$ and the total harmonic distortion of DAW [107] were used by Liu *et al.* [156], to quantify the nonlinearity of their experimentally observed waveforms. With $\kappa \to 0$, the wave attains a cosine waveform, and as $\kappa \to 1$, the waveform becomes nonlinear with the cosine wave getting converted to a cnoidal waveform. At $\kappa = 1$ when $cn^2(x,t;\ \kappa) = \text{sech}^2(x,t)$ [243], the cnoidal wave takes the form of a single soliton. Furthermore, the quantities $\phi$ and $\psi$ are defined as,

$$\phi(t) = \int F_s(t)\, dt \quad \text{and} \quad \psi(t) = \int \phi(t)\, dt. \tag{3.3}$$

The $\phi(t)$ and $\psi(t)$ can be calculated either analytically or numerically depending on the choice of the forcing profile. As a generalization of the work reported in Ref. [169], where only a sinusoidal form of $F_s(t)$ was used, we have considered a variety of functional forms for the drivers in our present work. These different forcing terms are listed in Table 3.1. For the case of a sinusoidal forcing profile, $\phi(t) = -\left(A_s/(2\pi f_2)\right)\cos(2\pi f_2 t)$ and $\psi(t) = -\left(A_s/(2\pi f_2)^2\right)\sin(2\pi f_2 t)$. Here $f_2$, $A_s$ and $\kappa_s$ are the forcing frequency, forcing amplitude and the forcing elliptic modulus corresponding to each forcing form $F_s(t)$, respectively.

Table 3.1: Functional form of different forcing profiles for which NLM is explored in the fKdV model

| Forcing profiles | $F_s(t)$ or $F_s(x,t)$ |
|---|---|
| Sinusoidal $F_{\sin}(t)$ | $A_s \sin(2\pi f_2 t)$ |
| Cnoidal $F_{cn}(t)$ | $A_s cn[4K(\kappa_s)f_2 t; \kappa_s]$ |
| Cnoidal-square $F_{cn^2}(t)$ | $A_s cn^2[2K(\kappa_s)f_2 t; \kappa_s]$ $F_{cn^2}(t) = F_{cn^2}(t) - \langle F_{cn^2}(t) \rangle$ |
| Travelling wave $F_s(x,t)$ | $A_s \sin(k_s x - 2\pi f_2 t)$ Solving fKdV numerically |
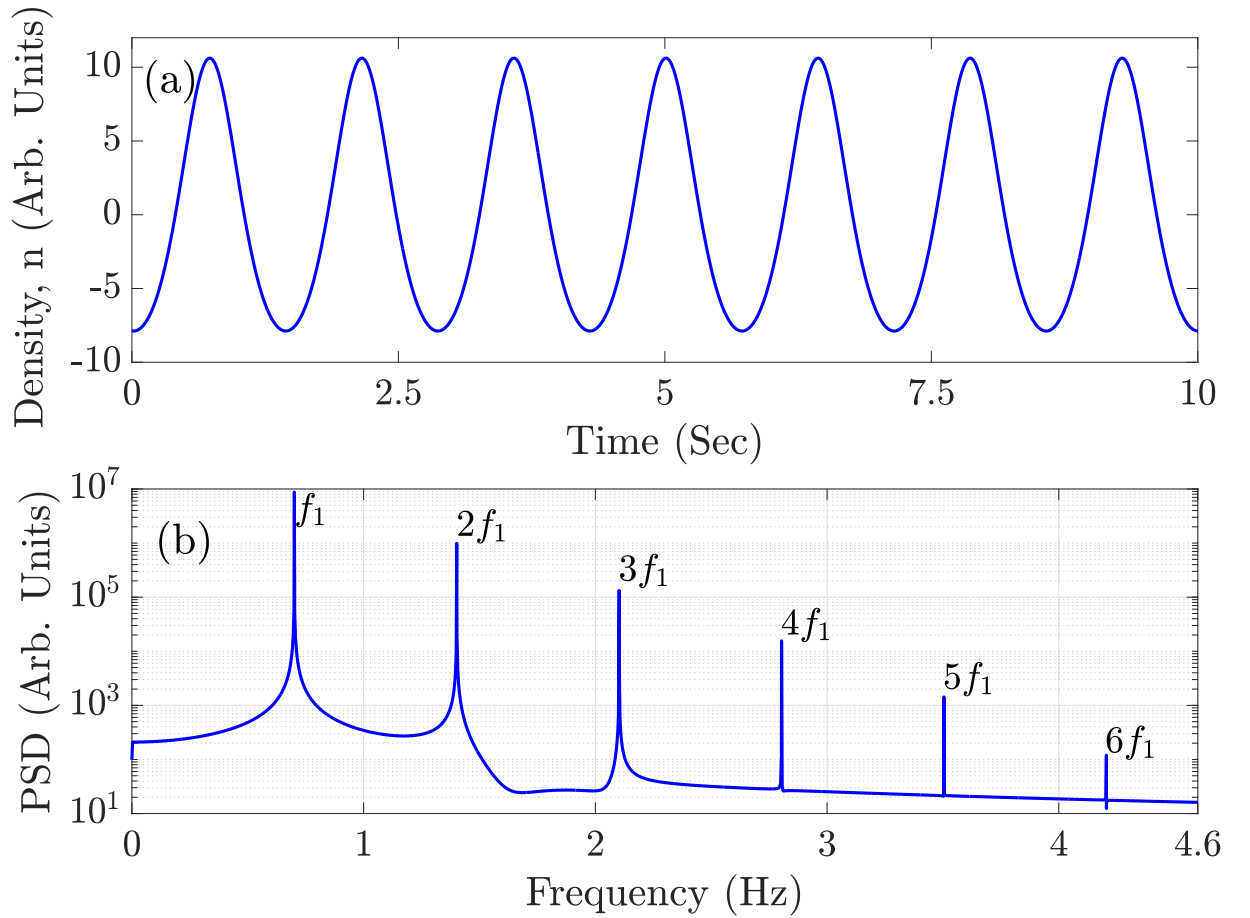


Figure 3.1: (a) Time series of KdV for $\mu = 18.5$, $\kappa = 0.7$ (such that $f_1 = 0.7$ Hz) with $\alpha = \beta = 1$. (b) Power spectrum of (a). The nonlinear wave (non-sinusoidal) nature is evident from both the time series (a) and the presence of harmonics in its PSD (b).

A truncated Fourier series expansion can approximate the non-sinusoidal forcing profiles. In the context of dusty plasma, Merlino *et al.* [57] obtained excellent fit to their experimental DAW profiles by retaining terms up to the second harmonic in the Fourier series expansion of the square of the cnoidal function, namely,

$$F_s(t) = F_{cn^2}(t) = A_s cn^2[2K(\kappa_s)f_2 t; \kappa_s]$$

$$F_{cn^2}(t) \approx (A_s/2)\{\cos(2\pi f_2 t) + 0.02A_s \cos(2\pi(2f_2)t) + 0.004A_s \cos(2\pi(3f_2)t)\}. \tag{3.4}$$

Such a Fourier series representation of a non-sinusoidal forcing term allows one to solve the fKdV system analytically by using the general solution described by (3.2) and (3.3). This facilitates the study of the nonlinear mixing phenomenon as a function of the various forms of the driver.

A nonlinear cnoidal time series solution of the KdV equation and its PSD are shown in Fig. 3.1(a) and Fig. 3.1(b), respectively. The PSD shows a fundamental frequency at $f_1 = 0.7$ Hz along with the even and odd harmonics of the wave at $2f_1$, $3f_1$ and so on.

### 3.2.2 Korteweg-de Vries model with spatio-temporal forcing, $F_s(x,t)$

The KdV equation with a spatio-temporal travelling waveform of the forcing is given by:

$$\frac{\partial n(x,t)}{\partial t} + \alpha\, n(x,t)\frac{\partial n(x,t)}{\partial x} + \beta\frac{\partial^3 n(x,t)}{\partial x^3} = A_s \sin(k_s x - 2\pi f_2 t). \tag{3.5}$$

We have numerically solved Eq. (3.5) using a finite difference scheme. The code has been validated by reproducing the results of Sen *et al.* [140]. The frequency corresponding to the forcing wave-vector $k_s$ is chosen to satisfy the linear dispersion relation obtained by setting $\alpha = 0$ in the standard KdV equation, namely $f_1 = -\beta k_s^3/(2\pi)$. Here, $k_s = nk_0$ with $k_0 = 2\pi/L$ being the minimum wavevector associated with a system of length $L$. For the numerical solution of Eq. (3.5), we have taken an initial condition of $n(x,0) = 0$.

## 3.3 Nonlinear mixing in the fKdV model with different forcing forms

To investigate the NLM process under various non-sinusoidal time-dependent forcing forms, we have used semi-analytic solutions by using (3.2) and (3.3). Exact analytic forms are possible for cases when $\phi$ and $\psi$ in (3.3) are exactly integrable. Sinusoidal forcing is one such example. While the solutions apply to all nonlinearity regimes and dispersion, we have taken one parameter set throughout the work for uniformity. We have used $\mu = 18.5$, $\kappa = 0.7$ (such that $f_1 = 0.7$ Hz) and $\alpha = \beta = 1$ for all cases in the manuscript unless specified otherwise.

The frequencies in the power spectrum as displayed in Fig. 3.2 are for (a) sinusoidal, (b) cnoidal wave, and (c) cnoidal-square wave driver in the fKdV equation. Their values are tabulated in Table 3.2. All listed frequencies match the sum and difference frequencies of $f_1$ (natural KdV mode), $f_2$ (fundamental forcing mode) and their harmonics. These additional modes are generated via the three-wave mixing mechanism, which is further confirmed via a bispectral analysis described in section 3.4.

The spectrum shown in Fig. 3.2 for each non-sinusoidal forcing form is qualitatively similar to the sinusoidal forcing case in the range of frequencies that carry significant power. A noticeable difference is
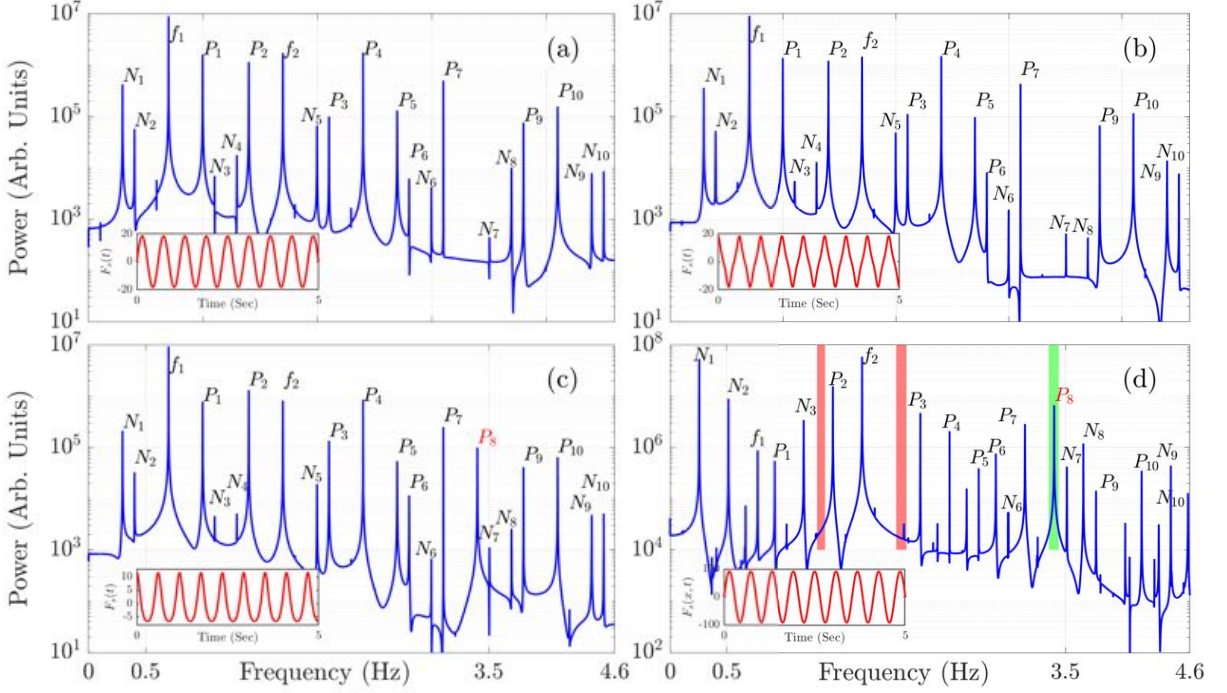
Figure 3.2: Power spectrum of time series obtained from fKdV model for (a) sinusoidal forcing $F_s(t) = F_{\sin}(t) = A_s \sin(2\pi f_2 t)$ , (b) cnoidal wave forcing $F_s(t) = F_{cn}(t) = A_s cn[4K(\kappa_s)f_2 t; \kappa_s]$, (c) cnoidal-square wave forcing $F_s(t) = F_{cn^2}(t) = A_s cn^2[2K(\kappa_s)f_2 t; \kappa_s]$. Here $A_s = \mu$, $\kappa_s = 0.9$ and $f_2 = 1.7$ Hz. (d) Travelling wave forcing $F_s(x,t) = A_s \sin(k_s x - 2\pi f_2 t)$ with no initial condition, i.e., $n(x,0) = 0$. Here $A_s = 5\mu$, $k_s = 9k_0$ with $k_0 = (2\pi)/L$, which corresponds to frequency $f_1 = k_s^3/(2\pi) = 0.7$ Hz for a system of length $L = 11\pi$ and $f_2 = 1.7$ Hz. Also, $\alpha = \beta = 1$ in each case.

for the cnoidal-square forcing case where we obtain an additional frequency $P_8 = 2f_2$ that also exists in the power spectrum of the fluctuations measured in the dusty plasma experiment of Nosenko *et al.* [15]. However, this could be because the cnoidal-square forcing form inherently contains the frequency mode at $P_8 = 2f_2$ in contrast to other forcing forms, as can be seen in Table 3.2.

We have also observed NLM in fKdV model with a travelling wave forcing form $F_s(x,t) = A_s \sin(k_s x - 2\pi f_2 t)$. The spectrum due to travelling wave forcing is shown in Fig. 3.2(d) and is also tabulated in Table 3.2. The spectrum obtained for this case is unique compared to all time-dependent forcing cases in two ways. First, certain frequencies are missing in the spectrum and are named $N_4$ and $N_5$ in Table 3.2. The same has been shown as red bands in Fig. 3.2(d). Second, we have also observed a frequency peak $P_8 = 2f_2$ marked in green patch in Fig. 3.2(d). Both the missing and the extra frequency are consistent with the observations in the dusty plasma experiment [15]. In this case, the extra frequency is not due to the inherent property of the driver but is a genuine outcome of an NLM process.

## 3.4   Bispectral analysis of nonlinear mixing

The bispectral analysis is a statistical tool that provides a quantitative measure of a coherent nonlinear interaction process. If a coherent nonlinear interaction exists between three oscillations at frequencies $F_1$, $F_2$ and $F_1 + F_2$, a peak will be generated in the principal domain of the bispectrum at the intersection between $F_1$ and $F_2$. The bispectrum of a dynamic process is always a complex quantity and is defined

Table 3.2: Dominant frequencies observed in the fKdV model for various forcing forms as shown in Fig. 3.2.

| Frequency (Hz) | Fig. 3.2(a) $F_{\sin}(t)$ $A_s = \mu$ | Fig. 3.2(b) $F_{cn}(t)$ $A_s = \mu$ $\kappa_s = 0.9$ | Fig. 3.2(c) $F_{cn^2}(t)$ $A_s = \mu$ $\kappa_s = 0.9$ | Fig. 3.2(d) $F_s(x,t)$ $A_s = 5\mu$ $k_s = 9k_0$ |
|---|---|---|---|---|
| $f_1 = 0.7$ | ✓ | ✓ | ✓ | ✓ |
| $f_2 = 1.7$ | ✓ | ✓ | ✓ | ✓ |
| $P_1 = f_2 - f_1$ | ✓ | ✓ | ✓ | ✓ |
| $P_2 = 2f_1$ | ✓ | ✓ | ✓ | ✓ |
| $P_3 = 3f_1$ | ✓ | ✓ | ✓ | ✓ |
| $P_4 = f_1 + f_2$ | ✓ | ✓ | ✓ | ✓ |
| $P_5 = 2f_2 - f_1$ | ✓ | ✓ | ✓ | ✓ |
| $P_6 = 4f_1$ | ✓ | ✓ | ✓ | ✓ |
| $P_7 = 2f_1 + f_2$ | ✓ | ✓ | ✓ | ✓ |
| $P_8 = 2f_2$ | | | ✓ | ✓ |
| $P_9 = 3f_1 + f_2$ | ✓ | ✓ | ✓ | ✓ |
| $P_{10} = 2f_2 + f_1$ | ✓ | ✓ | ✓ | ✓ |
| $N_1 = f_2 - 2f_1$ | ✓ | ✓ | ✓ | ✓ |
| $N_2 = 3f_1 - f_2$ | ✓ | ✓ | ✓ | ✓ |
| $N_3 = 4f_1 - f_2$ | ✓ | ✓ | ✓ | ✓ |
| $N_4 = 2f_2 - 3f_1$ | ✓ | ✓ | ✓ | |
| $N_5 = 2(f_2 - f_1)$ | ✓ | ✓ | ✓ | |
| $N_6 = 3(f_2 - f_1)$ | ✓ | ✓ | ✓ | ✓ |
| $N_7 = 5f_1$ | ✓ | ✓ | ✓ | ✓ |
| $N_8 = 3f_2 - 2f_1$ | ✓ | ✓ | ✓ | ✓ |
| $N_9 = 3f_2 - f_1$ | ✓ | ✓ | ✓ | ✓ |
| $N_{10} = 4f_1 + f_2$ | ✓ | ✓ | ✓ | ✓ |

by [226–228, 232, 244]

$$B(F_1, F_2) = \langle F(f_1)F(f_2)F^\star(f_1 + f_2) \rangle \tag{3.6}$$

where $\langle ... \rangle$ is the ensemble average over multiple samples, $F$ is the Fourier transform, $F^\star$ is the corresponding complex conjugate and $f_1$, $f_2$ are the two frequencies of the triad $(F_1, F_2, F_1 + F_2)$. The bispectrum $B(F_1, F_2)$ is a function of two frequencies and is a non-zero quantity only if a phase coupling exists between the frequency triplet $F_1$, $F_2$ and $F_1 + F_2$. $B(F_1, F_2)$ is identically zero for spontaneously generated modes, i.e., the modes generated without phase coupling. The bispectrum's ability to retain the phase information lost by the power spectrum (the Fourier transform of a signal) makes it a useful tool for analyzing coherent nonlinear interactions.

The normalized bispectrum of a time series [227, 228, 231, 232, 244] gives the bicoherence and is given by:

$$\gamma^2(F_1, F_2) = \frac{|B(F_1, F_2)|^2}{\langle|F(f_1)F(f_2)|^2\rangle\langle|F^\star(f_1 + f_2)|^2\rangle}. \tag{3.7}$$

Bicoherence gives a measure of phase coherence between the coupled modes. It is a measure of the fraction of power retained by modes due to phase coupling. Theoretically, bicoherence is 1 for phase coupled modes, *i.e.,* modes generated due to coherent nonlinear interaction and 0 for uncoupled modes, *i.e.,* modes generated spontaneously.

Bicoherence is symmetric about the line $F(f_1) = F(f_2)$ because $\gamma^2(F_1, F_2) = \gamma^2(F_2, F_1)$. For our analysis, we used $M = 8192$ sampling data points and $N = 16$ time series segments so that the total length of a time series was $K = M \times N$. A statistically significant correlation between the coherent modes is determined by the condition $\gamma^2 > \sqrt{6/2N} = 0.433$ as discussed in Siu *et al.* [232].
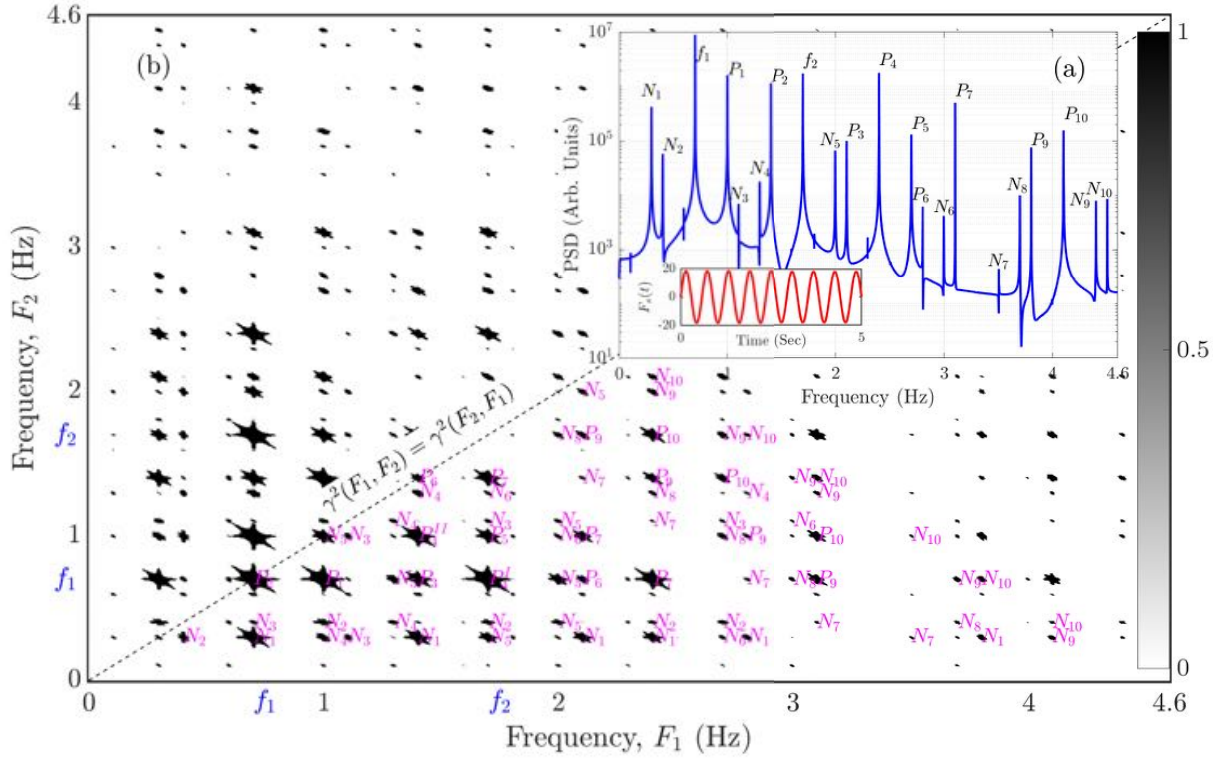


Figure 3.3: PSD (a) and bicoherence (b) of fKdV for sinusoidal forcing. Inset (a) is the PSD of fKdV for $F_s(t) = F_{\sin}(t) = A_s \sin(2\pi f_2 t)$ with $A_s = 18.5$ and $f_2 = 1.7$ Hz. Initial parameters are $\mu = 18.5$, $\kappa = 0.7$ (such that $f_1 = 0.7$ Hz) and $\alpha = \beta = 1$. The small inset within (a) shows the form of a sinusoidal forcing profile. The bicoherence map shows patches ($\gamma^2 \approx 1$) indicating that the waves at $F(f_1)$, $F(f_2)$ and $F(f_1) + F(f_2)$ are not only frequency coupled but are phase coupled as well. This confirms coherent nonlinear interaction between the waves at $F(f_1)$ and $F(f_2)$.

### 3.4.1   Time-dependent sinusoidal forcing

In Fig. 3.3 we show the power spectrum (inset) and the bicoherence of the time series obtained for a sinusoidal forcing in the fKdV model. The frequencies in the power spectrum as shown in Fig. 3.3(a) [inset] are listed in column (II) of Table 3.2. All the listed frequencies match the sum and difference

frequencies of $f_1$(fundamental KdV mode), $f_2$ and their harmonics. While the power spectrum confirms the presence of new modes, it does not confirm any frequency or phase coupling.

To confirm the origin of excited modes, we calculated the bicoherence of the same time series as in Fig. 3.3(b). Peaks in the power spectrum map to the dark patches in the bicoherence space shown in Fig. 3.3. For example, $P_4 = 2.4$ Hz in the power spectrum generates a patch ($P_4^I$) that is at the intersection of $F_1 = f_1 = 0.7$ Hz and $F_2 = f_2 = 1.7$ Hz confirming a phase coupled and frequency-coupled mode excitation. $P_4 = 2.4$ Hz also generates another patch in bicoherence ($P_4^{II}$) at the intersection of $F_1 = 2f_1 = 1.4$ Hz and $F_2 = f_2 - f_1 = 1.0$ Hz. Table 3.3, column (IV) lists all possible combinations of frequencies leading to patches in the bicoherence space with $P$ and $N$ nomenclature. Peaks marked with $P$ and $N$ are the ones that were observed and missing (not observed), respectively, in the dusty plasma experiment [15], which was used for validating nonlinear mixing in the fKdV model [169]. Many patches in bicoherence space suggest multiple possible combinations of sum and difference of frequencies leading to a single peak in the power spectrum. Thus the present bispectral analysis confirms the three-wave mixing results for a sinusoidal forcing of the fKdV as presented earlier by Mir *et al.* [169].

It should be mentioned that some of the specific patches, marked with a $\star$ in column (IV) of Table 3.3, do not follow the standard sum rules but are present in the power spectrum as well as in the bicoherence plot. We believe they represent one of the frequencies $F_1$ or $F_2$ that appears on the coordinate axes of Fig. 3.3. We have independently confirmed their source and presence by constructing a frequency and phase-coupled time series generated using all frequencies observed in the power spectrum and switching them on and off to see their impact on the bicoherence plot.

### 3.4.2 Time-dependent non-sinusoidal forcing

In practical scenarios, non-sinusoidal forcing patterns are more probable. The plasma-based nonlinear dynamical study carried out by Chaubey *et al.* [39] is one such example, where two nonlinearly excited ion acoustic modes interact with each other. But the studies can easily be generalized for any dispersive media.

This section provides the bispectral analysis for the time series obtained from the fKdV model with cnoidal and cnoidal-square forms (Fig. 3.4). Columns III-IV in Table 3.2 list frequencies observed in the power spectra for the two cases as mentioned earlier. Similarly, columns VI-VII in Table 3.3 contains all possible frequency combinations due to coherent phase coupling.

For all non-sinusoidal forcing cases, the general appearance of the power spectra and bicoherence diagrams appear nearly similar to the earlier discussed sinusoidal forcing case within the frequency range of significant amplitudes. An exception is a cnoidal-square case (Fig. 3.4), where we notice an additional frequency at $P_8 = 2f_2$. Such a frequency has also been observed in the referred dusty plasma experiment [15]. However, it should be noted that this frequency of $P_8 = 2f_2$ is also inherently present in the power spectrum of the driver on account of the nature of its profile. So, in this case, it is impossible
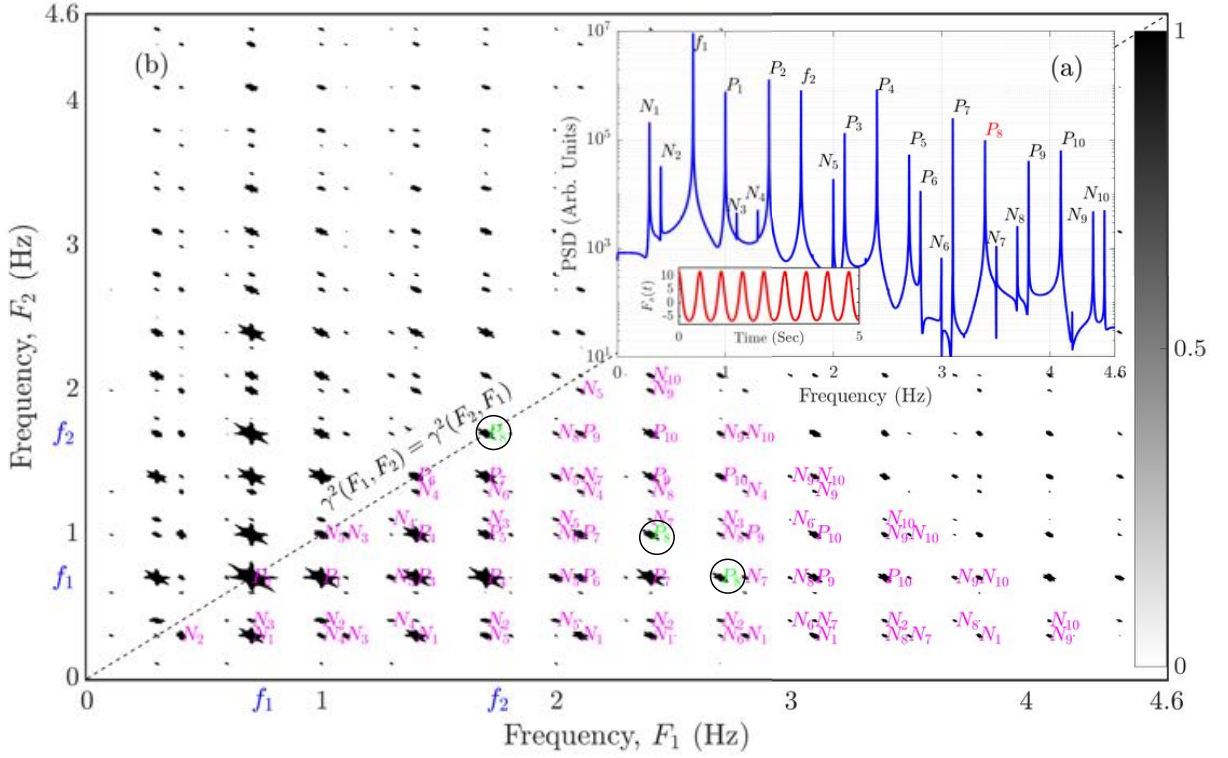
Figure 3.4: PSD (a) and bicoherence (b) of fKdV for cnoidal-square forcing. Inset (a) is the PSD of fKdV for $F_s(t) = F_{cn^2}(t) = A_s cn^2[2K(\kappa_s)f_2 t; \kappa_s]$ with $A_s = 18.5$, $f_2 = 1.7$ Hz and $\kappa_s = 0.9$. Initial parameters are $\mu = 18.5$, $\kappa = 0.7$ (such that $f_1 = 0.7$ Hz) and $\alpha = \beta = 1$. The small inset within (a) shows the form of the cnoidal-square forcing profile. Both the PSD (a) and bicoherence (b) show a peak at $P_8 = 2f_2$ (encircled), which is inherent in the cnoidal-square wave forcing.

to unambiguously assert that the appearance of this frequency in the response spectrum is a result of three-wave mixing.

### 3.4.3   Travelling wave forcing

The bicoherence spectrum of the time series obtained with a travelling wave forcing is shown in Fig. 3.5 with its quantitative values listed in column VIII of Table 3.3. It shows an absence of the $N_4$ and $N_5$ frequencies and the presence of $P_8 = 2f_2$ frequency in agreement with the power spectrum analysis. We reiterate that the observation is in contrast to the purely time-dependent sinusoidal forcing and agrees with the results reported in the dusty plasma experiment [15]. Also, unlike in the case of a cnoidal-square forcing, the presence of the $P_8 = 2f_2$ frequency is not an artifact of such a frequency being present in the driver itself. In this case, it is a genuine result of a three-wave mixing process.

## 3.5   Tailoring the mixing pattern through frequency tuning of the driver

Based on our above-discussed analysis of the influence of the functional form of the driver on the nonlinear mixing process, as seen in the power spectra and bicoherence spectra, we now discuss a possible means of tailoring the nonlinear mixing pattern through the driver parameters. We adopted two approaches for
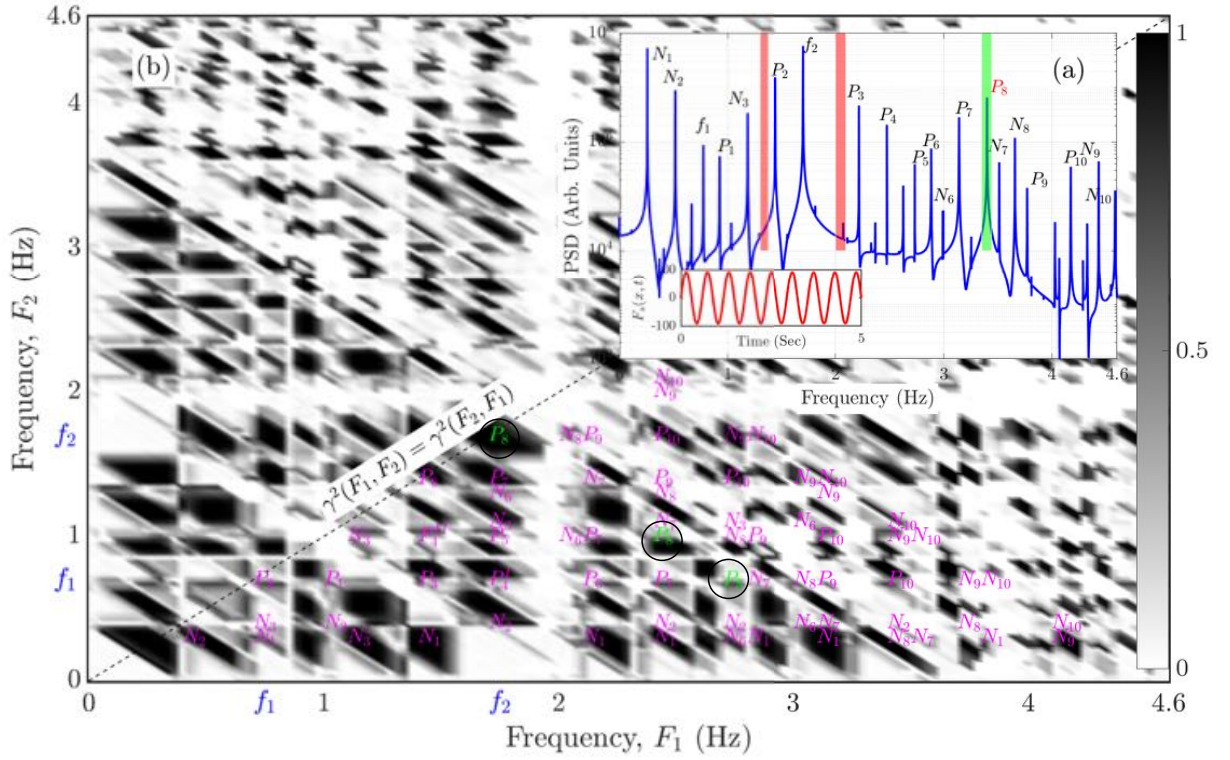
Figure 3.5: (a) PSD, and (b) bicoherence of fKdV for travelling wave forcing $F_s(x,t) = A_s \sin(k_s x - 2\pi f_2 t)$ with no initial perturbation, $i.e.$, $n(x,0) = 0$. Here $A_s = 5\mu$, $k_s = 9k_0$ with $k_0 = (2\pi)/L$, which corresponds to frequency $f_1 = k_s^3/(2\pi) = 0.7$ Hz for a system of length $L = 11\pi$ and $f_2 = 1.7$ Hz. Also $\alpha = \beta = 1$. The PSD and the bicoherence show a peak at $P_8 = 2f_2$ (encircled) generated via a coherent nonlinear interaction.
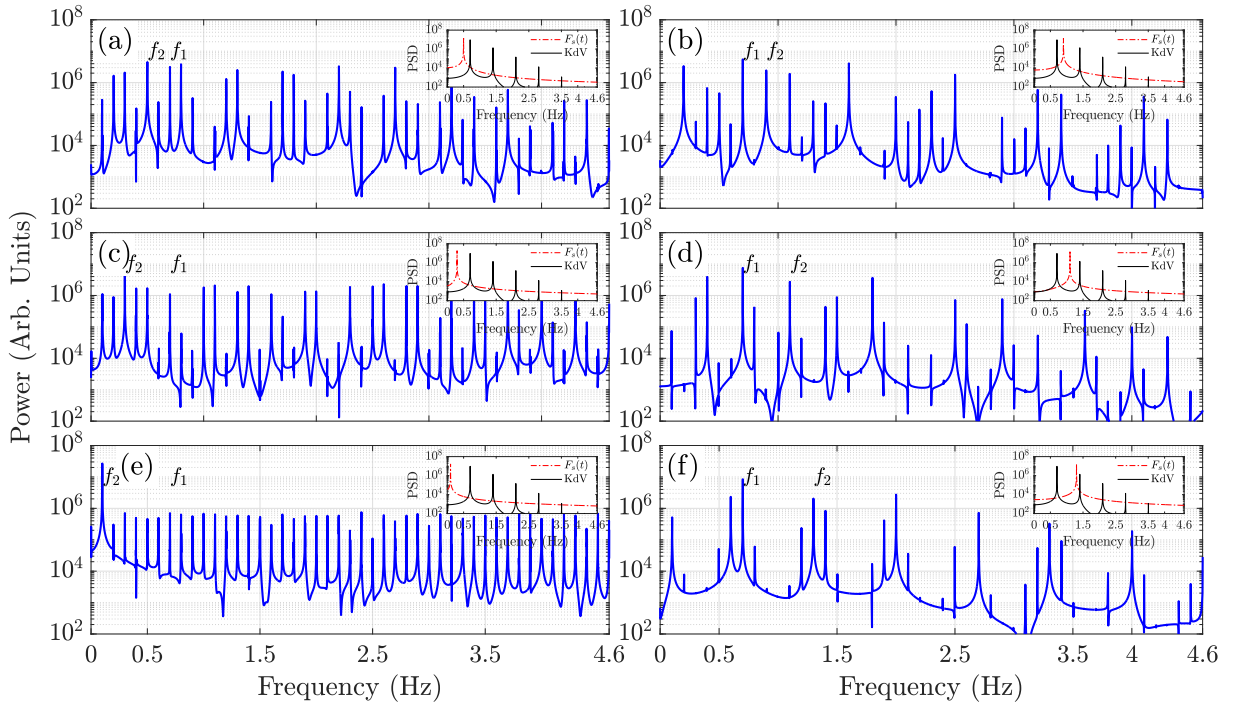


Figure 3.6: Tailoring the nonlinear mixing profiles of the fKdV model with forcing frequency $f_2 < f_1$ (left panel) and $f_2 > f_1$ (right panel). Left panel: (a, c, and e) with $f_2 = 0.5$ Hz, $f_2 = 0.3$ Hz and $f_2 = 0.1$ Hz, respectively. Right panel: (b, d, and f) with $f_2 = 0.9$ Hz, $f_2 = 1.1$ Hz and $f_2 = 1.3$ Hz, respectively. Insets in each case display the power spectrum of the KdV equation (black bold line) and forcing form (red dash-dotted line), $i.e.$, $F_s(t) = A_s \sin(2\pi f_2 t)$. Here $\alpha = \beta = 1$, $\mu = 18.5$, $\kappa = 0.7$ (such that $f_1 = 0.7$ Hz) and $A_s = \mu$ in each case.

this objective.

First, we varied the driver frequency $f_2$ towards lower or higher values than the system's natural frequency $f_1$. Second, we added specific additional frequency signals to enhance the power in the harmonics of the forcing profiles considered above. In the first case, we found that when the forcing frequency $f_2 < f_1$, where $f_1$ is the natural frequency of the KdV model, the resultant mixing pattern has a broad spectral form. This is seen in subplots (a), (c) and (e) of Fig. 3.6 for cases $f_2 = f_1 - 0.1$, $f_2 = f_1 - 0.3$ and $f_2 = f_1 - 0.5$ respectively. On the other hand, when the forcing frequency $f_2 > f_1$, the spectrum of the mixing pattern is sparse and contains fewer frequencies. This is shown in subplots (b), (d) and (f) of the Fig. 3.6 for cases $f_2 = f_1 + 0.1$, $f_2 = f_1 + 0.3$ and $f_2 = f_1 + 0.5$ respectively.
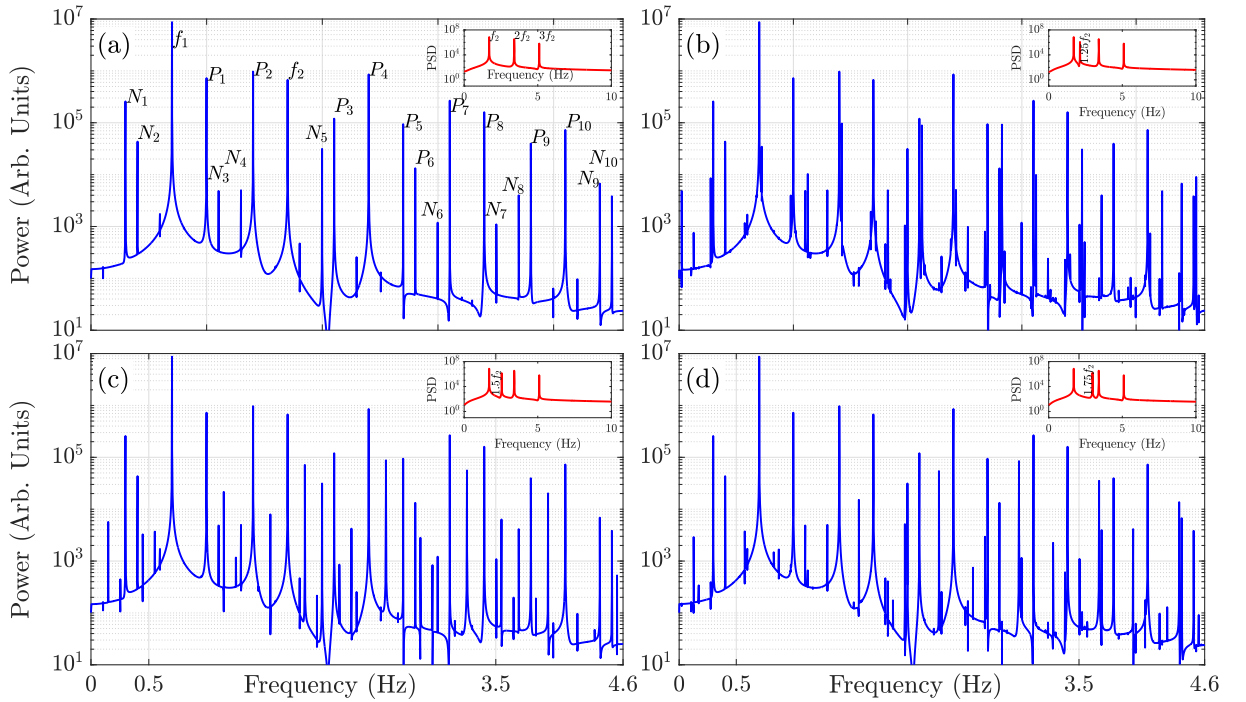


Figure 3.7: Tailoring the nonlinear mixing profiles by tuning the forcing form. The approximate form of cnoidal-square forcing as in [57] $F_s(t) = (A_s/2)\{\cos(2\pi f_2 t) + A_1 \cos(2\pi(2f_2)t) + A_2 \cos(2\pi(3f_2)t) + A_3 \cos(2\pi(f_T)t)\}$. (a) $A_3 = 0$, (b) $A_3 = 0.01A_s$, and $f_T = 1.25f_2$ Hz, (c) $A_3 = 0.01A_s$, and $f_T = 1.50f_2$ Hz, and (d) $A_3 = 0.01A_s$, and $f_T = 1.75f_2$ Hz. Here, $A_s = \mu$, $f_2 = 1.7$ Hz, $A_1 = 0.02A_s$ and $A_2 = 0.004A_s$ for each case.

Such an asymmetry in the nonlinear response of a system to the variation of the driver frequency towards or away from its natural frequency has been observed in other systems such as microwave mixers [245, 246]. The underlying physical mechanism responsible for this behaviour is a higher-order wave mixing phenomenon called inter-modulation distortion (IMD). Basically the output frequencies of the primary three-wave mixing, namely, $f_1 + f_2$, $f_1 - f_2$, $2f_1$ and $2f_2$, further mix with the primary modes $f_1$ and $f_2$ to give rise to 3rd order inter-modulation products such as $2f_1 - f_2$ and $2f_2 - f_1$. The 3rd order products may further lead to IMD if they are in proximity of the frequency of the primary modes $f_1$ and $f_2$. This higher-order IMD condition is better fulfilled for the condition $f_2 < f_1$ as compared to $f_2 > f_1$. This results in a broad mixing spectrum for the former case compared to the latter. The additional frequency content created by the 3rd order distortion is also known as "Spectral Regrowth" that has not

been observed before for the forced KdV model. Controlled regulation of such spectral regrowth through frequency tuning of the driver could prove useful in exploring the nonlinear characteristics of weakly dispersive and small amplitude nonlinear excitations in various plasma and fluid media.

We next discuss our second approach towards influencing the nature of the system response spectra by tuning the driver characteristics. As mentioned earlier, we had found that the effects of typical non-sinusoidal (*e.g.*, a cnoidal wave and a cnoidal-square wave) drivers on mixing were very similar to that of a sinusoidal driver (refer to Fig. 3.2), within a dominant frequency range. The standard driver limits both the amplitude and frequency of their harmonics, restricting the richness of nonlinear mixing. The non-sinusoidal drivers show dominant interactions because of their fundamental mode only, as the amplitudes of their harmonics drop significantly. Hence, in our second approach, we considered tuning the driver by externally pumping up the power in a frequency close to one of the harmonics of the driver. This is done by adding an extra sinusoidal component at a specific frequency and amplitude to the Fourier series representation of a non-sinusoidal forcing term.

Fig. 3.7(a) shows the time series spectrum obtained from fKdV with a cnoidal-square forcing. The spectrum is similar to the pure sinusoidal forcing case with an additional frequency at $P_8 = 2f_2$ due to the driver's inherent profile. The power at the first harmonic ($2f_2$) is significantly reduced and lies far away from the natural mode ($f_1$). Hence, the fundamental forcing mode ($f_2$) shows more interaction with the natural mode ($f_1$) and inhibits the interaction of the first harmonic with the natural mode. Figs. 3.7(b), 3.7(c) and 3.7(d) show the spectrum of mixing due to an extra tailoring mode ($f_T$) at $f_T = 1.25f_2$, $f_T = 1.50f_2$ and $f_T = 1.75f_2$ respectively, each with amplitude of $50\% A_{f_2}$, where $A_{f_2}$ is the amplitude of the fundamental mode. This results in a frequency bunching due to the fractional frequency mode (*i.e.*, the mode in between the fundamental mode and the first harmonic) close to the fundamental mode leading to an altered frequency spectrum. Thus both these techniques offer one a simple but effective means of tailoring the response spectrum of the driven KdV system.

Table 3.3: Phase coherent modes observed in bicoherence for different forcing forms given in Table 3.1.

| (I) | (II) | (III) | (IV) | (V) | (VI) | (VII) | (VIII) |
|---|---|---|---|---|---|---|---|
| $F_1$ (Hz) | $F_2$ (Hz) | $F_1 + F_2$ (Hz) | Interpretation | $F_{\sin}(t)$ | $F_{cn}(t)$ | $F_{cn^2}(t)$ | $F_s(x,t)$ |
| $f_2 - f_1$ | $f_1$ | $f_2 - f_1$ | $P_1^\star$ | ✓ | ✓ | ✓ | ✓ |
| $f_1$ | $f_1$ | $2f_1$ | $P_2$ | ✓ | ✓ | ✓ | ✓ |
| $2f_1$ | $f_1$ | $3f_1$ | $P_3$ | ✓ | ✓ | ✓ | ✓ |
| $f_2$ | $f_1$ | $f_1 + f_2$ | $P_4$ | ✓ | ✓ | ✓ | ✓ |
| $2f_1$ | $f_2 - f_1$ | $f_1 + f_2$ | $P_4$ | ✓ | ✓ | ✓ | ✓ |
| $f_2$ | $f_2 - f_1$ | $2f_2 - f_1$ | $P_5$ | ✓ | ✓ | ✓ | ✓ |
| $3f_1$ | $f_1$ | $4f_1$ | $P_6$ | ✓ | ✓ | ✓ | ✓ |
| $2f_1$ | $2f_1$ | $4f_1$ | $P_6$ | ✓ | ✓ | ✓ | ✓ |
| $f_1 + f_2$ | $f_1$ | $2f_1 + f_2$ | $P_7$ | ✓ | ✓ | ✓ | ✓ |

| | | | | | | | |
|---|---|---|---|---|---|---|---|
| $3f_1$ | $f_2 - f_1$ | $2f_1 + f_2$ | $P_7$ | ✓ | ✓ | ✓ | ✓ |
| $f_2$ | $2f_1$ | $2f_1 + f_2$ | $P_7$ | ✓ | ✓ | ✓ | ✓ |
| $f_2$ | $f_2$ | $2f_2$ | $P_8$ | | | ✓ | ✓ |
| $2f_2 - f_1$ | $f_1$ | $2f_2$ | $P_8$ | | | ✓ | ✓ |
| $f_2 + f_1$ | $f_2 - f_1$ | $2f_2$ | $P_8$ | | | ✓ | ✓ |
| $2f_1 + f_2$ | $f_1$ | $3f_1 + f_2$ | $P_9$ | ✓ | ✓ | ✓ | ✓ |
| $4f_1$ | $f_2 - f_1$ | $3f_1 + f_2$ | $P_9$ | ✓ | ✓ | ✓ | ✓ |
| $f_1 + f_2$ | $2f_1$ | $3f_1 + f_2$ | $P_9$ | ✓ | ✓ | ✓ | ✓ |
| $3f_1$ | $f_2$ | $3f_1 + f_2$ | $P_9$ | ✓ | ✓ | ✓ | ✓ |
| $2f_2$ | $f_1$ | $f_1 + 2f_2$ | $P_{10}$ | | | ✓ | ✓ |
| $2f_1 + f_2$ | $f_2 - f_1$ | $f_1 + 2f_2$ | $P_{10}$ | ✓ | ✓ | ✓ | ✓ |
| $2f_2 - f_1$ | $2f_1$ | $f_1 + 2f_2$ | $P_{10}$ | ✓ | ✓ | ✓ | ✓ |
| $f_1 + f_2$ | $f_2$ | $f_1 + 2f_2$ | $P_{10}$ | ✓ | ✓ | ✓ | ✓ |
| $f_1$ | $f_2 - 2f_1$ | $f_2 - 2f_1$ | $N_1^\star$ | ✓ | ✓ | ✓ | ✓ |
| $2f_1$ | $f_2 - 2f_1$ | $f_2 - 2f_1$ | $N_1^\star$ | ✓ | ✓ | ✓ | ✓ |
| $3f_1$ | $f_2 - 2f_1$ | $f_2 - 2f_1$ | $N_1^\star$ | ✓ | ✓ | ✓ | ✓ |
| $f_2 + f_1$ | $f_2 - 2f_1$ | $f_2 - 2f_1$ | $N_1^\star$ | ✓ | ✓ | ✓ | ✓ |
| $4f_1$ | $f_2 - 2f_1$ | $f_2 - 2f_1$ | $N_1^\star$ | ✓ | ✓ | ✓ | ✓ |
| $2f_1 + f_2$ | $f_2 - 2f_1$ | $f_2 - 2f_1$ | $N_1^\star$ | | | ✓ | ✓ |
| $3f_1 + f_2$ | $f_2 - 2f_1$ | $f_2 - 2f_1$ | $N_1^\star$ | ✓ | ✓ | ✓ | ✓ |
| $3f_1 - f_2$ | $f_2 - 2f_1$ | $3f_1 - f_2$ | $N_2^\star$ | ✓ | ✓ | ✓ | ✓ |
| $f_2 - f_1$ | $3f_1 - f_2$ | $3f_1 - f_2$ | $N_2^\star$ | ✓ | ✓ | ✓ | ✓ |
| $f_2$ | $3f_1 - f_2$ | $3f_1 - f_2$ | $N_2^\star$ | ✓ | ✓ | ✓ | ✓ |
| $f_1 + f_2$ | $3f_1 - f_2$ | $3f_1 - f_2$ | $N_2^\star$ | ✓ | ✓ | ✓ | ✓ |
| $2f_2 - f_1$ | $3f_1 - f_2$ | $3f_1 - f_2$ | $N_2^\star$ | ✓ | ✓ | ✓ | ✓ |
| $2f_2$ | $3f_1 - f_2$ | $3f_1 - f_2$ | $N_2^\star$ | | | ✓ | ✓ |
| $f_1$ | $3f_1 - f_2$ | $4f_1 - f_2$ | $N_3$ | ✓ | ✓ | ✓ | ✓ |
| $4f_1 - f_2$ | $f_2 - 2f_1$ | $4f_1 - f_2$ | $N_3^\star$ | ✓ | ✓ | ✓ | ✓ |
| $4f_1 - f_2$ | $f_2 - f_1$ | $4f_1 - f_2$ | $N_3^\star$ | ✓ | ✓ | ✓ | ✓ |
| $f_2$ | $4f_1 - f_2$ | $4f_1 - f_2$ | $N_3^\star$ | ✓ | ✓ | ✓ | ✓ |
| $2f_2 - f_1$ | $4f_1 - f_2$ | $4f_1 - f_2$ | $N_3^\star$ | ✓ | ✓ | ✓ | ✓ |
| $f_2 - f_1$ | $f_2 - 2f_1$ | $2f_2 - 3f_1$ | $N_4$ | ✓ | ✓ | ✓ | |
| $2f_2 - 3f_1$ | $3f_1 - f_2$ | $2f_2 - 3f_1$ | $N_4^\star$ | ✓ | ✓ | ✓ | |
| $2f_2 - 3f_1$ | $4f_1 - f_2$ | $2f_2 - 3f_1$ | $N_4^\star$ | ✓ | ✓ | ✓ | |
| $2f_1$ | $2f_2 - 3f_1$ | $2f_2 - 3f_1$ | $N_4^\star$ | ✓ | ✓ | ✓ | |
| $3f_1$ | $2f_2 - 3f_1$ | $2f_2 - 3f_1$ | $N_4^\star$ | | | ✓ | |
| $4f_1$ | $2f_2 - 3f_1$ | $2f_2 - 3f_1$ | $N_4^\star$ | ✓ | ✓ | ✓ | |

| | | | | | | | |
|---|---|---|---|---|---|---|---|
| $f_2$ | $f_2 - 2f_1$ | $2(f_2 - f_1)$ | $N_5$ | ✓ | ✓ | ✓ | |
| $2(f_2 - f_1)$ | $3f_1 - f_2$ | $2(f_2 - f_1)$ | $N_5^\star$ | ✓ | ✓ | ✓ | |
| $2f_2 - 3f_1$ | $f_1$ | $2(f_2 - f_1)$ | $N_5$ | ✓ | ✓ | ✓ | |
| $2(f_2 - f_1)$ | $f_1$ | $2(f_2 - f_1)$ | $N_5^\star$ | ✓ | ✓ | ✓ | |
| $f_2 - f_1$ | $f_2 - f_1$ | $2(f_2 - f_1)$ | $N_5$ | ✓ | ✓ | ✓ | |
| $2(f_2 - f_1)$ | $4f_1 - f_2$ | $2(f_2 - f_1)$ | $N_5^\star$ | ✓ | ✓ | ✓ | |
| $2(f_2 - f_1)$ | $2f_1$ | $2(f_2 - f_1)$ | $N_5^\star$ | | | ✓ | |
| $3f_1$ | $2(f_2 - f_1)$ | $2(f_2 - f_1)$ | $N_5^\star$ | ✓ | ✓ | ✓ | |
| $2f_2 - f_1$ | $f_2 - 2f_1$ | $3(f_2 - f_1)$ | $N_6$ | ✓ | ✓ | ✓ | ✓ |
| $3(f_2 - f_1)$ | $3f_1 - f_2$ | $3(f_2 - f_1)$ | $N_6^\star$ | | | ✓ | ✓ |
| $2(f_2 - f_1)$ | $f_2 - f_1$ | $3(f_2 - f_1)$ | $N_6$ | ✓ | ✓ | ✓ | ✓ |
| $3(f_2 - f_1)$ | $4f_1 - f_2$ | $3(f_2 - f_1)$ | $N_6^\star$ | ✓ | ✓ | ✓ | ✓ |
| $f_2$ | $2f_2 - 3f_1$ | $3(f_2 - f_1)$ | $N_6$ | ✓ | ✓ | ✓ | ✓ |
| $2f_1 + f_2$ | $3f_1 - f_2$ | $5f_1$ | $N_7$ | ✓ | ✓ | ✓ | ✓ |
| $5f_1$ | $f_2 - 2f_1$ | $5f_1$ | $N_7^\star$ | ✓ | ✓ | ✓ | ✓ |
| $4f_1$ | $f_1$ | $5f_1$ | $N_7$ | ✓ | ✓ | ✓ | ✓ |
| $f_1 + f_2$ | $4f_1 - f_2$ | $5f_1$ | $N_7$ | ✓ | ✓ | ✓ | ✓ |
| $3f_1$ | $2f_1$ | $5f_1$ | $N_7$ | ✓ | ✓ | ✓ | ✓ |
| $2f_2$ | $f_2 - 2f_1$ | $3f_2 - 2f_1$ | $N_8$ | | | ✓ | ✓ |
| $3f_2 - 2f_1$ | $3f_1 - f_2$ | $3f_2 - 2f_1$ | $N_8^\star$ | ✓ | ✓ | ✓ | ✓ |
| $3(f_2 - f_1)$ | $f_1$ | $3f_2 - 2f_1$ | $N_8$ | ✓ | ✓ | ✓ | ✓ |
| $f_1 + f_2$ | $2f_2 - 3f_1$ | $3f_2 - 2f_1$ | $N_8$ | ✓ | ✓ | ✓ | ✓ |
| $2(f_2 - f_1)$ | $2f_2 - 3f_1$ | $3f_2 - 2f_1$ | $N_8$ | ✓ | ✓ | ✓ | ✓ |
| $2(f_2 - f_1)$ | $f_2$ | $3f_2 - 2f_1$ | $N_8$ | ✓ | ✓ | ✓ | ✓ |
| $2f_2 + f_1$ | $f_2 - 2f_1$ | $3f_2 - f_1$ | $N_9$ | ✓ | ✓ | ✓ | ✓ |
| $3f_2 - 2f_1$ | $f_1$ | $3f_2 - f_1$ | $N_9$ | ✓ | ✓ | ✓ | ✓ |
| $2f_2$ | $f_2 - f_1$ | $3f_2 - f_1$ | $N_9$ | | | ✓ | ✓ |
| $2f_1 + f_2$ | $2f_2 - 3f_1$ | $3f_2 - f_1$ | $N_9$ | ✓ | ✓ | ✓ | ✓ |
| $3(f_2 - f_1)$ | $2f_1$ | $3f_2 - f_1$ | $N_9$ | ✓ | ✓ | ✓ | ✓ |
| $2f_2 - f_1$ | $f_2$ | $3f_2 - f_1$ | $N_9$ | ✓ | ✓ | ✓ | ✓ |
| $f_1 + f_2$ | $2(f_2 - 2f_1)$ | $3f_2 - f_1$ | $N_9$ | ✓ | ✓ | ✓ | ✓ |
| $2f_2 + f_1$ | $3f_1 - f_2$ | $4f_1 + f_2$ | $N_{10}$ | ✓ | ✓ | ✓ | ✓ |
| $3f_1 + f_2$ | $f_1$ | $4f_1 + f_2$ | $N_{10}$ | ✓ | ✓ | ✓ | ✓ |
| $5f_1$ | $f_2 - f_1$ | $4f_1 + f_2$ | $N_{10}$ | ✓ | ✓ | ✓ | ✓ |
| $2f_2$ | $4f_1 - f_2$ | $4f_1 + f_2$ | $N_{10}$ | | | ✓ | ✓ |
| $2f_1 + f_2$ | $2f_1$ | $4f_1 + f_2$ | $N_{10}$ | ✓ | ✓ | ✓ | ✓ |
| $f_1 + f_2$ | $3f_1$ | $4f_1 + f_2$ | $N_{10}$ | ✓ | ✓ | ✓ | ✓ |

## 3.6 Summary

To summarize, we have carried out a detailed numerical study of the driven response of a model KdV equation to a variety of driving sources that range from a simple time-varying sine wave to a spatio-temporally varying plane wave to nonlinear cnoidal waveforms. One of the first objectives of this study is to firmly establish the nature of the process underlying the wave mixing taking place in the system. An earlier study [169], using a simple time-varying sinusoidal driver, had concluded that three-wave couplings were responsible for the wave mixing in the system. The conclusion was based on identifying some of the combination frequencies in the power spectrum of the nonlinear fluctuations. However, the power spectrum information alone is not sufficient to establish the existence of a three-wave coupling event. This is because the power spectrum does not have phase coupling information about the interactions. A more precise tool for establishing the existence of three-wave coupling is a bispectral analysis that looks at the triple correlation of the time series of any dynamical quantity. A finite correlation is obtained for a frequency triad when they are formed by a coherent phase coupling mechanism. In this work, we have subjected the earlier data of Ref. [169] to bispectral analysis and have confirmed that the mixing process arising from a simple time-varying sinusoidal driver is indeed due to three-wave interactions.

We have next gone on to generalize the findings of Ref. [169] by changing the nature of the driving source and studying the impact of such changes on the mixing process. In particular, we have chosen time-varying nonlinear drivers in the form of cnoidal waves and the square of cnoidal waves and compared the resultant power spectra and bicoherence spectra with those of the purely sinusoidal driver. The absence of certain spectral lines or the presence of new ones in the response spectra have been identified, and their origin is traced to the changing nature of the natural spectra of the nonlinear driving terms. We have also considered a linear driving term with both a temporal and spatial variation and constitutes a travelling waveform. In this case, we find an additional response frequency that was not present in the case of the sinusoidal driver but had been experimentally observed in Ref. [15]. This is not surprising as the sine wave driver, in the earlier model calculation, was adopted as an approximation to the long wavelength $(k \rightarrow 0)$ dust acoustic wave that had been excited in the experimental system by an external laser. Such external perturbations can also give rise to a nonlinear excitation *e.g.,* as a cnoidal wave that can then act as a driver of the KdV system. Thus both the nonlinear waveforms and the travelling waveform considered as drivers in our model calculation can find useful applications in experimental scenarios.

Looking at the sensitivity of the response spectra to the nature of the driver, we have further extended our explorations to alter not just the form of the driver but also the frequency of the driver with respect to the natural frequency of the KdV system. Our results point to a novel means of altering the spectral density of the response spectra by manipulating the driver frequency to be smaller or larger than the system's natural frequency or by artificially injecting power in the driver at a frequency that is somewhat removed from its fundamental frequency. The physical origin of these spectral changes lies in higher-order wave interactions that can create additional frequencies and alter the spectrum's nature.

Finally, we would like to remark that our results have broad applicability and relevance for understanding nonlinear phenomena in plasmas. Nonlinear mixing is at the heart of wave-wave interactions in plasmas [10] and is responsible for such processes as harmonic generation parametric instabilities [247], the onset of weak turbulence, *etc.*. Such interactions have been widely studied in the context of laser heating of plasmas [248], radiofrequency heating in magnetic confinement devices [249, 250], and understanding a variety of electrostatic and electromagnetic fluctuations in space plasmas [9]. One of the principal objectives of such studies is identifying the precise nature of the wave-wave interaction responsible for a particular phenomenon. This becomes a challenging task because many of the nonlinear phenomena often take place simultaneously. The bispectral analysis is a convenient and accurate tool for carrying out such an analysis. The KdV-based model used in our analysis is a convenient semi-analytic framework for demonstrating the power and utility of this diagnostic. The conclusions are by no means limited to this model. They are also applicable to any physical scenario where an external (or internally generated) wave drives the plasma and induces nonlinear wave mixing. Our present results can be the basis for understanding nonlinear mixing in plasma systems that are weakly nonlinear and weakly dispersive. Such plasma systems are widely found in space and laboratory setups and have served as convenient media for the study of solitons and other coherent structures. We hope that our work will stimulate further theoretical work in extending the present studies to plasma models of higher dimensions and stronger nonlinearities.

In this chapter, we have identified the physical origin of the modes using the bispectral analysis and found them an outcome of three-wave mixing. We also extended the mathematical model to include any form of periodic forcing form, sinusoidal, cnoidal, or travelling waveform. Dusty plasma, the physical system we use as a testbed for studies, has a unique property to show traits of different phases and their intermediate states. The present model needs more flexibility to explore all such phases to understand nonlinear mixing comprehensively. For this purpose, we have carried out a kinetic study based on the Langevin molecular dynamics simulation to understand the nonlinear mixing of DLWs in strongly coupled plasma where dust particles interact via Yukawa or Debye-Hückel pair-wise interaction potential.

# Chapter 4

# Nonlinear Mixing of Dust Lattice Waves in Strongly Coupled Dusty Plasma

In this chapter, in pursuit of analyzing nonlinear mixing in dusty plasma using a kinetic approach, we treat them as an ensemble of charged particles interacting via pairwise Debye-Hückel form of potential. This kinetic system evolution is then studied using classical molecular dynamics simulations. This simulation model includes viscosity as an inherent property and has the flexibility to include the neutral drag explicitly via Langevin dynamics. The model intrinsically includes correlation effects controlled by dust species' charge, density, and temperature. The presented results in the fluid regime of dusty plasma are in excellent synchrony with the experimental and fKdV-based model proposed in Chapters 2, 3. As a future scope, we plan to extend molecular dynamics model-based studies to visualize the effects of correlations, drag, and background shielding.

## 4.1 Introduction

The dusty plasma medium is treated as an ensemble of charged particles interacting via a Yukawa pair-wise potential. We have studied the nonlinear mixing of waves in such a system using kinetic simulations based on the Langevin molecular dynamics (MD) simulations. In the present work, we have carried out the two-dimensional classical Langevin simulations to study the nonlinear mixing of two lattice waves in YOCP. The coherent nonlinear interaction in the excited modes is primarily due to a three-wave coupling mechanism, confirmed using the bispectral analysis. In this chapter, we will see how the kinetic nature affects the mixing patterns in a dusty plasma medium. We will establish a link between the fluid-based fKdV model and the kinetic approach based on the MD simulations for mixing dust lattice waves in a dusty plasma. Interestingly, we found that the fKdV model shows a good agreement with the kinetic simulations of the YOCP based on the Langevin MD simulations.

The strongly coupled plasmas (SCPs), in which the Coulomb interaction energy exceeds the thermal energy, are often modelled as one-component plasmas, which include pure Coulomb and screened Coulomb (Yukawa) systems [181]. The Coulomb coupling parameter $\Gamma$ characterises the frictionless pure Coulomb systems in thermodynamic equilibrium. In contrast, the Yukawa systems are characterised by the Debye screening parameter $\kappa_D$ and Coulomb coupling parameter $\Gamma$ [251, 252]. Studying the frictional Coulomb and Yukawa systems' thermodynamic equilibrium requires one additional parameter, the frictional damping rate $\nu$. The characteristic length scale of OCPs in 2D is characterised by the average inter-particle separation or the Wigner-Seitz radius $a = (\pi n)^{-1/2}$, where $n$ is the areal number density of particles. The time evolution dynamics of OCP in 2D is characterised by the inverse of its characteristic frequency $\omega_{pd} = \sqrt{nQ_d^2/(2a\epsilon_0 M_d)}$, where $Q_d$ and $M_d$ are the charge and mass of the particles. The phase-transition in OCP is characterised by strong coupling parameter $\Gamma$ and Debye screening/shielding parameter $\kappa$ The effective coupling strength $\Gamma^\star = \Gamma \exp(-\kappa_D)$ [253] due to the screening effect of charges. The effective coupling strength $\Gamma^\star = \Gamma(1 + \kappa_D + \kappa_D^2/2) \exp(-\kappa_D)$ was also proposed [254] and whose value alone determines the location of melting line in dusty plasma. The limit $\kappa_D \to 0$ represents a pure Coulomb system while the limit $\kappa_D \to \infty$ represents the hard-sphere-like interactions.

A rich variety of Yuwaka/Debye-Hückel systems exists in nature that includes soft-matter systems like colloid suspensions [255–257], charged colloids [258–262] and bio-molecules [263, 264]; plasmas like quark-gluon plasma [265, 266], dusty plasma [267], and ultracold plasma [268, 269]; and many ionic-liquids [270, 271]. A vast literature is available where different collective phenomena observed in dusty plasma are often modelled using the Yukawa potential [15, 131, 272, 273]. Recently, the KdV-type solitons in dusty plasma modelled by Yukawa interaction are revealed using MD simulations [274, 275]. We will also model the dusty plasma using kinetic simulations in which the particles interact via Yukawa pair-wise interaction and try to figure out the resemblance of the mixing profiles in YOCP as were found in the fKdV model.

The work is organized into three sections. The Langevin MD simulations are discussed in section 4.2. The PSD and bispectral analysis of the velocity-squared times series is explained in section 4.3. Finally,

the work done in this chapter is summarized in section 4.4.

## 4.2 Langevin molecular dynamics simulations

The 2D Langevin MD simulations [15, 276–279] have been performed using open-source Large-scale Atomic/Molecular Massively Parallel Simulator (LAMMPS) [280] code to study the dynamics of particles in strongly coupled Yukawa fluids. The Langevin dynamics models collisions with neutral atoms, providing frictional drag and random kicks. The Langevin simulations consider the dissipation due to frictional gas damping, which is evident in experimental scenarios. To model the experimental configuration, we suppose that the wave is excited by a localized external perturbation force $F_L$ and the particles are confined by an external confinement force $F_C$ at the boundaries in the x-direction. The Langevin equation of motion, which mimics the dynamics of each particle in frictional Yukawa fluids along with laser external excitation and confinement forces, is given by

$$M_d \ddot{\mathbf{r}} = -\nabla \phi^Y - m\bar{\nu}\dot{\mathbf{r}} + \xi(t) + F_L + F_C. \tag{4.1}$$

The particle trajectories $\mathbf{r}(t)$ are generated for all particles by integrating Eq. (4.1) using standard Langevin dynamics [281]. The repulsive Yukawa/Debye-Hückel [282, 283] interaction potential, which is the only source of nonlinearity, between the particles of mass $M_d$ and charges $Q_d$ separated by a distance $r$ and is given by

$$\phi^Y(r) = \frac{Q_d^2}{4\pi\epsilon_0 r} \exp(-r/\lambda_D). \tag{4.2}$$

The system is confined on the left and right boundaries by the Gaussian profile force of the form [284, 285]

$$F_C^{Left} = A_C^{Left} \exp(-(x - x_C^{Left})^2/\sigma^2); \tag{4.3}$$

$$A_C^{Left} = 100 \ ma\omega_{pd}^2, x_C^{Left} = 0, \sigma = 2a.$$

$$F_C^{Right} = A_C^{Right} \exp(-(x - x_C^{Right})^2/\sigma^2); \tag{4.4}$$

$$A_C^{Right} = 100 \ ma\omega_{pd}^2, x_C^{Right} = L_x, \sigma = 2a.$$

The wave is excited by laser force by taking a Gaussian profile of the form [286]

$$F_L^{f_1} = A_L^{f_1} \exp(-(x - x_L^{f_1})^2/\sigma^2) \left[1 - \cos(2\pi f_1 t)\right]; \tag{4.5}$$

$$A_L^{f_1} = 0.25 \ ma\omega_{pd}^2, x_L^{f_1} = 0.2L_x, \sigma = 2a.$$

$$F_L^{f_2} = A_L^{f_2} \exp(-(x - x_L f_2)^2/\sigma^2) \left[1 - \cos(2\pi f_2 t)\right]; \tag{4.6}$$

$$A_L^{f_2} = 0.25 \ ma\omega_{pd}^2, x_L^{f_2} = 0.8L_x, \sigma = 2a.$$

The term $m\bar{\nu}\dot{\mathbf{r}}$ is the neutral drag force with neutral drag coefficient $\bar{\nu}$ and $\xi(t)$ is the random Brownian/Langevin force due to random kicking of neutral gas molecules [276, 278]. We assume that the random force $\xi(t)$ has Gaussian distribution with zero mean *i.e.,* $\langle\xi(t)\rangle = 0$. In the Langevin simulation,

Table 4.1: Particle parameters for the Langevin MD simulations.

| Particle parameter | Rectangular configuration ($L_x = 10L_y$) |
|---|---|
| No. of particles, $N$ | $10^4$ |
| Number density, $n$ | $2.923 \times 10^6$ m$^{-2}$ |
| Charge of particle, $Q$ | $16 \times 10^3$ e<br>e = Electron charge |
| Mass of particle, $m$ | $6.9 \times 10^{-13}$ kg |

the heating quantified by temperature $T_d$ and friction quantified by friction coefficient $\bar{\nu}$ is explicitly coupled by the fluctuation-dissipation theorem. In other words, the frictional drag and Langevin kick in combination act as a heat bath and are coupled through the fluctuation-dissipation theorem.

According to the fluctuation-dissipation theorem, the magnitude of random force, characterized by the width of force, helps to achieve the desired temperature $T_d$ [287–289]

$$\langle \xi_{i\alpha}(0)\xi_{j\beta}(t)\rangle = 2k_B T_d m \bar{\nu} \delta(t) \delta_{ij} \delta_{\alpha\beta}, \tag{4.7}$$

where the Dirac delta function $\delta(t)$ indicates localized nature of the random force $\xi(t)$ in time. $\delta_{ij}$ and $\delta_{\alpha\beta}$ are the Kronecker delta symbols with $i, j \in \{1, ..., N\}$ are particle indices and $\alpha, \beta \in \{x, y\}$ denote space-coordinates. $\langle \xi_{i\alpha}(0)\xi_{j\beta}(t)\rangle$ is the standard deviation of Gaussian white noise $\xi(t)$. Therefore in thermodynamic equilibrium, the system is completely described by three dimensionless parameters: the inverse Debye screening length $\kappa_D$, the friction coefficient $\nu = \bar{\nu}/\omega_{pd}$ and the Coulomb coupling parameter $\Gamma$.
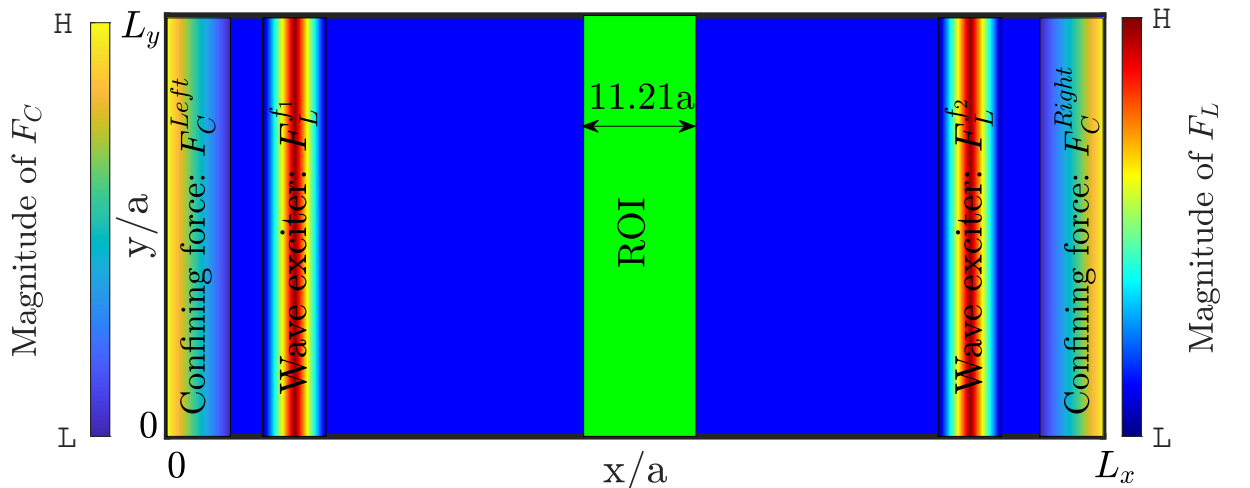


Figure 4.1: A cartoon to study NLM using the Langevin simulation in LAMMPS. The system is bound at $x = 0$ and $x = L_x$ by confining force $F_C$. Two waves are excited by laser forces $F_L$, each with a different frequency. Both the $F_C$ and $F_L$ are Gaussian in nature. Periodic boundary conditions are imposed along the y-direction. The region-of-interest (ROI) used to collect time series is the green-coloured region at the centre of the rectangular ($L_x = 10L_y$) simulation box.

To carry out the Langevin MD simulations using LAMMPS, we created a rectangular box ($L_x = 10L_y$) with periodic boundary conditions in the y-direction and reflecting boundary conditions in the x-direction. To begin with, we created point-charged particles homogeneously distributed inside the box with the particle parameters given in Table 4.1. Further, we gave random velocity to the particles corresponding to temperature $T_d$. To study a dynamical system at a particular coupling strength $\Gamma$ (corresponding to temperature $T_d$), we let it evolve along with Nosé-Hoover [290, 291] thermostat (under NVT condition). We found that 400 $\omega_{pd}^{-1}$ is a reasonable time for the system to attain an equilibrium around this temperature. As a next step, we let the system evolve freely (under NVE conditions) for another 400 $\omega_{pd}^{-1}$ after detaching it from the thermostat. During this phase of evolution, we use the system for energy conservation and its equilibrium maintenance around desired temperature $T_d$. We found the total energy conserved up to $10^{-2}\%$. We also validate the system by calculating the RDF and comparing it with available results in the literature for similar systems. The Langevin thermostat was also imposed during the NVE evolution.

## 4.3 Bispectral analysis of NLM in strongly coupled dusty plasma

The Langevin molecular dynamics simulation has been carried out to study NLM in strongly coupled YOCP. We have excited two waves of frequency $f_1 = 0.7$ Hz and $f_2 = 1.7$ Hz with laser forces modelled theoretically. The Langevin dynamics is used to maintain the temperature of dust species and include the effects of dust-neutral collisions. The speciality of MD simulations is that we can know the complete information about the phase-space of the system by solving Newton's equation of motion for each particle in the ensemble.

The system is equilibrated under the Langevin dynamics till it attains the desired temperature and maintains the thermal equilibrium corresponding to a chosen strong coupling parameter $\Gamma$. Then we performed the non-equilibrium simulations to study the mixing of waves in the ensemble of particles. We created three regions in a rectangular box with confined boundaries in the wave propagation direction and periodic boundary conditions at other boundaries. Two regions were used for wave excitation by laser force, and one region was used to download the velocity time-series of the evolution called the region-of-interest (ROI) shown in Fig. 4.1.

As a benchmark test, we first excite one wave to find out the nature and frequency of the wave by turning on only one laser beam and running the simulation for a sufficient time. After validation, we turned on both lasers to study mixing due to the two waves simultaneously at two locations shown in Fig. 4.1. The time-series of the system's evolution was collected in the ROI. The PSD was used to study the mixing frequency spectrum, and bicoherence was calculated to establish the physical origin of different modes in the mixing profiles.

Figure 4.2 shows the PSD (a) and bicoherence (b) of mixing of lattice waves using Langevin MD simulations with two laser wave exciter in Yukawa fluids. The nonlinear interaction is due to the three-
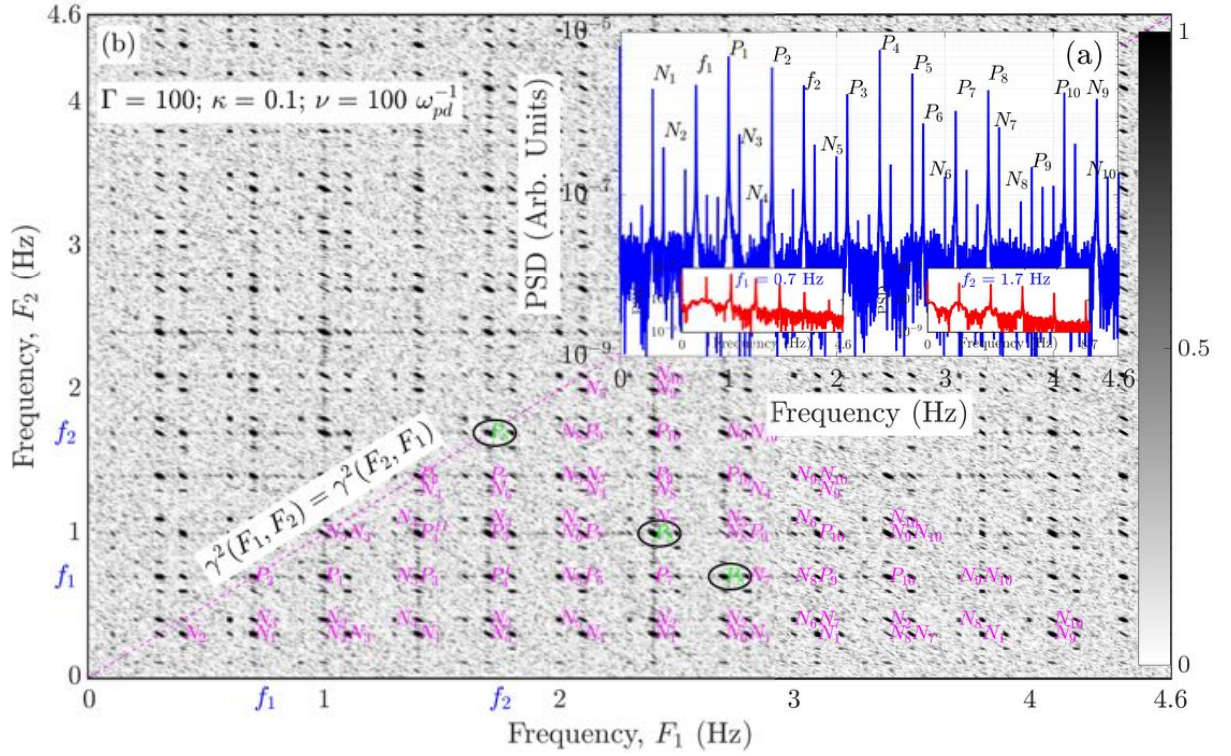
Figure 4.2: NLM in strongly coupled YOCP using the Langevin MD simulations. (a) PSD and (b) bicoherence of the time-series obtained in YOCP for $\Gamma = 100$, $\kappa = 0.1$ and damping rate $\nu = 100\ \omega_{pd}^{-1}$. The small insets show the PSD of individual waves with frequency $f_1 = 0.7$ Hz and $f_2 = 1.7$ Hz.

wave mixing mechanism, confirmed using bispectral analysis. The Langevin MD simulations show an excellent agreement with our earlier proposed fKdV model [45] in a weak screening regime ($\kappa = 0.1$). Table 4.2 show the dominant frequency spectrum observed in the YOCP and the fKdV model [45].

Table 4.2: Dominant frequencies observed in the fKdV model [45] and the Langevin MD simulations of YOCP.

| Frequency (Hz) | fKdV [45] | YOCP | Frequency (Hz) | fKdV [45] | YOCP |
|---|---|---|---|---|---|
| $f_1$ | 0.7 | 0.7 | $P_{10} = 2f_2 + f_1$ | ✓ | ✓ |
| $f_2$ | 1.7 | 1.7 | $N_1 = f_2 - 2f_1$ | ✓ | ✓ |
| $P_1 = f_2 - f_1$ | ✓ | ✓ | $N_2 = 3f_1 - f_2$ | ✓ | ✓ |
| $P_2 = 2f_1$ | ✓ | ✓ | $N_3 = 4f_1 - f_2$ | ✓ | ✓ |
| $P_3 = 3f_1$ | ✓ | ✓ | $N_4 = 2f_2 - 3f_1$ | ✓ | ✓ |
| $P_4 = f_1 + f_2$ | ✓ | ✓ | $N_5 = 2(f_2 - f_1)$ | ✓ | ✓ |
| $P_5 = 2f_2 - f_1$ | ✓ | ✓ | $N_6 = 3(f_2 - f_1)$ | ✓ | ✓ |
| $P_6 = 4f_1$ | ✓ | ✓ | $N_7 = 5f_1$ | ✓ | ✓ |
| $P_7 = 2f_1 + f_2$ | ✓ | ✓ | $N_8 = 3f_2 - 2f_1$ | ✓ | ✓ |
| $P_8 = 2f_2$ | ✓ | ✓ | $N_9 = 3f_2 - f_1$ | ✓ | ✓ |
| $P_9 = 3f_1 + f_2$ | ✓ | ✓ | $N_{10} = 4f_1 + f_2$ | ✓ | ✓ |

We have used M = 4096 sampling data points and N = 8 time-series segments so that the total length of a time series was $K = M \times N$ to get the bicoherence of the times series obtained from the MD simulations. A statistically significant correlation between the coherent modes is determined by the condition $\gamma^2 > \sqrt{6/2N} = 0.6124$ [232]. The fKdV model shows a similar frequency and bicoherence with the same two frequencies $f_1 = 0.7$ Hz and $f_2 = 1.7$ Hz. Table 4.2 shows the dominant frequencies obtained in the fKdV model [45] and the current Langevin MD simulations for YOCP.

We have found an excellent agreement between the Langevin simulations and the fKdV model. The Langevin MD simulations show an excellent agreement with our earlier proposed fKdV model [45]. However, there is a difference between the fKdV model and the Langevin MD simulations, possibly due to the neutral gas damping in the latter case.

## 4.4 Summary

We have reported nonlinear mixing in strongly coupled Yukawa one-component plasma using two-dimensional classical Langevin molecular dynamics simulations. The Langevin dynamics relaxes all modes indiscriminately regardless of their wavelength. The mixing patterns observed in the Langevin MD simulations in weak screening regime ($\kappa = 0.1$) are in agreement with the fKdV model [45]. A cascade of modes generated by the nonlinear interaction of two DLWs in the YOCP is revealed through the PSD of the times-series obtained from the Langevin simulations. Also, the coherent nonlinear interaction is primarily due to the three-wave mixing mechanism, confirmed using the bispectral analysis. The kinetic origin of the nonlinear mixing lie in the nonlinear pair-wise Yukawa interaction, which is the only source of nonlinearity at the kinetic level.

In this chapter, we extended nonlinear mixing studies from the fluid-based model to the kinetic model of dusty plasma that includes the effect of viscosity, neutral drag, and correlations. The study has much of future scope and will be worked upon separately. In the next chapter, we return to the fluid-based model and study characteristic synchronization features in dusty plasma by including viscous damping. The model we present is the first to include fluid-like nonlinearity effects.

# Chapter 5

# Synchronization of dust acoustic waves in a forced Korteweg–de Vries–Burgers model

In this chapter, we formulate a theoretical model based on the fKdV-B equation to model the synchronization of dust acoustic waves. Previous experimental investigations use the Van-der-Pol oscillator model to explain results qualitatively. The oscillator-based model does not include convective nonlinearity in its mathematical formulation. To bridge this gap, we propose the fKdV-B model, which includes convective nonlinearity, dispersion, and dissipation, all three essential components to explain dusty plasma dynamics. Results from the fKdV-B model closely agree with experiments and include 1:1 and 1:2 synchronized states. Finally, an Arnold tongue diagram consolidates all observed synchronization features from the proposed model.

## 5.1  Introduction

The nonlinear phenomenon of frequency synchronization is ubiquitous in many physical, chemical, and biological systems and has been the subject of a large number of studies over the past several years [4, 185, 292]. The simplest mathematical model describing this phenomenon consists of an ensemble of globally coupled nonlinear point oscillators that adjust their intrinsic frequencies to a common collective frequency as the coupling strength is increased [2, 32, 293, 294]. Such a nonlinear phenomenon can also be observed in a continuum medium (a fluid) where a self-excited oscillation or a wave can interact with a driving force and adjust its oscillation or wave frequency [190, 295–299]. A plasma system, with its wide variety of collective modes and complex nonlinear dynamics, provides a rich and challenging medium for the exploration of synchronization phenomena. A number of past experimental studies have examined the driven response of plasma to an external frequency source [36, 38, 41, 42, 190, 296, 297, 300–305]. These studies include the synchronization of waves and oscillations at ion and dust dynamical scales as well as chaos and wave turbulence. A few studies have also been devoted to investigating mutual synchronization between two plasma devices [39, 40, 191].

More recently, synchronization phenomena have been experimentally explored in dusty plasma devices where it is easy to visualize the low-frequency wave activity using fast video imaging. A dusty plasma is a four-component plasma of electrons, ions, neutral gas atoms, and micron-size particles of solid matter [51, 56, 131]. It can be produced in a laboratory device like a glow discharge plasma, by introducing micron-sized solid particles  [104, 105, 111, 203]. These small solid particles (dust) get negatively charged by absorbing more electrons which have higher mobility than ions. Such a charged medium consisting of dust, ions and electrons can sustain a variety of collective modes [51, 98, 108, 306]. The dust acoustic wave (DAW) or dust density wave (DDW) first theoretically predicted by Rao, Shukla and Yu [138] is one such well-known low-frequency compressional mode that is analogous to the ion acoustic wave [51, 156]. A DAW can be spontaneously excited due to the onset of an ion-streaming instability. The DAW has a very low frequency (typically 10–100 Hz) [36, 105] due to the large mass of the dust particles and can consequently be visually observed; through its images and video recording [111, 307–309]. The term 'dust density wave' originated as a generalization of 'dust acoustic wave', after observing wavefronts (visible in the dust cloud) that appeared to be oblique with respect to the ion drift direction [101]. Two key factors led to the use of the term DDW: the presence of ion drift and an oblique orientation of the wavefront and its propagation with respect to the ion drift. Since then, many research groups have used the term 'dust density wave' and 'dust acoustic wave' synonymously [36, 108, 111, 112, 116, 128]. The present work focuses on the synchronization of DAW using the forced Korteweg-de Vries-Burgers (fKdV-B) model.

Synchronization of dust acoustic waves has been studied in an anodic plasma [41], radio-frequency (RF) and direct-current (DC) plasmas [36–38]. Pilch *et al.* [41] reported the entrainment of DAWs through a driving modulation to the anode. Ruhunusiri *et al.* [36] reported observation of harmonic, super-harmonic, and sub-harmonic synchrony of self-excited cnoidal DAWs. This was achieved through the driven modulation of the streaming ions in the dust cloud. Their experiments showed parametric

regions for the occurrence of such synchrony in the form of Arnold tongue diagrams in the state space
of the driving frequency and driving amplitude. They also observed features like the branching of the
tongues and the existence of an amplitude threshold for synchronization to occur. Williams *et al.* [38]
compared DAW synchronization in RF and DC-generated plasmas. Their results suggested that in an
RF plasma, synchronization was restricted to a part of the dust cloud volume, unlike the complete dust
cloud synchrony in a DC discharge plasma. Deka *et al.* [37] observed the synchronization of self-excited
DDW, through the suppression mechanism, by modulating ion streaming using an external sinusoidal
driver. Recently, Liu *et al.* [187] carried out experiments in the Plasma Kristall-4 (PK-4) device on
board the International Space Station (ISS) under micro-gravity conditions and reported phase locking
for harmonic synchronization. The present work is motivated by Ruhunusiri *et al.* [36] experiment on
global synchronization of a DDW driven by an ion flow. Unlike the DDW in some experiments [101,
310], the wavefronts were not obliquely propagating, as the experiment was designed to have a planar
symmetry, provided by proximity to a planar electrode, so the wavefronts were nearly perpendicular to
the ion flow direction.

Theoretical efforts towards interpretation and physical understanding of these experimental results
have so far been limited to providing qualitative comparisons with results obtained from very simple
dynamical models. One of the commonly employed mathematical model is the periodically forced Van
der Pol (fVdP) oscillator [4, 185, 311],

$$\frac{d^2x}{dt^2} - (c_1 - c_2 x^2)\frac{dx}{dt} + \omega_0^2 x = A_{dr}\cos(2\pi f_{dr}t) \qquad (5.1)$$

which describes the displacement $x$ of a harmonic oscillator with a natural frequency $\omega_0$, with terms for
a nonlinear damping $c_2 x^2 dx/dt$, a source of energy for self-excitation $c_1 dx/dt$, and a periodic driving
source of amplitude $A_{dr}$ at a frequency $f_{dr}$. The fVdP oscillator can exhibit synchronization not only
at $f_{dr}/f_0 \approx 1$, which is called "harmonic" synchronization but at ratios that are rational numbers.
If $f_{dr}/f_0 > 1$, the synchronization is said to be "super-harmonic", whereas if $f_{dr}/f_0 < 1$ it is "sub-
harmonic". Although the VdP oscillator model has been used in the past as a reference for characterizing
synchronization phenomena in plasmas and other media that support the propagation of waves [36, 37, 39,
190, 192, 297, 300]. It should be pointed out that as a point oscillator model, its dynamics is restricted
to nonlinear oscillations, and it cannot correctly represent nonlinear waves. This is also evident from
the fact that the VdP model is an ordinary differential equation in time and therefore has no spatial
dynamics that characterize a propagating wave. In addition, for nonlinear dust acoustic or dust density
waves, dispersion plays an important role in defining their propagation characteristics and this is not
built into the VdP model. As a promising step in capturing spatial properties of a wave, one modelling
approach to explain cluster or partial synchronization of propagating DDWs [120] under microgravity
conditions [101] used a chain of coupled Van der Pol oscillators [193]. As a further advance, however,
there remains a need to develop a simple theoretical model based on a wave equation that successfully
describes the global synchronization of waves exhibiting both nonlinearity and dispersion in a plasma
medium.

In this work, we present such a model and use it to demonstrate the synchronization of nonlinear dust acoustic waves to an external driver. The fKdV-B model is a generalization of the fKdV model that was developed by Sen *et al.* [140] for driven nonlinear acoustic waves and subsequently extensively used to study nonlinear precursor solitons in dusty plasma experiments [154, 155]. For our study, we include viscous dissipation in the model, an important feature of most laboratory studies of dusty plasmas [161, 162], which converts the fKdV to a fKdV-B model. Such a model provides a proper theoretical framework for the study of synchronization in a realistic dispersive plasma system that includes natural growth and dissipation of waves. The driving term is chosen to have an oscillatory form that has both a temporal and spatial periodicity. Our numerical solution of the model equation shows clear signatures of harmonic (1:1) and super-harmonic (1:2) synchronization. The characteristic features of the synchronization are delineated using power spectral density (PSD) plots, phase space plots and Lissajous plots obtained from the time-series data collected at one spatial location. A parametric plot in the form of an Arnold tongue diagram shows multiple tongues, each corresponding to the existence region of a harmonic or a higher-order super-harmonic synchronized state. The harmonic tongue also shows a branching behaviour.

The rest of the work is organized as follows. Section 5.2 briefly describes the fKdV-B model and the numerical approach adopted to solve it. The section also presents some numerical results for the undriven KdV and KdV-B equations as background information on the characteristic nonlinear features of the waves. It describes the diagnostic tools to be used for identifying synchronization phenomena. Section 5.3 presents our main results on harmonic and super-harmonic synchronization using the fKdV-B model. A brief summary and some concluding discussion are provided in section 5.4.

## 5.2 The forced Korteweg-de Vries-Burgers model

The fKdV-B equation, a one-dimensional driven nonlinear partial differential equation, is of the form:

$$\frac{\partial n(x,t)}{\partial t} + \alpha n(x,t)\frac{\partial n(x,t)}{\partial x} + \beta\frac{\partial^3 n(x,t)}{\partial x^3} - \eta\frac{\partial^2 n(x,t)}{\partial x^2} = F_s(x,t). \tag{5.2}$$

Here $n(x,t)$ is the dependent variable (the perturbed density in this case) and $F_s(x,t)$ is an external spatio-temporal forcing term. $\alpha$, $\beta$, and $\eta$ are positive quantities representing the strength of nonlinearity, dispersion, and viscous damping, respectively. The spatial coordinate $x$ and time $t$ are normalized by the plasma Debye length $\lambda_D$ and the dust plasma period $\omega_{pd}^{-1}$, respectively.

It should be mentioned that the KdV equation (*i.e.,* Eq. (5.2) in the absence of the viscous damping and driving term) has been shown to model the evolution of weakly nonlinear waves in dusty plasmas both in the presence [156] and in the absence [138] of ion-streaming. Hence it can correctly represent both nonlinear dust density and dust acoustic waves. Recently Liu *et al.* [156] showed that the cnoidal solution of the KdV shows excellent agreement with the DDW profiles observed in the dusty plasma experiments [107, 242]. Theoretically, the experimental DDW evolution was modelled by the KdV model in which the ion-streaming was taken into consideration [156]. Earlier, a theoretical model based on the

fKdV equation [169] was used to explore the nonlinear mixing of longitudinal dust lattice waves observed in the dusty plasma experiment [15]. Nonlinear mixing means the natural mode and the external forcing mode retain their identity after interaction and excited frequencies are different combinations of addition and subtraction of the natural and forcing mode. The present theoretical fKdV-B model is proposed to understand the global synchronization of the dust acoustic wave as was observed in the dusty plasma experiment [36]. Synchronization means the natural mode loses its identity and the system is controlled by the external driver. Here, we model synchronization by incorporating the viscous damping instead of nonlinear mixing as was done in Ref. [169]. The fKdV-B equation can be derived from the full fluid-Poisson set of equations in the weakly nonlinear, dispersive and dissipative regime by using a reductive perturbation method [162, 165]. Such a derivation in the absence of the viscosity term has been given in detail by Sen *et al.* [140]. The KdV-B equation (*i.e.,* Eq. (5.2) in the absence of the driving term) is well known in the literature [161, 162, 165] and has been employed in the past to model oscillatory shocks in dusty plasmas [162, 312]. The model has also been used to study temporal chaos or spatial chaos by using a randomly time-varying [194] or randomly space-varying [195] driving term. In earlier work by Sen *et al.* [140], the source term was taken to be a constant, while in this work, we use a spatio-temporally varying periodic source and carry out a numerical investigation of Eq. (5.2) to study the synchronization of DAWs based on the fKdV-B model.

The driving source is taken to be in the form of a cnoidal-square travelling wave,

$$F_s(x,t) = A_s cn^2[2K(\kappa_s)\{x/\lambda_s - f_s t\}; \ \kappa_s] \tag{5.3}$$

where $cn$ is the Jacobi elliptic function, $A_s$ is the driving amplitude, $\lambda_s$ is the spatial wave length and $f_s$ is the driving frequency. $K(\kappa)$ is the complete elliptic integral of the first kind, and the elliptic parameter $\kappa$ is a measure of the nonlinearity of the wave. The cnoidal-square travelling wave is an exact solution of the KdV equation. It can therefore mimic the driving of the system by a DAW arising from an external (coupled) plasma source. For the numerical solution of Eq. (5.2), the initial waveform is also taken to be of the form,

$$n(x, t = 0) = A_0 cn^2[2K(\kappa_0)\{x/\lambda_0\}; \ \kappa_0], \tag{5.4}$$

with the values of $A_0$, $f_0$ and $\lambda_0$ different from those of the driving source. The idea is to see whether the final driven modes of the system synchronize to the frequency of the driver. Equation (5.2) is solved for various values of $f_s$ and $A_s$ in order to find the regions of synchronization in the parameter space of $(A_s, f_s)$.

### 5.2.1 The numerical solution of the fKdV-B equation

Our numerical investigation of the fKdV-B equation is based on the pseudo-spectral method [198] and uses periodic boundary conditions. The code is first bench marked by reproducing earlier results [45, 140] obtained for the fKdV equation. The various parameter values associated with the model are taken to be as follows: The Jacobi elliptic parameters $\kappa_0 = \kappa_s = 0.98$ for Eqs. (5.3) and (5.4). The wave vector of

the initial perturbation *i.e.,* $k_0 = 12k_m$ where $k_m = (2\pi)/L_x$ being the minimum wave vector associated with a system of length $L_x = 6\pi$. The corresponding wavelength *i.e.,* $\lambda_0 = (2\pi)/k_0$ and amplitude $A_0$ of the initial perturbation (*i.e.,* Eq. (5.4)) are kept fixed throughout the analysis. We have taken $k_s = 12k_m$ and $k_s = 2 \times 12k_m$ for studying harmonic (1:1), and super-harmonic (1:2) synchronization states. The corresponding forcing wavelength is $\lambda_s = (2\pi)/k_s$. Throughout the analysis, we have only varied the forcing amplitude, $A_s$ and forcing frequency, $f_s$. The coefficient $\alpha$ in Eq. (5.2) is given by following expression $\alpha = \left[\delta^2 + (3\delta + \sigma)\sigma + (\delta/2)(1 + \sigma^2)\right]/(\delta - 1)^2$ [154] and $\beta = 0.5$. We evaluate $\alpha = 2.3$ with $\sigma = T_{i0}/T_{e0} = 0.0036$ where electron and ion temperatures are $T_{e0} = 7$ eV and $T_{i0} = 0.025$ eV, respectively and $\delta = n_{i0}/n_{e0} = 3.4$ where electron and ion densities are $n_{e0} = 2 \times 10^{14}$ m$^{-3}$ and $n_{i0} = 6.8 \times 10^{14}$ m$^{-3}$, respectively. The nonlinearity parameter $\alpha$ was measured from experimental parameters reported by Flanagan *et al.* [107] for a wave experiment using a setup similar to that of Ruhunusiri *et al.* [36]. Since there is no measurement of the viscosity parameter in Flanagan *et al.* [107] and no value is reported for the experimental setup of Ruhunusiri *et al.* [36], we treat the viscosity coefficient to be a free parameter, which we adjust to obtain a good quantitative agreement with the signatures of dissipation in the experimental data of Ruhunusiri *et al.* [36], namely the Arnold tongues. A value of $\eta = 0.0025$ best fits the experimental data. Using the experimental plasma parameters [107] and assuming dust temperature $T_d = 2$ eV, we calculate Coulomb coupling strength $\Gamma = 92$ and Debye screening parameter $\kappa_D = 2.8$. Referring to molecular dynamics simulations for dusty plasmas for the corresponding closest $\Gamma = 100$ and $\kappa_D = 3$, the value of normalized viscosity is $\eta^* = 0.04$ [273, 313]. This value of viscosity translates to $\eta = 0.0027$ as per the KdV-B equation normalization, which is fairly close to our chosen value of viscosity for the simulations of the fKdV-B model. Furthermore, we take the same experimental values of the natural and driver frequencies as reported in the experiment [36] to carry out numerical solutions of the fKdV-B model *i.e.,* Eq. (5.2). Also, based on the chosen parameters $\alpha$, $\beta$, $\kappa_0$ and $k_0$, the initial perturbation has amplitude $A_0 = 46.32$ and frequency $f_0 = 22$ Hz, which is derived using the relationship provided in Mir *et al.* [169]. The amplitude of the initial perturbation chosen in this fashion will be governed by the exact solution of the KdV and will be a stable solution of KdV for this particular amplitude.

We evolve the initial perturbation in Eq. (5.2) over long times for these various different parameter values. During the spatio-temporal evolution, we collect a time series of the density field at a fixed spatial location and use it to calculate the power spectral density. The PSD provides a useful tool for distinguishing between synchronized and un-synchronized states.

As an illustrative example, we show in Fig. 5.1 the PSD, the time-series and the phase space plot of the solution, obtained for a KdV (solid line) equation (Eq. (5.2) for $\eta = A_s = 0$). The time-series data has been collected up to $t_{max} = 80 \; \omega_{pd}^{-1}$ with a time step $dt = 10^{-5} \; \omega_{pd}^{-1}$. The maximum sampling frequency $f_S = 1/dt$ and the Nyquist frequency is $f_N = f_S/2$. This leads to a frequency resolution of $df = 1/t_{max}$ for the collected time-series. The time-series data corresponding to the first few tens of periods is discarded to remove transient effects while constructing the PSD. In Fig. 5.1 the nonlinear character of the mode is evident from the presence of the higher harmonics in the PSD and from the shape of wave form in the

time-series. The natural mode of KdV has a frequency $f_0 = 22$ Hz. The single cycle phase space plot (solid line) with its form resembling a separatrix curve indicates an undamped nonlinear periodic wave, in this case, the exact cnoidal-square wave. Also, for comparison, we present in Fig. 5.1 the corresponding results for the undriven KdV-B (dash-dotted) equation (Eq. (5.2) for $\eta = 0.0025$ and $A_s = 0$) on top of the KdV (solid line) equation. The effect of viscous damping is seen in the frequency shift of the fundamental component in the PSD towards a lower value of $f_0^\eta = 15$ Hz, the reduced amplitude in the time-series and the spiralling of the phase space plot (dash-dotted) towards the origin. It is clear that in
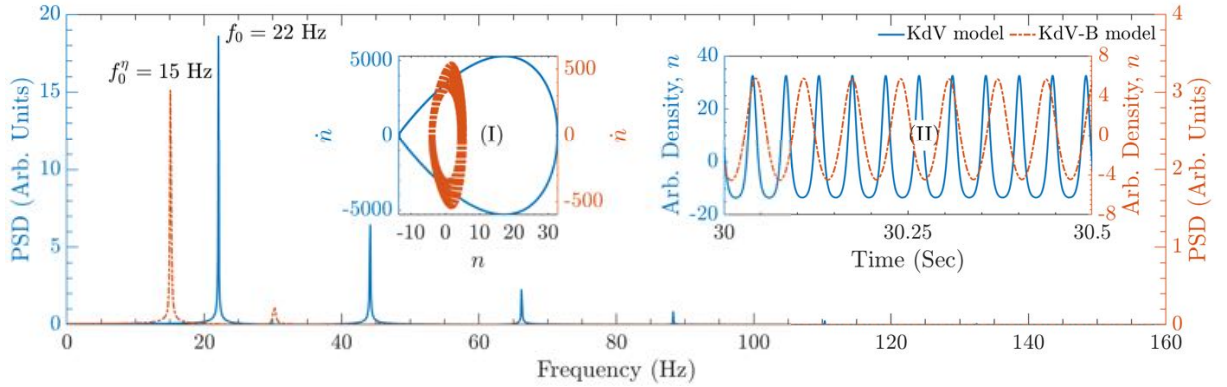


Figure 5.1: PSD for the times-series of KdV (solid line) and KdV-B (dash-dotted line) equations with initial perturbation Eq. (5.4). Insets (I) and (II) show the phase space plots and time series, respectively for KdV (solid line) and KdV-B (dash-dotted line) models.

the presence of finite viscosity the cnoidal-square wave can no longer be sustained as a nonlinear solution of Eq. (5.2) with $F_s = 0$ and the initial perturbation decays in time. The question is whether by driving the system with a periodic source one can revive and sustain a nonlinear solution that is also synchronized with the driver. The answer is in the positive and we next present our results on such a phenomenon.

## 5.3 Synchronization in the fKdV-B model

Here, we present the main results of our work, namely, the synchronization of the solutions of Eq. (5.2) to an external driver of the form given by Eq. (5.3). We begin by discussing harmonic (1:1) synchronization for which we choose the driving frequency to be slightly away from the fundamental frequency of $f_0 = 22$ Hz that is characteristic fundamental frequency of the undriven system. Two cases are considered, namely, $f_s = 21$ Hz and $f_s = 23$ Hz. The driving amplitude in both cases is taken to be $A_s = 0.40A_0$. Figure 5.2 shows the attainment of harmonic (1:1) synchronization for both these cases with subplots (a, b) devoted to $f_s = 21$ Hz and (c, d) to $f_s = 23$ Hz, respectively. As can be seen from the time-series plots in (a) and (c) the driven solutions are indeed locked to the driver. This is also clearly seen in the PSDs where the fundamental frequencies of the driven solutions are indeed at the frequency of the driver. Furthermore, the phase space plots in (b) and (d) show that these solutions constitute undamped nonlinear periodic waves that are maintained by a balance between the nonlinear steepening, dispersive broadening, viscous damping and amplification due to the external pumping by the driving term. The resultant phase space curve, that has the characteristic shape of a separatrix, represents a stationary cnoidal wave solution. The presence of dissipation seems to be necessary for sustaining this synchronized driven solution. We
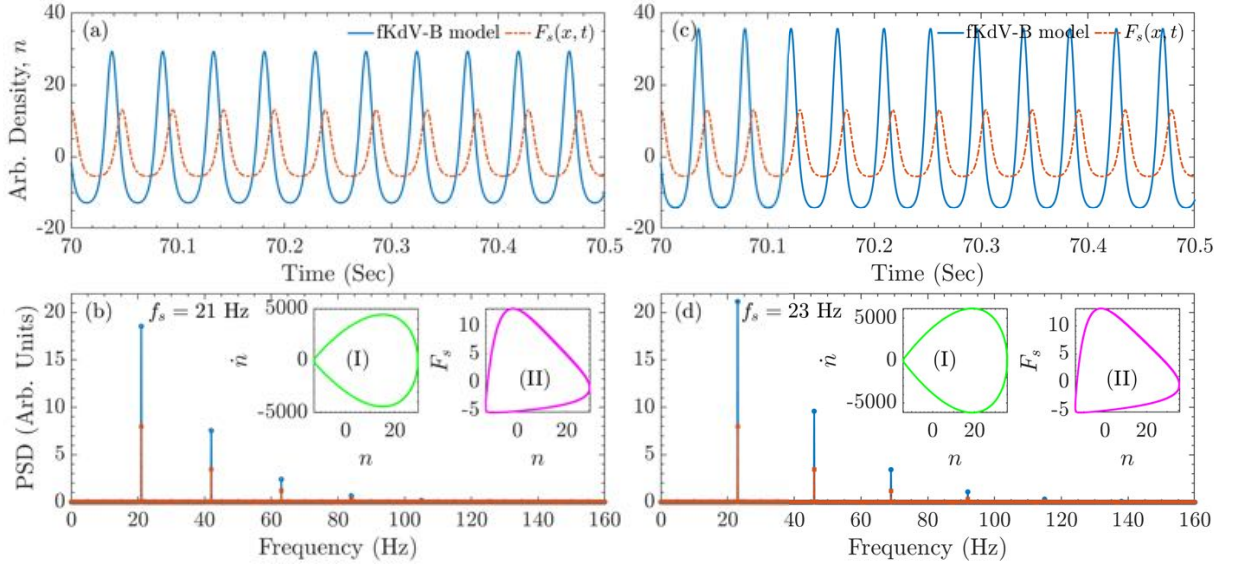
Figure 5.2: The harmonic (1:1) synchronization in the fKdV-B model with $f_s < f_0$ and $f_s > f_0$. The time-series of the fKdV-B model (solid line) and the forcing (dash-dotted line) at driver frequency (a) $f_s = 21$ Hz with threshold amplitude $A_s = 0.40A_0$ and (b) $f_s = 23$ Hz with threshold amplitude $A_s = 0.40A_0$. (c) PSD of times-series (a). (d) PSD of time-series (b). The inset (I) is the phase space plot, and the inset (II) is the Lissajous figure which reflects the frequency locking at the driver frequency.
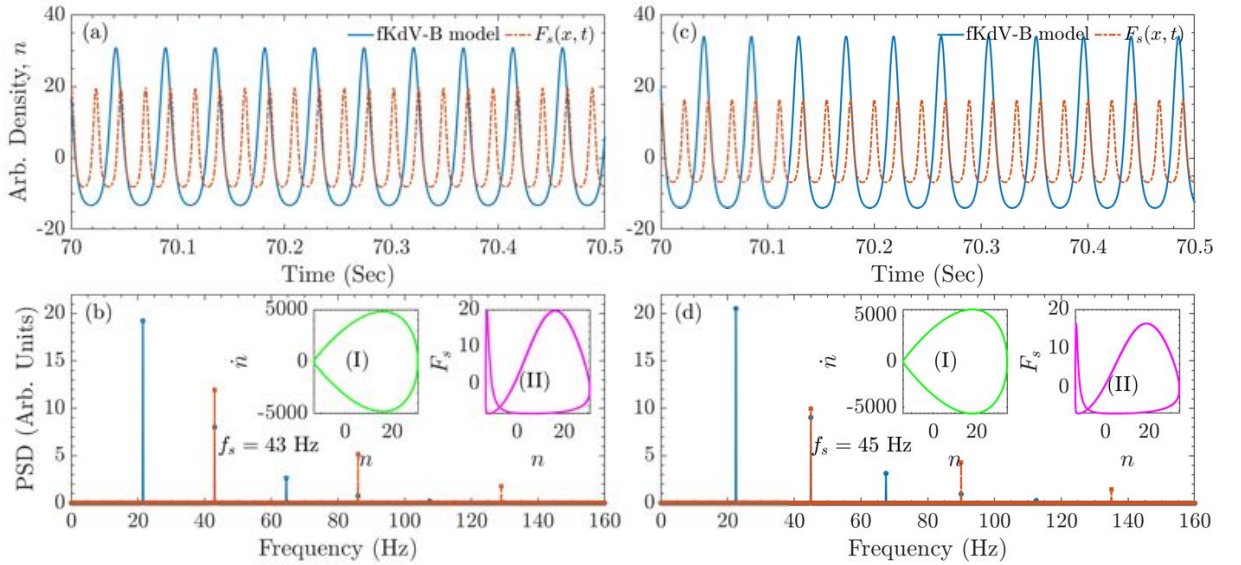


Figure 5.3: The super-harmonic (1:2) synchronization in the fKdV-B model with $f_s < 2f_0$ and $f_s > 2f_0$. The time-series of the fKdV-B model (solid line) and the forcing (dash-dotted line) at driver frequency (a) $f_s = 43$ Hz with threshold amplitude $A_s = 0.60A_0$ and (b) $f_s = 45$ Hz with threshold amplitude $A_s = 0.50A_0$. (c) PSD of times-series (a). (d) PSD of time-series (b). The inset (I) is the phase space plot and the inset (II) is the Lissajous figure which reflects the frequency locking at half of the driver frequency.

have found that in the partial differential equation Eq. (5.2), including not just nonlinear and dispersive terms, but also a linear dissipative term, allowed achieving synchronization of a wave. When we turned off dissipation, by setting the viscosity coefficient to zero in Eq. (5.2), we did not observe synchronization of the wave, for the conditions that we studied here. This is different from the case of a point oscillator, as described by the Van der Pol oscillator Eq. (5.1), which requires a nonlinear dissipation term to obtain synchronization. In the absence of viscosity, one only gets nonlinear mixing from the model as has been reported earlier in Mir *et al.* [45, 169]. The amount of viscosity also determines the threshold condition
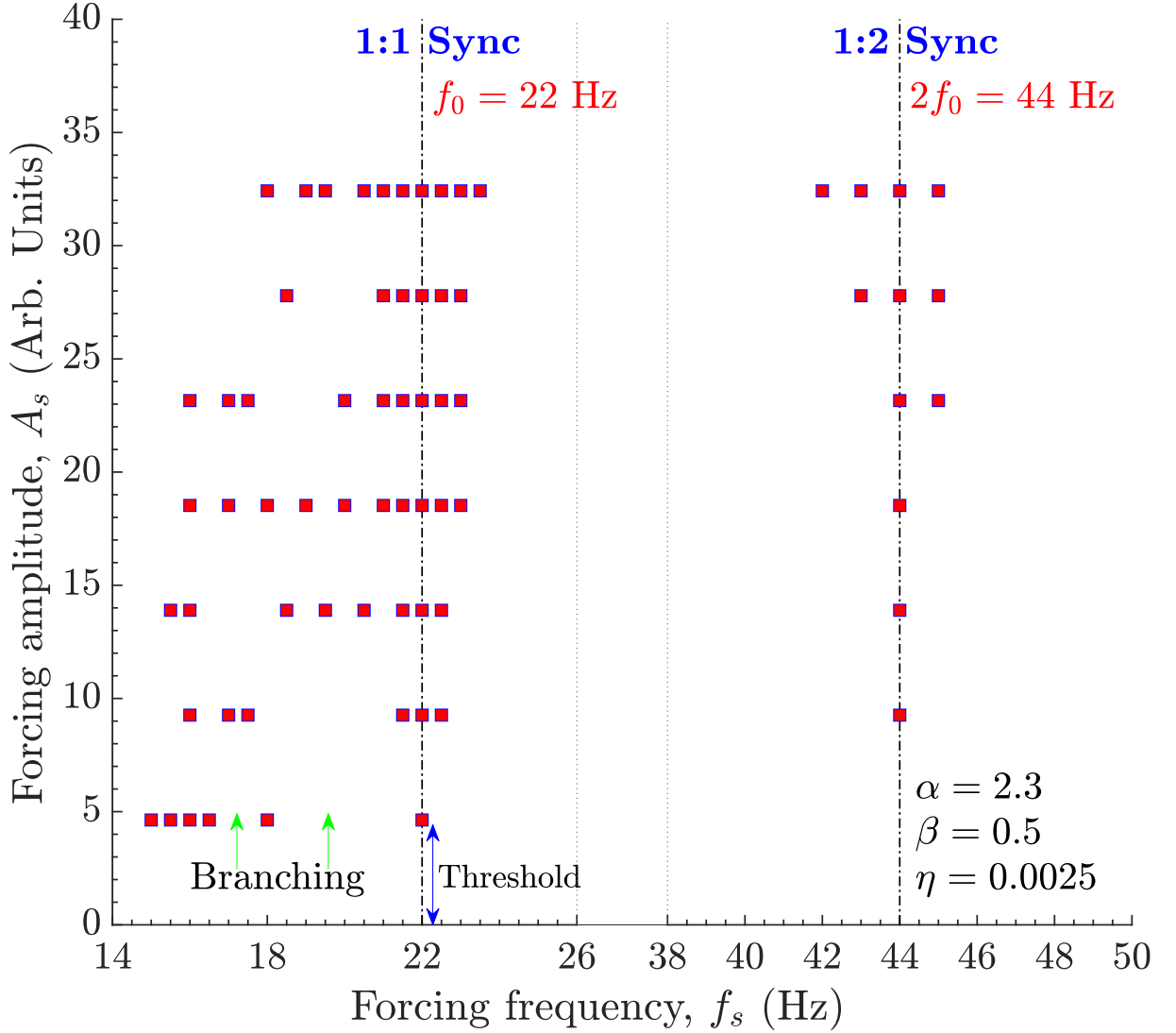
Figure 5.4: The Arnold tongue diagram for harmonic (1:1) and super-harmonic (1:2) synchronization states in the fKdV-B model. The amplitude is varied from $A_s = 0.10A_0$ to $A_s = 0.70A_0$ for 1:1, and $A_s = 0.20A_0$ to $A_s = 0.70A_0$ for 1:2 synchronization.

for the driver amplitude.

To explore super-harmonic (1:2) synchronization, we again consider two cases of $f_s = 43$ Hz and $f_s = 45$ Hz, which are slightly below and above the first harmonic frequency $2f_0 = 44$ Hz of the undriven system. The results are shown in Fig. 5.3 where the subplots (a,c) are devoted to $f_s = 43$ Hz and (b,d) to $f_s = 45$ Hz, respectively. As in the previous case of harmonic synchronization, we see clear evidence of super-harmonic (2:1) synchronization in the time-series plots, the PSDs and the phase space plots. The Lissajous figures have a figure eight-like trajectory which is indicative of a (1:2) synchronized state. One significant difference from the harmonic synchronization case is that the minimum threshold amplitude for the driver to achieve a (1:2) state is different for the cases $f_s < 2f_0$ and $f_s > 2f_0$. They are $A_s = 0.60A_0$ and $A_s = 0.50A_0$, respectively.

Finally, in Fig. 5.4, we present a consolidated picture of the existence domain of these synchronized states in the parameter space of the driver frequency $f_s$ and driver amplitude $A_s$ in the form of an Arnold

tongue diagram. To obtain the Arnold tongue diagram, $A_s$ is varied in steps of 4.63 (which is $0.10A_0$) from 0 to 32.42 (which is $0.70A_0$) while $f_s$ is varied in steps of 0.5 Hz for harmonic synchronization and 1.0 Hz for the super-harmonic case. Fig. 5.4 shows the (1:1) and (1:2) entrained state tongues in the fKdV-B model.

We observe several interesting features in the Arnold tongue diagram. To start with, there is always a threshold amplitude $A_s$ below which no synchronization occurs. For the harmonic (1:1) synchronization it is $A_s = 0.10A_0$ for $\eta = 0.0025$. This is unlike the harmonic synchronization phenomenon observed in a driven Van der Pol model where no such threshold is found [314]. Another important feature is a distinctive branching of the Arnold tongue that is clearly seen for the (1:1) states at low forcing amplitudes marked with arrows. The branching gives rise to a non-synchronized region between the frequencies $f_s = 22$ Hz to $f_s = 18$ Hz at driver amplitude $A_s = 0.10A_0$. This branching narrows down with the increase in $A_s$. Another branch is seen in between $f_s = 18$ Hz and $f_s = 16.5$ Hz, which also narrows down with increase in $A_s$. A third feature is the asymmetric nature of the tongue structures about $f_0$. The frequency width over which synchronization can be obtained is much broader for $f_s < f_0$ compared to $f_s > f_0$.

## 5.4 Summary

To summarize, we have studied the phenomenon of synchronization of dust acoustic waves to an external periodic driver in a model system described by the forced Korteweg-de Vries-Burgers equation. This equation provides a proper theoretical framework and a better physical model compared to the Van der Pol oscillator model for studying the dynamics of nonlinear dust acoustic waves by properly accounting for nonlinear, dispersive and dissipative influences on the waves. Using the model, we have successfully demonstrated harmonic (1:1) and super-harmonic (1:2) synchronization states of DAWs for the experimental values reported by Ruhunusiri *et al.* [36]. In particular, a comparison of our theoretical Arnold tongue diagram with their experimental one shows the following common features. As in the experimental Arnold tongue diagram, we see the existence of amplitude thresholds as well as clear evidence of the branching phenomena. However, there are also important differences. With our model, we have not been able to obtain the sub-harmonic synchronization that has been observed in the experiment. Furthermore, our model uses an external driver that closely resembles a nonlinear natural mode of the system whereas in the experiment, a purely time-varying external sinusoidal driver has been used. However, it is not clear what form this driver takes inside the plasma system and whether it manifests itself as a spatio-temporally varying perturbation. These and other questions, such as the absence of sub-harmonic synchronization in the equation, and the neglect of dissipation arising from gas friction on the dust particles, remain to be explored in the future in order to further improve the model.

# Chapter 6

# Conclusion and Future Outlook

In this chapter, we enlist the primary findings of this thesis work and their future scope. We propose an alternate and comprehensive theoretical model to represent nonlinear physical processes that can reasonably be represented via a one-dimensional mathematical model. This fKdV-based model description is more quantitatively agreeable than typical oscillator-based model descriptions. Inclusion of effects due to correlation, full nonlinearity and higher dimensionality are domains for extending present dusty plasma studies. Further, the current models can be helpful to different media governed by the characteristic spatio-temporal convective nonlinearity.

---

## 6.1 Conclusion

This thesis contributes a set of theoretical models to study the nonlinear phenomena of mixing and synchronization in dusty plasma. Both models are built upon the forced-KdV equation incorporating the convective nonlinearity, a feature of fluids. The proposed models reasonably represent the dynamics of charged dust fluid in the weakly nonlinear regime. Besides dusty plasma, the models have applicability and extendibility to other fluid mediums. This thesis advances the theoretical understanding of nonlinear mixing and synchronization-like collective phenomena in dusty plasma experiments. Previously, driven nonlinear oscillator models only provided qualitative theoretical support and did not appropriately include the medium's nonlinearity. The broad observations of this thesis are as follows:

1. We observe nonlinear mixing of the natural dust acoustic and dust lattice modes with a) time-dependent oscillations and b) sinusoidal travelling wave. While former mixing had good agreement with the experimental findings by Nosenko *et al.* [15], the mystery of missing harmonic mode and some other modes was resolved with the latter case making it a more appropriate model close to experiments.

2. The power spectral analysis is used to capture the presence of individual modes in the mixing profiles. We have used the bispectral analysis to explore the origin of these modes further. The bispectral technique provided conclusive evidence that each generated mode constituting the time-series from the fKdV model is due to three-wave mixing that leads to generating modes having a frequency at an addition or subtraction of the original two modes.

3. The kinetic simulations of dusty plasmas treated as one component strongly coupled plasma based on the Langevin molecular dynamics has shown excellent agreement with the fluid-based fKdV model. The power spectral and bispectral analyses confirmed the modes' presence and physical origin. The kinetic picture of dusty plasmas confirmed our fluid-based simulations.

4. We have demonstrated, for the first time, the synchronization of nonlinear waves using the fKdV-B model. The proposed model showed an excellent quantitative agreement with the synchronization of dust acoustic waves done by Ruhunusiri *et al.* [154]. The model helps us understand the contribution of the damping mechanism in achieving the synchronization of nonlinear propagating waves. The features of harmonic and super-harmonic synchronization in the fKdV-B were captured using the spectral diagrams, Lissajous figures and the Arnold tongue diagram.

5. The thesis provided the theoretical model for nonlinear mixing and synchronization of waves in nonlinear dispersive systems with experimental validation from the dusty plasma experiments. The fKdV model, which doesn't incorporate any dissipation mechanism, showed the nonlinear mixing of waves. While the fKdV-B model, which incorporates the dissipation mechanism, showed the synchronising propagating waves. The fKdV and fKdV-B models apply to other driven charged or neutral fluid or fluid-like systems governed by spatio-temporal convective nonlinearity.

## 6.2 Future Outlook

The two fKdV-based models we presented in this thesis were derived from the full set of fluid-Poisson equations. We could simplify the mathematical model as a single partial differential equation using the reductive perturbation approach. Yet, the model retains the essence of the nonlinearity and dispersion of the medium. Also, the simplification helped in finding exact analytic solutions in certain parameter regimes. While results from the simplified models show excellent agreement with experiments, there is a scope for improvement by studying collective dynamics with the help of full-fluid modelling. With full model equations, we will not only have access to a full nonlinear medium but also can access the effect of dimensionality. The transition from weakly nonlinear to fully nonlinear dynamics of the medium effects may significantly differ for mixing and synchronization processes. We also expect the possibility of transition to bifurcation, chaos, and driven turbulence in this regime.

The fKdV model found its applicability to space debris-related problems in recent studies. It includes understanding the nonlinear plasma excitation by space junk or space debris in LEO and helps predict and control the threat due to the space debris to future space missions [140, 177]. We may also utilize the fKdV model to study the effect of external sources on the precursor solitons created due to a charged bunch moving in a plasma [222]. Another important aspect of the KdV-based model description is its applicability to other fluid-like physical systems. The nonlinear mixing and synchrony of surface, internal, and strain waves are a few topics where present studies are readily extendable.

Dusty plasmas have a unique property to exist in different phases of matter depending on the background plasma environment and the charge over dust grains. Mostly they reflect traits of the intermediate phase of fluid and solid. The standard fluid-Poisson model can not represent the medium's dynamics in strong coupling regimes. The dusty plasma is phenomenologically closer to the visco-elastic fluids in intermediate coupling regimes. It will be interesting to see how nonlinear mixing and synchronization responses alter in these regimes using a phenomenological visco-elastic model. The generalized hydro-dynamic (GHD) visco-elastic model [147] can be the initiation point for such studies. A quantitatively appropriate approach is to model the dusty plasma at a kinetic level using classical molecular dynamics simulation. It is because the pair-wise interactions for charged dust particles are the form of shielded Coulomb potential. This model intrinsically includes correlation, viscosity, and neutral drag effects. The MD simulation can be utilized for a qualitative picture of correlation effects. The large-angle collisions cause these correlation effects and can not be included in the standard fluid models. In the present thesis, we initially attempted to model nonlinear mixing using MD simulations. Results align with the fluid model in the fluid regime, *i.e.,* weak correlation domain. Mixing and synchronization studies need to be extended for strong correlation domains.

On the model development front, magnetized dusty plasma is an important domain with the scope for improvement in fKdV-based models. We explore a simplified two-dimensional model using a perturbation technique appropriate to magnetized plasma. It will be interesting to see how an external driving can

affect nonlinear physical processes such as the instabilities and localized structure evolution, especially in the presence of two characteristic frequencies associated with the plasma and the magnetic field, respectively.

Another related topic worth exploring is the study of coupled plasma systems with different plasma parameters. The coupled nonlinear oscillators have shown complete, lag, phase, and generalized synchronization features in the literature [315–318]. An ensemble of coupled nonlinear oscillators has shown frequency clustering and the Chimera states [319–321]. It is an interesting domain to explore how two coupled KdV-B systems will reflect synchronization features.

# List of publications

## Journals

1. **Ajaz Mir**, Sanat Tiwari, Abhijit Sen, Chris Crabtree, Gurudas Ganguli, and John Goree:
   Synchronization of Dust Acoustic Waves in a forced Korteweg-de Vries-Burgers model.
   *Phys. Rev. E* **107**, *035202 (2023)*

2. **Ajaz Mir**, Sanat Tiwari, and Abhijit Sen:
   Bispectral analysis of nonlinear mixing in a periodically driven Korteweg–de Vries system.
   *Phys. Plasmas* **29**, *032303 (2022)*

3. **Ajaz A. Mir**, Sanat K. Tiwari, John Goree, Abhijit Sen, Chris Crabtree, and Gurudas Ganguli:
   A forced Korteweg–de Vries model for nonlinear mixing of oscillations in a dusty plasma.
   *Phys. Plasmas* **27**, *113701 (2020)*

4. Farida Batool, **Ajaz Mir**, Sachin Sharma, Sanat Tiwari, and Abhijit Sen:
   Comparison of Korteweg-de Vries model-based nonlinear dispersion relations for dust acoustic wave.
   *[Under preparation]*

## Other work

1. Rauoof Wani, **Ajaz Mir**, Farida Batool and Sanat Tiwari:
   Rayleigh–Taylor Instability in Strongly Coupled Plasma.
   *Sci. Rep.* **12**, *11557 (2022)*

2. **Ajaz Mir**, Sanat Tiwari, and Abhijit Sen:
   Two-Stream Instability in Strongly Coupled Plasma.
   *[Under preparation]*

# Bibliography

[1]   Paul E. Dimotakis. "Turbulent Mixing". In: *Annu. Rev. Fluid Mech.* 37.1 (2005), pp. 329–356.

[2]   Juan A. Acebrón et al. "The Kuramoto model: A simple paradigm for synchronization phenomena". In: *Rev. Mod. Phys.* 77.04 (1 2005), pp. 137–185.

[3]   Uriel Frisch. *Turbulence: the legacy of A. N. Kolmogorov.* Cambridge University Press, Cambridge, 1995.

[4]   Arkady Pikovsky, Michael Rosenblum, and Jürgen Kurths. *Synchronization: A Universal Concept in Nonlinear Sciences.* Cambridge University Press, Cambridge, 2001.

[5]   Tamás Vicsek et al. "Novel Type of Phase Transition in a System of Self-Driven Particles". In: *Phys. Rev. Lett.* 75.8 (6 1995), pp. 1226–1229.

[6]   Thomas Leweke, Stéphane Le Dizès, and Charles H.K. Williamson. "Dynamics and Instabilities of Vortex Pairs". In: *Annu. Rev. Fluid Mech.* 48.1 (2016), pp. 507–541.

[7]   David C Aveline et al. "Observation of Bose–Einstein condensates in an Earth-orbiting research lab". In: *Nature* 582.7811 (2020), pp. 193–197.

[8]   Vıctor M. Pérez-Garcıa et al. "Dynamics of Bose-Einstein condensates: Variational solutions of the Gross-Pitaevskii equations". In: *Phys. Rev. A* 56.8 (2 1997), pp. 1424–1432.

[9]   AC-L Chian. "Nonlinear wave-wave interactions in astrophysical and space plasmas". In: *Astrophys. Space Sci.* 242.1 (1996), pp. 249–295.

[10]  H. Wilhelmsson. "Wave-wave interaction in plasmas". In: *Physica B* 82.1 (1976), pp. 52–60. ISSN: 0378-4363.

[11]  Noriyoshi Sato. "Nonlinear Mixing of Ion Acoustic Waves in a Plasma". In: *Phys. Fluids* 13.8 (1970), pp. 2198–2200.

[12]  V. Stefan, B. I. Cohen, and C. Joshi. "Nonlinear Mixing of Electromagnetic Waves in Plasmas". In: *Science* 243.4890 (1989), pp. 494–500.

[13]  George C. Papen and John A. Tataronis. "Transient nonlinear wave mixing in collisional plasmas". In: *J. Plasma Phys.* 42.3 (1989), pp. 457–478.

[14]  I. Fidone, G. Granata, and J. Teichmann. "Nonlinear Wave Mixing at Hybrid Frequencies in an Inhomogeneous Plasma". In: *Phys. Fluids* 14.3 (1971), pp. 737–745.

[15] V. Nosenko et al. "Nonlinear Interaction of Compressional Waves in a 2D Dusty Plasma Crystal". In: *Phys. Rev. Lett.* 92.2 (8 2004), p. 085001.

[16] P. Blanloeuil et al. "Nonlinear mixing of non-collinear guided waves at a contact interface". In: *Ultrasonics* 110 (2021), p. 106222. ISSN: 0041-624X.

[17] Maoxun Sun et al. "Experimental and numerical investigations of nonlinear interaction of counter-propagating Lamb waves". In: *Appl. Phys. Lett.* 114.1 (2019), p. 011902.

[18] Joel D. Cox and F. Javier García de Abajo. "Plasmon-Enhanced Nonlinear Wave Mixing in Nanostructured Graphene". In: *ACS Photonics* 2.2 (2015), pp. 306–312.

[19] Jan Renger et al. "Free-Space Excitation of Propagating Surface Plasmon Polaritons by Nonlinear Four-Wave Mixing". In: *Phys. Rev. Lett.* 103.12 (26 2009), p. 266802.

[20] Stefano Palomba and Lukas Novotny. "Nonlinear Excitation of Surface Plasmon Polaritons by Four-Wave Mixing". In: *Phys. Rev. Lett.* 101.8 (5 2008), p. 056802.

[21] V. M. Agranovich et al. "Linear and nonlinear wave propagation in negative refraction metamaterials". In: *Phys. Rev. B* 69.4 (16 2004), p. 165112.

[22] Aref Chowdhury and John A. Tataronis. "Nonlinear wave mixing and susceptibility properties of negative refractive index materials". In: *Phys. Rev. E* 75.1 (1 2007), p. 016603.

[23] L. Misoguti et al. "Nonlinear wave-mixing processes in the extreme ultraviolet". In: *Phys. Rev. A* 72.12 (6 2005), p. 063803.

[24] F. Lenzini et al. "Optical vortex interaction and generation via nonlinear wave mixing". In: *Phys. Rev. A* 84.12 (6 2011), p. 061801.

[25] John R. Thompson and Rajarshi Roy. "Nonlinear dynamics of multiple four-wave mixing processes in a single-mode fiber". In: *Phys. Rev. A* 43.5 (9 1991), pp. 4987–4996.

[26] Alexey Belyanin et al. "Three-terminal semiconductor laser for wave mixing". In: *Phys. Rev. A* 65.5 (5 2002), p. 053824.

[27] Alon Bahabad et al. "Unveiling Quasiperiodicity through Nonlinear Wave Mixing in Periodic Media". In: *Phys. Rev. Lett.* 98.5 (20 2007), p. 205501.

[28] Haifeng Li et al. "Growth mechanism of interfacial fluid-mixing width induced by successive nonlinear wave interactions". In: *Phys. Rev. E* 103.5 (5 2021), p. 053109.

[29] Leon Glass. "Synchronization and rhythmic processes in physiology". In: *Nature* 410.6825 (2001), pp. 277–284.

[30] Didier Gonze et al. "Spontaneous Synchronization of Coupled Circadian Oscillators". In: *Biophys. J.* 89.1 (2005), pp. 120–129. ISSN: 0006-3495.

[31] Dongming Cai, Ying-Cheng Lai, and Raimond L. Winslow. "Complex Dynamics in Coupled Cardiac Pacemaker Cells". In: *Phys. Rev. Lett.* 71.10 (15 1993), pp. 2501–2504.

[32] Yoshiki Kuramoto. *Chemical Oscillations, Waves, and Turbulence.* Dover, New York, 2003.

[33] J. M. Cruz, M. Rivera, and P. Parmananda. "Experimental observation of different types of chaotic synchronization in an electrochemical cell". In: *Phys. Rev. E* 75.3 (3 2007), p. 035201.

[34] Tony E. Lee and H. R. Sadeghpour. "Quantum Synchronization of Quantum van der Pol Oscillators with Trapped Ions". In: *Phys. Rev. Lett.* 111.12 (23 2013), p. 234101.

[35] Arif Warsi Laskar et al. "Observation of Quantum Phase Synchronization in Spin-1 Atoms". In: *Phys. Rev. Lett.* 125.7 (1 2020), p. 013601.

[36] W. D. Suranga Ruhunusiri and J. Goree. "Synchronization mechanism and Arnold tongues for dust density waves". In: *Phys. Rev. E* 85.4 (4 2012), p. 046401.

[37] Tonuj Deka et al. "Suppression of a spontaneous dust density wave by modulation of ion streaming". In: *Plasma Sci. Technol.* 22.4 (2020), p. 045002.

[38] Jeremiah Williams. "Synchronization of the Dust Acoustic Wave in an RF and a DC Discharge Plasma". In: *IEEE Trans. Plasma Sci.* 46.4 (2018), pp. 806–814.

[39] Neeraj Chaubey et al. "Synchronization between two coupled direct current glow discharge plasma sources". In: *Phys. Plasmas* 22.2 (2015), p. 022312.

[40] T. Fukuyama et al. "Spatiotemporal Synchronization of Coupled Oscillators in a Laboratory Plasma". In: *Phys. Rev. Lett.* 96.1 (2 2006), p. 024101.

[41] Iris Pilch, Torben Reichstein, and Alexander Piel. "Synchronization of dust density waves in anodic plasmas". In: *Phys. Plasmas* 16.12 (2009), p. 123709.

[42] J. D. Williams. "Time-resolved measurement of global synchronization in the dust acoustic wave". In: *Phys. Rev. E* 90.10 (4 2014), p. 043103.

[43] Jiteng Sheng et al. "Self-Organized Synchronization of Phonon Lasers". In: *Phys. Rev. Lett.* 124.2 (5 2020), p. 053604.

[44] Caitlin R. S. Williams et al. "Synchronization states and multistability in a ring of periodic oscillators: Experimentally variable coupling delays". In: *Chaos* 23.4 (2013), p. 043117.

[45] Ajaz Mir, Sanat Tiwari, and Abhijit Sen. "Bispectral analysis of nonlinear mixing in a periodically driven Korteweg–de Vries system". In: *Phys. Plasmas* 29.3 (2022), p. 032303.

[46] Ajaz Mir et al. "Synchronization of dust acoustic waves in a forced Korteweg–de Vries–Burgers model". In: *Phys. Rev. E* 107.3 (3 2023), p. 035202.

[47] H. Thomas et al. "Plasma Crystal: Coulomb Crystallization in a Dusty Plasma". In: *Phys. Rev. Lett.* 73.8 (5 1994), pp. 652–655.

[48] J. H. Chu and Lin I. "Direct observation of Coulomb crystals and liquids in strongly coupled rf dusty plasmas". In: *Phys. Rev. Lett.* 72.6 (25 1994), pp. 4009–4012.

[49] A. Melzer, A. Homann, and A. Piel. "Experimental investigation of the melting transition of the plasma crystal". In: *Phys. Rev. E* 53.3 (3 1996), pp. 2757–2766.

[50] K. Qiao and T. W. Hyde. "Structural phase transitions and out-of-plane dust lattice instabilities in vertically confined plasma crystals". In: *Phys. Rev. E* 71.2 (2 2005), p. 026406.

[51] P. K. Shukla and A. A. Mamun. *Introduction to Dusty Plasma Physics*. Institute of Physics, Bristol, 2001.

[52] Robert Merlino. "Dusty plasmas: from Saturn's rings to semiconductor processing devices". In: *Adv. Phys.: X* 6.1 (2021), p. 1873859.

[53] Frank Verheest. *Waves in dusty space plasmas*. Vol. 245. Kluwer Academic, Dordrecht, 2000.

[54] G.A. Wurden, A.J. Wurden, and I.M. Gladstone. "Plasma tails: Comets Hale-Bopp and Hyakutake". In: *IEEE Trans. Plasma Sci.* 27.1 (1999), pp. 142–143.

[55] C. K. Goertz. "Dusty plasmas in the solar system". In: *Rev. Geophys.* 27.2 (1989), pp. 271–292.

[56] P. K. Shukla and B. Eliasson. "Colloquium: Fundamentals of dust-plasma interactions". In: *Rev. Mod. Phys.* 81.1 (1 2009), pp. 25–44.

[57] R. L. Merlino et al. "Nonlinear dust acoustic waves and shocks". In: *Phys. Plasmas* 19.5 (2012), p. 057301.

[58] Yoshiko Bailung et al. "Vortex formation in a strongly coupled dusty plasma flow past an obstacle". In: *Phys. Plasmas* 27.12 (2020), p. 123702.

[59] Garima Arora et al. "Effect of size and shape of a moving charged object on the propagation characteristics of precursor solitons". In: *Phys. Plasmas* 26.9 (2019), p. 093701.

[60] A. Melzer, D. Maier, and S. Schütt. "Analyzing phase separation processes in binary dusty plasmas using a polarization-sensitive camera". In: *Phys. Plasmas* 29.8 (2022), p. 083701.

[61] Birger Buttenschön, Michael Himpel, and André Melzer. "Spatially resolved three-dimensional particle dynamics in the void of dusty plasmas under microgravity using stereoscopy". In: *New J. Phys.* 13.2 (2011), p. 023042.

[62] C. A. Knapek et al. "Kinetic Characterization of Strongly Coupled Systems". In: *Phys. Rev. Lett.* 98.1 (1 2007), p. 015001.

[63] M. G. Hariprasad et al. "Experimental observation of a dusty plasma crystal in the cathode sheath of a DC glow discharge plasma". In: *Phys. Plasmas* 25.12 (2018), p. 123704.

[64] M. G. Hariprasad et al. "Thermodynamics and self-organization of strongly coupled Coulomb clusters: An experimental study". In: *Phys. Plasmas* 28.7 (2021), p. 073702.

[65] L. Couëdel et al. "First Direct Measurement of Optical Phonons in 2D Plasma Crystals". In: *Phys. Rev. Lett.* 103.11 (21 2009), p. 215001.

[66] S. Nunomura et al. "Dispersion relations of longitudinal and transverse waves in two-dimensional screened Coulomb crystals". In: *Phys. Rev. E* 65.6 (6 2002), p. 066402.

[67] S. Nunomura, D. Samsonov, and J. Goree. "Transverse Waves in a Two-Dimensional Screened-Coulomb Crystal (Dusty Plasma)". In: *Phys. Rev. Lett.* 84.5 (22 2000), pp. 5141–5144.

[68] S. Nunomura et al. "Phonon Spectrum in a Plasma Crystal". In: *Phys. Rev. Lett.* 89.6 (3 2002), p. 035001.

[69] S. Nunomura et al. "Wave Spectra in Solid and Liquid Complex (Dusty) Plasmas". In: *Phys. Rev. Lett.* 94.2 (4 2005), p. 045001.

[70] S. Nunomura et al. "Instability of Dust Particles in a Coulomb Crystal due to Delayed Charging". In: *Phys. Rev. Lett.* 83.9 (10 1999), pp. 1970–1973.

[71] L. Couëdel et al. "Direct Observation of Mode-Coupling Instability in Two-Dimensional Plasma Crystals". In: *Phys. Rev. Lett.* 104.5 (19 2010), p. 195001.

[72] J. K. Meyer et al. "Coupling of Noncrossing Wave Modes in a Two-Dimensional Plasma Crystal". In: *Phys. Rev. Lett.* 119.12 (25 2017), p. 255001.

[73] Krishan Kumar et al. "Kelvin-Helmholtz instability in a compressible dust fluid flow". In: *Sci. Rep.* 13.1 (2023), p. 3979.

[74] D. A. Law et al. "Probe-Induced Particle Circulation in a Plasma Crystal". In: *Phys. Rev. Lett.* 80.5 (19 1998), pp. 4189–4192.

[75] M. Klindworth et al. "Laser-excited intershell rotation of finite Coulomb clusters in a dusty plasma". In: *Phys. Rev. B* 61.3 (12 2000), pp. 8404–8410.

[76] M. R. Akdim and W. J. Goedheer. "Modeling of self-excited dust vortices in complex plasmas under microgravity". In: *Phys. Rev. E* 67.5 (5 2003), p. 056405.

[77] Mierk Schwabe et al. "Collective Effects in Vortex Movements in Complex Plasmas". In: *Phys. Rev. Lett.* 112.3 (11 2014), p. 115002.

[78] S. Mitic et al. "Convective Dust Clouds Driven by Thermal Creep in a Complex Plasma". In: *Phys. Rev. Lett.* 101.12 (23 2008), p. 235001.

[79] T. M. Flanagan and J. Goree. "Gas flow driven by thermal creep in dusty plasma". In: *Phys. Rev. E* 80.10 (4 2009), p. 046402.

[80] Hubertus M Thomas and Gregor E Morfill. "Melting dynamics of a plasma crystal". In: *Nature (London)* 379.6568 (1996), pp. 806–809.

[81] M. G. Hariprasad et al. "Experimental observation of a first-order phase transition in a complex plasma monolayer crystal". In: *Phys. Rev. E* 101.4 (4 2020), p. 043209.

[82] S. A. Khrapak et al. "Fluid-solid phase transitions in three-dimensional complex plasmas under microgravity conditions". In: *Phys. Rev. E* 85.6 (6 2012), p. 066407.

[83] MG Hariprasad et al. "Self-sustained non-equilibrium co-existence of fluid and solid states in a strongly coupled complex plasma system". In: *Sci. Rep.* 12.1 (2022), p. 13882.

[84] S Jaiswal and E Thomas. "Melting transition of two-dimensional complex plasma crystal in the DC glow discharge". In: *Plasma Res. Express* 1.2 (2019), p. 025014.

[85] V. Nosenko et al. "2D Melting of Plasma Crystals: Equilibrium and Nonequilibrium Regimes". In: *Phys. Rev. Lett.* 103.6 (1 2009), p. 015001.

[86] A. Wysocki et al. "Kinetics of Fluid Demixing in Complex Plasmas: Role of Two-Scale Interactions". In: *Phys. Rev. Lett.* 105.7 (4 2010), p. 045001.

[87]   D. Samsonov et al. "Shock Melting of a Two-Dimensional Complex (Dusty) Plasma". In: *Phys. Rev. Lett.* 92.6 (25 2004), p. 255004.

[88]   Anton Kananovich and J. Goree. "Experimental determination of shock speed versus exciter speed in a two-dimensional dusty plasma". In: *Phys. Rev. E* 101.54 (4 2020), p. 043211.

[89]   Anton Kananovich and J. Goree. "Shocks propagate in a 2D dusty plasma with less attenuation than due to gas friction alone". In: *Phys. lasmas* 27.11 (2020), p. 113704.

[90]   Anton Kananovich and J. Goree. "Shock width measured under liquid and solid conditions in a two-dimensional dusty plasma". In: *Phys. Rev. E* 104.11 (5 2021), p. 055201.

[91]   Garima Arora et al. "Excitation of dust acoustic shock waves in an inhomogeneous dusty plasma". In: *Phys. Plasmas* 27.8 (2020), p. 083703.

[92]   Sumita K. Sharma et al. "Observation of dust acoustic shock wave in a strongly coupled dusty plasma". In: *Phys. Plasmas* 23.5 (2016), p. 053702.

[93]   D. Samsonov et al. "Kinetic measurements of shock wave propagation in a three-dimensional complex (dusty) plasma". In: *Phys. Rev. E* 67.3 (3 2003), p. 036404.

[94]   D. Samsonov et al. "Mach Cones in a Coulomb Lattice and a Dusty Plasma". In: *Phys. Rev. Lett.* 83.11 (18 1999), pp. 3649–3652.

[95]   D. Samsonov et al. "Mach cone shocks in a two-dimensional Yukawa solid using a complex plasma". In: *Phys. Rev. E* 61.5 (5 2000), pp. 5557–5572.

[96]   K. Jiang et al. "Mach cones in a three-dimensional complex plasma". In: *Europhy. Lett.* 85.4 (Mar. 2009), p. 45002.

[97]   L. Couëdel et al. "Three-Dimensional Structure of Mach Cones in Monolayer Complex Plasma Crystals". In: *Phys. Rev. Lett.* 109.10 (17 2012), p. 175001.

[98]   P. Bandyopadhyay et al. "Experimental Study of Nonlinear Dust Acoustic Solitary Waves in a Dusty Plasma". In: *Phys. Rev. Lett.* 101.8 (6 2008), p. 065006.

[99]   T. E. Sheridan, V. Nosenko, and J. Goree. "Experimental study of nonlinear solitary waves in two-dimensional dusty plasma". In: *Phys. Plasmas* 15.7 (2008), p. 073703.

[100]  H. Bailung, S. K. Sharma, and Y. Nakamura. "Observation of Peregrine Solitons in a Multicomponent Plasma with Negative Ions". In: *Phys. Rev. Lett.* 107.12 (25 2011), p. 255005.

[101]  A. Piel et al. "Obliquely Propagating Dust-Density Plasma Waves in the Presence of an Ion Beam". In: *Phys. Rev. Lett.* 97.11 (20 2006), p. 205009.

[102]  Robert L. Merlino. "Dust-acoustic waves driven by an ion-dust streaming instability in laboratory discharge dusty plasma experiments". In: *Phys. Plasmas* 16.12 (2009), p. 124501.

[103]  Robert L. Merlino. "25 years of dust acoustic waves". In: *J. Plasma Phys.* 80.6 (2014), pp. 773–786.

[104]  A. Barkan, R. L. Merlino, and N. D'Angelo. "Laboratory observation of the dust-acoustic wave mode". In: *Phys. Plasmas* 2.10 (1995), pp. 3563–3565.

[105] C. Thompson et al. "Dust acoustic waves in a direct current glow discharge". In: *Phys. Plasmas* 4.7 (1997), pp. 2331–2335.

[106] R. L. Merlino et al. "Laboratory studies of waves and instabilities in dusty plasmas". In: *Phys. Plasmas* 5.5 (1998), pp. 1607–1614.

[107] T. M. Flanagan and J. Goree. "Observation of the spatial growth of self-excited dust-density waves". In: *Phys. Plasmas* 17.12 (2010), p. 123702.

[108] Tonuj Deka et al. "Observation of self-excited dust acoustic wave in dusty plasma with nanometer size dust grains". In: *Phys. Plasmas* 24.9 (2017), p. 093706.

[109] V. E. Fortov et al. "Mechanism of dust-acoustic instability in a direct current glow discharge plasma". In: *Phys. Plasmas* 7.5 (2000), pp. 1374–1380.

[110] Edward Thomas. "Measurements of spatially growing dust acoustic waves in a dc glow discharge plasma". In: *Phys. Plasmas* 13.4 (2006), p. 042107.

[111] M. Schwabe et al. "Highly Resolved Self-Excited Density Waves in a Complex Plasma". In: *Phys. Rev. Lett.* 99.8 (9 2007), p. 095002.

[112] Lee-Wen Teng et al. "Wave-Particle Dynamics of Wave Breaking in the Self-Excited Dust Acoustic Wave". In: *Phys. Rev. Lett.* 103.12 (24 2009), p. 245005.

[113] A. Melzer et al. "Dust-density waves in radio-frequency discharges under magnetic fields". In: *Phys. Plasmas* 27.3 (2020), p. 033704.

[114] Jeremiah D. Williams, Edward Thomas, and Lydia Marcus. "Observations of vertically propagating driven dust acoustic waves: Finite temperature effects". In: *Phys. Plasmas* 15.4 (2008), p. 043704.

[115] Benjamin Tadsen et al. "Self-excited dust-acoustic waves in an electron-depleted nanodusty plasma". In: *Phys. Plasmas* 22.11 (2015), p. 113701.

[116] P. Bajaj et al. "Spatial distribution of dust density wave properties in fluid complex plasmas". In: *Phys. Rev. E* 105.2 (2 2022), p. 025202.

[117] Simon Dap et al. "Cluster Agglomeration Induced by Dust-Density Waves in Complex Plasmas". In: *Phys. Rev. Lett.* 109.12 (24 2012), p. 245002.

[118] S.-H. Kim, J. R. Heinrich, and R. L. Merlino. "Diffraction of dust acoustic waves by a circular cylinder". In: *Phys. Plasmas* 15.9 (2008), p. 090701.

[119] J. B. Pieper and J. Goree. "Dispersion of Plasma Dust Acoustic Waves in the Strong-Coupling Regime". In: *Phys. Rev. Lett.* 77.10 (15 1996), pp. 3137–3140.

[120] K. O. Menzel, O. Arp, and A. Piel. "Spatial Frequency Clustering in Nonlinear Dust-Density Waves". In: *Phys. Rev. Lett.* 104.6 (23 2010), p. 235002.

[121] K. O. Menzel, O. Arp, and A. Piel. "Frequency clusters and defect structures in nonlinear dust-density waves under microgravity conditions". In: *Phys. Rev. E* 83.1 (1 2011), p. 016402.

[122] S. Khrapak et al. "Compressional waves in complex (dusty) plasmas under microgravity conditions". In: *Phys. Plasmas* 10.1 (2003), pp. 1–4.

[123] V. V. Yaroshenko et al. "Electrostatic modes in collisional complex plasmas under microgravity conditions". In: *Phys. Rev. E* 69.6 (6 2004), p. 066401.

[124] Mierk Schwabe et al. "Nonlinear waves externally excited in a complex plasma under microgravity conditions". In: *New J. Phys.* 10.3 (2008), p. 033037.

[125] S. Jaiswal et al. "Dust density waves in a dc flowing complex plasma with discharge polarity reversal". In: *Phys. Plasmas* 25.8 (2018), p. 083705.

[126] V. V. Yaroshenko et al. "Excitation of low-frequency dust density waves in flowing complex plasmas". In: *Phys. Plasmas* 26.5 (2019), p. 053702.

[127] H M Thomas et al. "Complex plasma research on the International Space Station". In: *Plasma Phys. Controlled Fusion* 61.1 (2018), p. 014004.

[128] S. Jaiswal et al. "Dust density waves in a dc flowing complex plasma with discharge polarity reversal". In: *Phys. Plasmas* 25.8 (2018), p. 083705.

[129] J. B. Pieper, J. Goree, and R. A. Quinn. "Three-dimensional structure in a crystallized dusty plasma". In: *Phys. Rev. E* 54.11 (5 1996), pp. 5636–5640.

[130] M. Zuzic et al. "Three-Dimensional Strongly Coupled Plasma Crystal under Gravity Conditions". In: *Phys. Rev. Lett.* 85.11 (19 2000), pp. 4064–4067.

[131] Gregor E. Morfill and Alexei V. Ivlev. "Complex plasmas: An interdisciplinary research field". In: *Rev. Mod. Phys.* 81.10 (4 2009), pp. 1353–1404.

[132] Swarnima Singh et al. "Square Lattice Formation in a Monodisperse Complex Plasma". In: *Phys. Rev. Lett.* 129.9 (11 2022), p. 115003.

[133] A. V. Zampetaki et al. "Buckling of two-dimensional plasma crystals with nonreciprocal interactions". In: *Phys. Rev. E* 102.10 (4 2020), p. 043204.

[134] A. Homann et al. "Laser-excited dust lattice waves in plasma crystals". In: *Phys. Lett. A* 242.3 (1998), pp. 173–180. ISSN: 0375-9601.

[135] A Piel, A Homann, and A Melzer. "Laser-excited waves in a plasma crystal". In: *Plasma Phys. Controlled Fusion* 41.3 (1999), A453–A461.

[136] Frank Melandsø. "Lattice waves in dust plasma crystals". In: *Phys. Plasmas* 3.11 (1996), pp. 3890–3901.

[137] Bin Liu, K. Avinash, and J. Goree. "Transverse Optical Mode in a One-Dimensional Yukawa Chain". In: *Phys. Rev. Lett.* 91.12 (25 2003), p. 255003.

[138] N. N. Rao, P. K. Shukla, and M. Y. Yu. "Dust-acoustic waves in dusty plasmas". In: *Planet. Space Sci.* 38 (4 1990), p. 543.

[139] Sanat Kumar Tiwari et al. "Observation of sharply peaked solitons in dusty plasma simulations". In: *New J. Phys.* 14.6 (2012), p. 063008.

[140] Abhijit Sen et al. "Nonlinear wave excitations by orbiting charged space debris objects". In: *Adv. Space Res.* 56.3 (2015), pp. 429–435. ISSN: 0273-1177.

[141] Lakhan Lal Yadav and R. Bharuthram. "Nonlinear Periodic Waves in Dusty Plasma with Variable Dust Charge". In: *AIP Conf. Proc.* 649.1 (2002), pp. 483–486.

[142] L. L. Yadav, S. V. Singh, and R. Bharuthram. "Dust–acoustic nonlinear periodic waves in a dusty plasma with charge fluctuation". In: *J. Plasma Phys.* 75.5 (2009), pp. 697–707.

[143] N. S. Saini and Papihra Sethi. "Dust ion-acoustic cnoidal waves in a plasma with two temperature superthermal electrons". In: *Phys. Plasmas* 23.10 (2016), p. 103702.

[144] R. E. Tolba et al. "Development of Cnoidal Waves in Positively Charged Dusty Plasmas". In: *IEEE Trans. Plasma Sci.* 45.9 (2017), pp. 2552–2560.

[145] S. K. Sharma, A. Boruah, and H. Bailung. "Head-on collision of dust-acoustic solitons in a strongly coupled dusty plasma". In: *Phys. Rev. E* 89.1 (1 2014), p. 013110.

[146] Y. Nakamura and I. Tsukabayashi. "Observation of Modified Korteweg—de Vries Solitons in a Multicomponent Plasma with Negative Ions". In: *Phys. Rev. Lett.* 52.6 (26 1984), pp. 2356–2359.

[147] P. K. Kaw and A. Sen. "Low frequency modes in strongly coupled dusty plasmas". In: *Phys. Plasmas* 5.10 (1998), pp. 3552–3559.

[148] Gustavo M. Monteiro and Sriram Ganeshan. "Nonlinear shallow water dynamics with odd viscosity". In: *Phys. Rev. Fluids* 6 (9 Sept. 2021), p. L092401.

[149] Atul Kumar et al. "Excitation of KdV magnetosonic solitons in plasma in the presence of an external magnetic field". In: *Plasma Phys. Controlled Fusion* 61.6 (May 2019), p. 065009.

[150] Krishan Kumar et al. "Reflection of a dust acoustic solitary wave in a dusty plasma". In: *Phys. Plasmas* 28.10 (2021), p. 103701.

[151] B Farokhi et al. "Linear and nonlinear dust lattice waves in plasma crystals". In: *Phys. Lett. A* 264.4 (1999), pp. 318–323. ISSN: 0375-9601.

[152] K. Avinash et al. "Nonlinear compressional waves in a two-dimensional Yukawa lattice". In: *Phys. Rev. E* 68.10 (4 2003), p. 046402.

[153] Garima Arora et al. "Experimental observation of pinned solitons in a flowing dusty plasma". In: *Phys. Rev. E* 103.1 (1 2021), p. 013201.

[154] Surabhi Jaiswal, P. Bandyopadhyay, and A. Sen. "Experimental observation of precursor solitons in a flowing complex plasma". In: *Phys. Rev. E* 93.4 (4 2016), p. 041201.

[155] Sanat Kumar Tiwari and Abhijit Sen. "Wakes and precursor soliton excitations by a moving charged object in a plasma". In: *Phys. Plasmas* 23.2 (2016), p. 022301.

[156] Bin Liu et al. "Experimental observation of cnoidal waveform of nonlinear dust acoustic waves". In: *Phys. Plasmas* 25.11 (2018), p. 113701.

[157] S. E. Cousens et al. "Nonlinear dust-acoustic solitary waves in strongly coupled dusty plasmas". In: *Phys. Rev. E* 86.12 (6 2012), p. 066404.

[158] R. S. Johnson. "A non-linear equation incorporating damping and dispersion". In: *J. Fluid Mech.* 42.1 (1970), pp. 49–60.

[159] A. González and A. Castellanos. "Korteweg–de Vries–Burgers equation for surface waves in non-ideal conducting liquids". In: *Phys. Rev. E* 49.4 (4 1994), pp. 2935–2940.

[160] Hui Du et al. "Experimental study of elevation- and depression-type internal solitary waves generated by gravity collapse". In: *Phys. Fluids* 31.10 (2019), p. 102104.

[161] Y. Nakamura and A. Sarma. "Observation of ion-acoustic solitary waves in a dusty plasma". In: *Phys. Plasmas* 8.9 (2001), pp. 3921–3926.

[162] Y. Nakamura, H. Bailung, and P. K. Shukla. "Observation of Ion-Acoustic Shocks in a Dusty Plasma". In: *Phys. Rev. Lett.* 83.8 (8 1999), pp. 1602–1605.

[163] S. Jaiswal, P. Bandyopadhyay, and A. Sen. "Experimental investigation of flow induced dust acoustic shock waves in a complex plasma". In: *Phys. Plasmas* 23.8 (2016), p. 083701.

[164] P.K. Shukla and A.A. Mamun. "Dust-acoustic shocks in a strongly coupled dusty plasma". In: *IEEE Trans. Plasma Sci.* 29.2 (2001), pp. 221–225.

[165] B. M. Veeresha et al. "Nonlinear wave propagation in strongly coupled dusty plasmas". In: *Phys. Rev. E* 81.3 (3 2010), p. 036407.

[166] Stefan C. Mancas and Ronald Adams. "Dissipative periodic and chaotic patterns to the KdV–Burgers and Gardner equations". In: *Chaos, Solitons & Fractals* 126 (2019), pp. 385–393. ISSN: 0960-0779.

[167] A. Boruah et al. "Observation of dust acoustic multi-solitons in a strongly coupled dusty plasma". In: *Phys. Plasmas* 23.9 (2016), p. 093704.

[168] S. Y. El-Monier and A. Atteya. "Bifurcation Analysis for Dust-Acoustic Waves in a Four-Component Plasma Including Warm Ions". In: *IEEE Trans. Plasma Sci.* 46.4 (2018), pp. 815–824.

[169] Ajaz A. Mir et al. "A forced Korteweg–de Vries model for nonlinear mixing of oscillations in a dusty plasma". In: *Phys. Plasmas* 27.11 (2020), p. 113701.

[170] Yuanlin Zheng and Xianfeng Chen. "Nonlinear wave mixing in lithium niobate thin film". In: *Adv. Phys.: X* 6.1 (2021), p. 1889402.

[171] X. Liu et al. "Nonlinear four-wave mixing with enhanced diversity and selectivity via spin and orbital angular momentum conservation". In: *APL Photonics* 5.1 (2020), p. 010802.

[172] W. T. Buono et al. "Polarization-controlled orbital angular momentum switching in nonlinear wave mixing". In: *Opt. Lett.* 43.7 (2018), pp. 1439–1442.

[173] Przemyslaw Lewandowski et al. "Polarization dependence of nonlinear wave mixing of spinor polaritons in semiconductor microcavities". In: *Phys. Rev. B* 94.7 (4 2016), p. 045308.

[174] Da Huang et al. "Wave mixing in nonlinear magnetic metacrystal". In: *Appl. Phys. Lett.* 98.20 (2011), p. 204102.

[175] Ilya V. Shadrivov et al. "Tunable transmission and harmonic generation in nonlinear metamaterials". In: *Appl. Phys. Lett.* 93.16 (2008), p. 161903.

[176]  María Teresa Tejedor Sastre and Christian Vanhille. "A numerical model for the study of the difference frequency generated from nonlinear mixing of standing ultrasonic waves in bubbly liquids". In: *Ultrason. Sonochem.* 34 (2017), pp. 881–888. ISSN: 1350-4177.

[177]  Abhijit Sen et al. "Electromagnetic pinned solitons for space debris detection". In: *Phys. Plasmas* 30.1 (2023), p. 012301.

[178]  T. R. Akylas. "On the excitation of long nonlinear water waves by a moving pressure distribution". In: *J. Fluid Mech.* 141 (1984), pp. 455–466.

[179]  R. Camassa and T.Yao-tsu Wu. "Stability of some stationary solutions for the forced KdV equation". In: *Phys. D: Nonlinear Phenom.* 51.1 (1991), pp. 295–307. ISSN: 0167-2789.

[180]  S. Hamaguchi, R. T. Farouki, and D. H. E. Dubin. "Triple point of Yukawa systems". In: *Phys. Rev. E* 56.10 (4 1997), pp. 4671–4682.

[181]  Setsuo Ichimaru. "Strongly coupled plasmas: high-density classical plasmas and degenerate electron liquids". In: *Rev. Mod. Phys.* 54.10 (4 1982), pp. 1017–1059.

[182]  Christiaan Huygens. *Oeuvres Complètes de Christiaan Huygens*. Martinus Nijhoff, 1899.

[183]  Christiaan Huygens. *Horologium oscillatorium sive de motu pendulorum ad horologia aptato demonstrationes geometricae*. Apud F. Muguet, 1966.

[184]  Andrew Moiseff and Jonathan Copeland. "Firefly Synchrony: A Behavioral Strategy to Minimize Visual Clutter". In: *Science* 329.5988 (2010), pp. 181–181.

[185]  A. Balanov et al. *Synchronization: From Simple to Complex*. Springer-Verlag, Berlin, 2009.

[186]  J. D. Williams. "Evolution of frequency clusters in the naturally occurring dust acoustic wave". In: *Phys. Rev. E* 89.2 (2 2014), p. 023105.

[187]  Bin Liu et al. "Nonlinear Wave Synchronization in a Dusty Plasma Under Microgravity on the International Space Station (ISS)". In: *IEEE Trans. Plasma Sci.* 49.12 (2021), pp. 3958–3962.

[188]  G. V. Osipov and M. M. Sushchik. "Synchronized clusters and multistability in arrays of oscillators with different natural frequencies". In: *Phys. Rev. E* 58.12 (6 1998), pp. 7198–7207.

[189]  Alexey K. Kryukov et al. "Synchronous regimes in ensembles of coupled Bonhoeffer–van der Pol oscillators". In: *Phys. Rev. E* 79.4 (4 2009), p. 046209.

[190]  T. Klinger et al. "van der Pol behavior of relaxation oscillations in a periodically driven thermionic discharge". In: *Phys. Rev. E* 52.10 (4 1995), pp. 4316–4327.

[191]  Neeraj Chaubey et al. "Experimental observation of phase-flip transitions in two inductively coupled glow discharge plasmas". In: *Phys. Rev. E* 94.12 (6 2016), p. 061201.

[192]  Dmitry P. Kovalev and Peter D. Kovalev. "Synchronization of Long Ocean Waves by Coastal Relief on the Southeast Shelf of Sakhalin Island". In: *Int. J. Bifurc. Chaos* 27.13 (2017), p. 1750195.

[193]  K. O. Menzel, O. Arp, and A. Piel. "Chain of coupled van der Pol oscillators as model system for density waves in dusty plasmas". In: *Phys. Rev. E* 84.7 (1 2011), p. 016405.

[194] Arkadiusz Orłowski. "Randomly driven Korteweg–de Vries–Burgers equation". In: *Phys. Rev. E* 49.3 (3 1994), pp. 2465–2467.

[195] Paulo C Rech. "Nonlinear dynamics investigation in parameter planes of a periodically forced compound KdV-Burgers equation". In: *Eur. Phys. J. B* 86.8 (2013), pp. 1–5.

[196] M.A Malkov. "Spatial chaos in weakly dispersive and viscous media: A nonperturbative theory of the driven KdV-Burgers equation". In: *Phys. D: Nonlinear Phenom.* 95.1 (1996), pp. 62–80. ISSN: 0167-2789.

[197] Tay Kim Gaik and Hilmi Demiray. "Forced Korteweg-de Vries–Burgers equation in an elastic tube filled with a variable viscosity fluid". In: *Chaos, Solitons & Fractals* 38.4 (2008), pp. 1134–1145. ISSN: 0960-0779.

[198] John P Boyd. *Chebyshev and Fourier Spectral Methods.* Dover, New York, 2003.

[199] K. O. Hill et al. "cw three-wave mixing in single-mode optical fibers". In: *J. Appl. Phys.* 49.10 (1978), pp. 5098–5106.

[200] Peer Fischer et al. "Three-Wave Mixing in Chiral Liquids". In: *Phys. Rev. Lett.* 85.11 (20 2000), pp. 4253–4256.

[201] Yuan Shi. "Three-wave interactions in magnetized warm-fluid plasmas: General theory with evaluable coupling coefficient". In: *Phys. Rev. E* 99.6 (6 2019), p. 063212.

[202] A. Homann et al. "Determination of the dust screening length by laser-excited lattice waves". In: *Phys. Rev. E* 56.12 (6 1997), pp. 7138–7141.

[203] J. Heinrich, S.-H. Kim, and R. L. Merlino. "Laboratory Observations of Self-Excited Dust Acoustic Shocks". In: *Phys. Rev. Lett.* 103.9 (11 2009), p. 115002.

[204] P K Shukla and A A Mamun. "Solitons, shocks and vortices in dusty plasmas". In: *New J. Phys.* 5 (2003), pp. 17–17.

[205] P Bandyopadhyay et al. "Effect of polarization force on the propagation of dust acoustic solitary waves". In: *New J. Phys.* 12.7 (2010), p. 073002.

[206] G. M. Peradze and N. L. Tsintsadze. "Solitons in normal Fermi liquid". In: *Low Temp. Phys.* 45.1 (2019), pp. 103–106.

[207] A. Ludu and J. P. Draayer. "Nonlinear Modes of Liquid Drops as Solitary Waves". In: *Phys. Rev. Lett.* 80.3 (10 1998), pp. 2125–2128.

[208] D. A. Foga ça, F. S. Navarra, and L. G. Ferreira Filho. "Korteveg-de Vries solitons in a cold quark-gluon plasma". In: *Phys. Rev. D* 84.9 (5 2011), p. 054011.

[209] Y. C. Mo et al. "Experimental Observations of Soliton Wave Trains in Electron Beams". In: *Phys. Rev. Lett.* 110.2 (8 2013), p. 084802.

[210] D. Samsonov et al. "Dissipative Longitudinal Solitons in a Two-Dimensional Strongly Coupled Complex (Dusty) Plasma". In: *Phys. Rev. Lett.* 88.2 (9 2002), p. 095004.

[211] Hervé Leblond. "Half-cycle optical soliton in quadratic nonlinear media". In: *Phys. Rev. A* 78.7 (1 2008), p. 013807.

[212] A. Gasch, T. Berning, and D. Jäger. "Generation and parametric amplification of solitons in a nonlinear resonator with a Korteweg-de Vries medium". In: *Phys. Rev. A* 34.11 (5 1986), pp. 4528–4531.

[213] E. F. El-Shamy. "Nonlinear ion-acoustic cnoidal waves in a dense relativistic degenerate magnetoplasma". In: *Phys. Rev. E* 91.3 (3 2015), p. 033105.

[214] A. R. Osborne. "Numerical construction of nonlinear wave-train solutions of the periodic Korteweg–de Vries equation". In: *Phys. Rev. E* 48.7 (1 1993), pp. 296–309.

[215] M.W. Dingemans. *Water Wave Propagation Over Uneven Bottoms*. World Scientific, Singapore, 1997.

[216] Alvaro H. Salas. "Computing solutions to a forced KdV equation". In: *Nonlinear Anal. Real World Appl.* 12.2 (2011), pp. 1314–1320. ISSN: 1468-1218.

[217] Haruichi Washimi and Tosiya Taniuti. "Propagation of Ion-Acoustic Solitary Waves of Small Amplitude". In: *Phys. Rev. Lett.* 17.11 (19 1966), pp. 996–998.

[218] H.-Y. Hao and H. J. Maris. "Experiments with acoustic solitons in crystalline solids". In: *Phys. Rev. B* 64.7 (6 2001), p. 064302.

[219] Ivan Redor et al. "Experimental Evidence of a Hydrodynamic Soliton Gas". In: *Phys. Rev. Lett.* 122.5 (21 2019), p. 214502.

[220] T. Congy, A. M. Kamchatnov, and N. Pavloff. "Nonlinear waves in coherently coupled Bose-Einstein condensates". In: *Phys. Rev. A* 93.4 (4 2016), p. 043613.

[221] A. M. Kamchatnov and V. S. Shchesnovich. "Dynamics of Bose-Einstein condensates in cigar-shaped traps". In: *Phys. Rev. A* 70.8 (2 2004), p. 023604.

[222] Atul Kumar and Abhijit Sen. "Precursor magneto-sonic solitons in a plasma from a moving charge bunch". In: *New J. Phys.* 22.7 (July 2020), p. 073057.

[223] Yu. R. Vainberg, B. I. Meerson, and P. V. Sasorov. "Resonance excitation of nonlinear dispersive waves". In: *Radiophys. Quantum Electron.* 26 (10 Dec. 1983), pp. 1114–1119.

[224] L. Friedland, A. G. Shagalov, and S. V. Batalov. "Anomalous autoresonance threshold for chirped-driven Korteweg–de-Vries waves". In: *Phys. Rev. E* 92.10 (4 2015), p. 042924.

[225] Igor Aranson, Baruch Meerson, and Toshiki Tajima. "Excitation of solitons by an external resonant wave with a slowly varying phase velocity". In: *Phys. Rev. A* 45.5 (10 1992), pp. 7500–7510.

[226] T. Subba Rao and M. M. Gabr. *Lecture Notes in Statistics: An Introduction to Bispectral Analysis and Bilinear Time Series Models*. Springer-Verlag, New York, 1984.

[227] C. L. Nikias and M. R. Raghuveer. "Bispectrum estimation: A digital signal processing framework". In: *Proc. IEEE* 75.7 (1987), pp. 869–891.

[228] Y. C. Kim and E. J. Powers. "Digital Bispectral Analysis and Its Applications to Nonlinear Wave Interactions". In: *IEEE Trans. Plasma Sci.* 7.2 (1979), pp. 120–131.

[229] B. Ph. van Milligen, C. Hidalgo, and E. Sánchez. "Nonlinear Phenomena and Intermittency in Plasma Turbulence". In: *Phys. Rev. Lett.* 74.1 (3 1995), pp. 395–398.

[230] J. S. Kim et al. "Measurements of Nonlinear Energy Transfer in Turbulence in the Tokamak Fusion Test Reactor". In: *Phys. Rev. Lett.* 79.8 (5 1997), pp. 841–844.

[231] V. Nosenko, J. Goree, and F. Skiff. "Bispectral analysis of nonlinear compressional waves in a two-dimensional dusty plasma crystal". In: *Phys. Rev. E* 73.1 (1 2006), p. 016401.

[232] K. L. Siu et al. "Statistical Approach to Quantify the Presence of Phase Coupling Using the Bispectrum". In: *IEEE Trans. Biomed. Eng.* 55.5 (2008), pp. 1512–1520.

[233] G. Tacchino et al. "Bicoherence Interpretation in EEG Requires Signal to Noise Ratio Quantification: An Application to Sensorimotor Rhythms". In: *IEEE Trans. Biomed. Eng.* 67.9 (2020), pp. 2696–2704.

[234] Andrew J Hillis et al. "Global crack detection using bispectral analysis". In: *Proc. Math. Phys. Eng. Sci.* 462.2069 (2006), pp. 1515–1530.

[235] T. E. Hall and G. B. Giannakis. "Bispectral analysis and model validation of texture images". In: *IEEE Trans. Image Processing* 4.7 (1995), pp. 996–1009.

[236] Chengyang Mo et al. "Cnoidal wave propagation in an elastic metamaterial". In: *Phys. Rev. E* 100.7 (1 2019), p. 013001.

[237] Dora Kholmyansky and Omri Gat. "Optimal frequency combs from cnoidal waves in Kerr microresonators". In: *Phys. Rev. A* 100.12 (6 2019), p. 063809.

[238] Sarveshwar Sharma, Nishant Sirse, and Miles M Turner. "High frequency sheath modulation and higher harmonic generation in a low pressure very high frequency capacitively coupled plasma excited by sawtooth waveform". In: *Plasma Sources Sci. Technol.* 29.11 (Nov. 2020), p. 114001.

[239] Zhen Qi, Giuseppe D'Aguanno, and Curtis R. Menyuk. "Nonlinear frequency combs generated by cnoidal waves in microring resonators". In: *J. Opt. Soc. Am. B* 34.4 (Apr. 2017), pp. 785–794.

[240] D. Farina and S. V. Bulanov. "Relativistic Electromagnetic Solitons in the Electron-Ion Plasma". In: *Phys. Rev. Lett.* 86.6 (23 2001), pp. 5289–5292.

[241] S. Mahmood and F. Haas. "Ion-acoustic cnoidal waves in a quantum plasma". In: *Phys. Plasmas* 21.10 (2014), p. 102308.

[242] T. M. Flanagan and J. Goree. "Development of nonlinearity in a growing self-excited dust-density wave". In: *Phys. Plasmas* 18.1 (2011), p. 013705.

[243] Milton Abramowitz and Irene A Stegun. *Handbook of Mathematical Functions : With Formulas, Graphs, and Mathematical Tables.* New York: Dover Publications, 1965.

[244] D Raju, O Sauter, and J B Lister. "Study of nonlinear mode coupling during neoclassical tearing modes using bispectrum analysis". In: *Plasma Phys. Control. Fusion* 45.4 (Mar. 2003), pp. 369–378.

[245] Jose Carlos Pedro and Nuno Borges Carvalho. *Intermodulation Distortion in Microwave and Wireless Circuits*. Artech House, Boston, 2003.

[246] K. Y. Lau and A. Yariv. "Intermodulation distortion in a directly modulated semiconductor injection laser". In: *Appl. Phys. Lett.* 45.10 (1984), pp. 1034–1036.

[247] P. K. Shukla. "Parametric Instability of Dust Lattice Waves in a Turbulent Plasma Sheath". In: *Phys. Rev. Lett.* 84.6 (23 2000), pp. 5328–5330.

[248] Keith A. Brueckner and Siebe Jorna. "Laser-driven fusion". In: *Rev. Mod. Phys.* 46 (2 1974), pp. 325–367.

[249] V.N. Tsytovich and L. Stenflo. "Three wave interaction in turbulent plasmas". In: *Phys. Lett. A* 43.1 (1973), pp. 7–8. ISSN: 0375-9601.

[250] Ch. P. Ritz, E. J. Powers, and R. D. Bengtson. "Experimental measurement of three-wave coupling and energy cascading". In: *Phys. Fluids B: Plasma Phys.* 1.1 (1989), pp. 153–163.

[251] G. J. Kalman et al. "Two-Dimensional Yukawa Liquids: Correlation and Dynamics". In: *Phys. Rev. Lett.* 92.2 (6 2004), p. 065001.

[252] P. Hartmann et al. "Equilibrium properties and phase diagram of two-dimensional Yukawa systems". In: *Phys. Rev. E* 72.8 (2 2005), p. 026409.

[253] H. Ikezi. "Coulomb solid of small particles in plasmas". In: *Phys. Fluids* 29.6 (1986), pp. 1764–1766.

[254] O. Vaulina, S. Khrapak, and G. Morfill. "Universal scaling in complex (dusty) plasmas". In: *Phys. Rev. E* 66.7 (1 2002), p. 016404.

[255] F. Bitzer et al. "Dynamical test of interaction potentials for colloidal suspensions". In: *Phys. Rev. E* 50.10 (4 1994), pp. 2821–2826.

[256] Hartmut Löwen, Thomas Palberg, and Rolf Simon. "Dynamical criterion for freezing of colloidal liquids". In: *Phys. Rev. Lett.* 70.3 (10 1993), pp. 1557–1560.

[257] Kurt Kremer, Mark O. Robbins, and Gary S. Grest. "Phase Diagram of Yukawa Systems: Model for Charge-Stabilized Colloids". In: *Phys. Rev. Lett.* 57.11 (21 1986), pp. 2694–2697.

[258] H Lowen. "Structure and Brownian dynamics of the two-dimensional Yukawa fluid". In: *J. Phys.: Condens. Matter* 4.50 (Dec. 1992), pp. 10105–10116.

[259] H Löwen et al. "Charged colloids, polyelectrolytes and biomolecules viewed as strongly coupled Coulomb systems". In: *J. Phys. A: Math. Gen.* 36.22 (2003), p. 5827.

[260] Antti-Pekka Hynninen and Marjolein Dijkstra. "Melting line of charged colloids from primitive model simulations". In: *J. Chem. Phys.* 123.24 (2005), p. 244902.

[261] Dikeos Soumpasis. "Debye–Hückel theory of model polyelectrolytes". In: *J. Chem. Phys.* 69.7 (1978), pp. 3190–3196.

[262] Stefan Auer and Daan Frenkel. "Crystallization of weakly charged colloidal spheres: a numerical study". In: *J. Phys.: Condens. Matter* 14.33 (Aug. 2002), pp. 7667–7680.

[263] A. A. Kornyshev and S. Leikin. "Theory of interaction between helical molecules". In: *J. Chem. Phys.* 107.9 (1997), pp. 3656–3674.

[264] Anna Stradner et al. "Equilibrium cluster formation in concentrated protein solutions and colloids". In: *Nature (London)* 432.7016 (2004), pp. 492–495.

[265] Edward V. Shuryak and Ismail Zahed. "Toward a theory of binary bound states in the quark-gluon plasma". In: *Phys. Rev. D* 70.9 (5 2004), p. 054507.

[266] Munshi G. Mustafa, Markus H. Thoma, and Purnendu Chakraborty. "Screening of a moving parton in the quark-gluon plasma". In: *Phys. Rev. C* 71.1 (1 2005), p. 017901.

[267] S. Hamaguchi. "Strongly coupled Yukawa plasmas — models for dusty plasmas and colloidal suspensions". In: *Plasmas & Ions* 2.2 (1999), pp. 57–68. ISSN: 1288-3255.

[268] T.C. Killian et al. "Ultracold neutral plasmas". In: *Phys. Rep.* 449.4 (2007), pp. 77–130. ISSN: 0370-1573.

[269] P. K. Shukla and K. Avinash. "Phase Coexistence and a Critical Point in Ultracold Neutral Plasmas". In: *Phys. Rev. Lett.* 107.9 (13 2011), p. 135002.

[270] Guilherme Volpe Bossa and Sylvio May. "Stability of ionic liquid modeled by composite Coulomb-Yukawa potentials". In: *Phys. Rev. Res.* 2.8 (3 2020), p. 032040.

[271] Lubov V Zherenkova, Pavel V Komarov, and Alexander S Pavlov. "Long-range correlations in polymer-containing ionic liquids: the case of good solubility". In: *J. Phys. Chem. Lett.* 1.8 (2010), pp. 1186–1190.

[272] Bin Liu, J. Goree, and Yan Feng. "Non-Gaussian statistics and superdiffusion in a driven-dissipative dusty plasma". In: *Phys. Rev. E* 78 (4 Oct. 2008), p. 046403.

[273] Z. Donkó and P. Hartmann. "Shear viscosity of strongly coupled Yukawa liquids". In: *Phys. Rev. E* 78.8 (2 2008), p. 026408.

[274] Sanat Kumar Tiwari et al. "Molecular dynamics simulations of soliton-like structures in a dusty plasma medium". In: *Phys. Plasmas* 22.3 (2015), p. 033706.

[275] Sandeep Kumar, Sanat Kumar Tiwari, and Amita Das. "Observation of the Korteweg-de Vries soliton in molecular dynamics simulations of a dusty plasma medium". In: *Phys. Plasmas* 24.3 (2017), p. 033711.

[276] Yan Feng, Bin Liu, and J. Goree. "Rapid heating and cooling in two-dimensional Yukawa systems". In: *Phys. Rev. E* 78.8 (2 2008), p. 026415.

[277] O. S. Vaulina et al. "Determination of Pair Interaction Forces between Particles in Nonideal Dissipative Systems". In: *Phys. Rev. Lett.* 103.7 (3 2009), p. 035003.

[278] T. Ott and M. Bonitz. "Is Diffusion Anomalous in Two-Dimensional Yukawa Liquids?" In: *Phys. Rev. Lett.* 103.11 (19 2009), p. 195001.

[279] Yan Feng, J. Goree, and Bin Liu. "Identifying anomalous diffusion and melting in dusty plasmas". In: *Phys. Rev. E* 82.9 (3 2010), p. 036403.

[280] A. P. Thompson et al. "LAMMPS - a flexible simulation tool for particle-based materials modeling at the atomic, meso, and continuum scales". In: *Comp. Phys. Comm.* 271.2 (2022), p. 108171.

[281] Michael P Allen and Dominic J Tildesley. *Computer Simulation of Liquids*. Oxford University Press, New York, 2017.

[282] Hideki Yukawa. "On the interaction of elementary particles. I". In: *Proc. Phys. Math. Soc. Japan* 17 (1935), pp. 48–57.

[283] P Debye and E Hückel. "The interionic attraction theory of deviations from ideal behavior in solution". In: *Z. Phys* 24 (1923), p. 185.

[284] Pengwei Qiu, Tianyue Sun, and Yan Feng. "Observation of the solid and liquid separation after the shock propagation in a two-dimensional Yukawa solid". In: *Phys. Plasmas* 28.11 (2021), p. 113702.

[285] Wei Lin, M. S. Murillo, and Yan Feng. "Pressure and energy of compressional shocks in two-dimensional Yukawa systems". In: *Phys. Rev. E* 100.10 (4 2019), p. 043203.

[286] S. Nunomura et al. "Nonlinear longitudinal waves in a two-dimensional screened Coulomb crystal". In: *Phys. Rev. E* 68.8 (2 2003), p. 026407.

[287] R. K. Pathria. *Statistical Mechanics*. Pergamon Press, Oxford, 1972.

[288] W.F. van Gunsteren and H.J.C. Berendsen. "Algorithms for brownian dynamics". In: *Mol. Phys.* 45.3 (1982), pp. 637–647.

[289] Rep Kubo. "The fluctuation-dissipation theorem". In: *Rep. Prog. Phys.* 29.1 (1966), p. 255.

[290] Shūichi Nosé. "A molecular dynamics method for simulations in the canonical ensemble". In: *Mol. Phys.* 52.2 (1984), pp. 255–268.

[291] William G. Hoover. "Canonical dynamics: Equilibrium phase-space distributions". In: *Phys. Rev. A* 31.3 (3 1985), pp. 1695–1697.

[292] Steven Strogatz. *Sync: The Emerging Science of Spontaneous Order*. Penguin, UK, 2004.

[293] Yoshiki Kuramoto. "Cooperative dynamics of oscillator communitya study based on lattice of rings". In: *Progr. Theoret. Phys. Suppl.* 79 (1984), pp. 223–240.

[294] D.G. Aronson, G.B. Ermentrout, and N. Kopell. "Amplitude response of coupled oscillators". In: *Phys. D: Nonlinear Phenom.* 41.3 (1990), pp. 403–449. ISSN: 0167-2789.

[295] Jeremiah D. Williams and James Duff. "Observation of the coupling of the driven dust acoustic wave". In: *Phys. Plasmas* 17.3 (2010), p. 033702.

[296] D. Block et al. "Synchronization of drift waves". In: *Phys. Rev. E* 63.4 (5 2001), p. 056401.

[297] T. Klinger et al. "Van der Pol dynamics of ionization waves". In: *Phys. Lett. A* 182.2 (1993), pp. 312–318. ISSN: 0375-9601.

[298] Tomaž Gyergyek. "Experimental study of the nonlinear dynamics of a harmonically forced double layer". In: *Plasma Phys. Controlled Fusion* 41.2 (1999), p. 175.

[299] Md. Nurujjaman and A. N. Sekar Iyengar. "Dynamics of an excitable glow-discharge plasma under external forcing". In: *Phys. Rev. E* 82.11 (5 2010), p. 056210.

[300] B. E. Keen and W. H. W. Fletcher. "Suppression and Enhancement of an Ion-Sound Instability by Nonlinear Resonance Effects in a Plasma". In: *Phys. Rev. Lett.* 23.10 (14 1969), pp. 760–763.

[301] Th Mausbach et al. "Continuous control of ionization wave chaos by spatially derived feedback signals". In: *Phys. Lett. A* 228.6 (1997), pp. 373–377. ISSN: 0375-9601.

[302] M. E. Koepke et al. "Spatiotemporal signatures of periodic pulling during ionization-wave-mode transitions". In: *Phys. Plasmas* 8.4 (2001), pp. 1432–1436.

[303] F. Brochard et al. "Spatiotemporal control and synchronization of flute modes and drift waves in a magnetized plasma column". In: *Phys. Plasmas* 13.5 (2006), p. 052509.

[304] Christiane Schröder et al. "Mode Selective Control of Drift Wave Turbulence". In: *Phys. Rev. Lett.* 86.6 (25 2001), pp. 5711–5714.

[305] T Gyergyek et al. "Mode suppression of a two-dimensional potential relaxation instability in a weakly magnetized discharge plasma". In: *Phys. Lett. A* 177.1 (1993), pp. 54–60. ISSN: 0375-9601.

[306] A Piel and A Melzer. "Dynamical processes in complex plasmas". In: *Plasma Phys. Controlled Fusion* 44.1 (2001), pp. 1–26.

[307] C Thompson et al. "Video imaging of dust acoustic waves". In: *IEEE Trans. Plasma Sci.* 27.1 (1999), pp. 146–147.

[308] Wellalage Don, Suranga Ruhunusiri, and John Goree. "Imaging of the dust acoustic wave to explore synchronization". In: *IEEE Trans. Plasma Sci.* 42.10 (2014), pp. 2688–2689.

[309] Y. Feng, J. Goree, and Bin Liu. "Accurate particle position measurement from images". In: *Rev. Sci. Instrum.* 78.5 (2007), p. 053704.

[310] Sanjib Sarkar et al. "Spatiotemporal evolution of dielectric driven cogenerated dust density waves". In: *Phys. Plasmas* 20.6 (2013), p. 064502.

[311] Balth Van Der Pol. "Vii. forced oscillations in a circuit with non-linear resistance.(reception with reactive triode)". In: *Philos. Mag.* 3.13 (1927), pp. 65–80.

[312] S. Jaiswal, P. Bandyopadhyay, and A. Sen. "Experimental investigation of flow induced dust acoustic shock waves in a complex plasma". In: *Phys. Plasmas* 23.8 (2016), p. 083701.

[313] T. Saigo and S. Hamaguchi. "Shear viscosity of strongly coupled Yukawa systems". In: *Phys. Plasmas* 9.4 (2002), pp. 1210–1216.

[314] R. V. Jensen. "Synchronization of driven nonlinear oscillators". In: *Am. J. Phys.* 70.6 (2002), pp. 607–619.

[315] Louis M. Pecora and Thomas L. Carroll. "Synchronization in chaotic systems". In: *Phys. Rev. Lett.* 64.2 (8 1990), pp. 821–824.

[316] Epaminondas Rosa, Edward Ott, and Mark H. Hess. "Transition to Phase Synchronization of Chaos". In: *Phys. Rev. Lett.* 80.2 (8 1998), pp. 1642–1645.

[317] Michael G. Rosenblum, Arkady S. Pikovsky, and Jürgen Kurths. "From Phase to Lag Synchronization in Coupled Chaotic Oscillators". In: *Phys. Rev. Lett.* 78.6 (22 1997), pp. 4193–4196.

[318] L. Kocarev and U. Parlitz. "Generalized Synchronization, Predictability, and Equivalence of Unidirectionally Coupled Dynamical Systems". In: *Phys. Rev. Lett.* 76.3 (11 1996), pp. 1816–1819.

[319] O. I. Kanakov et al. "Cluster synchronization and spatio-temporal dynamics in networks of oscillatory and excitable Luo-Rudy cells". In: *Chaos* 17.1 (2007), p. 015111.

[320] Gautam C. Sethia, Abhijit Sen, and Fatihcan M. Atay. "Clustered Chimera States in Delay-Coupled Oscillator Systems". In: *Phys. Rev. Lett.* 100.4 (14 2008), p. 144102.

[321] Hiroya Nakao, Kensuke Arai, and Yoji Kawamura. "Noise-Induced Synchronization and Clustering in Ensembles of Uncoupled Limit-Cycle Oscillators". In: *Phys. Rev. Lett.* 98.5 (18 2007), p. 184101.